Chemistry–A European Journal

Supporting Information

Exceptional Substrate Diversity in Oxygenation Reactions Catalyzed by a Bis(μ-oxo) Copper Complex

Melanie Paul,[a] Melissa Teubner,[a, b] Benjamin Grimm-Lebsanft,[b] Christiane Golchert,[a] Yannick Meiners,[a] Laura Senft,[c] Kristina Keisers,[a] Patricia Liebhäuser,[a] Thomas Rösener,[a] Florian Biebl,[b] Sören Buchenau,[b] Maria Naumova,[d] Vadim Murzin,[d] Roxanne Krug,[e] Alexander Hoffmann,[a] Jörg Pietruszka,[e, f] Ivana Ivanović-Burmazović,[c] Michael Rübhausen,[b] and Sonja Herres-Pawlis*[a]

Author Contributions

S.H. Conceptualization: Lead; Funding acquisition: Lead; Investigation: Supporting; Project administration: Lead; Resources: Lead; Supervision: Lead; Validation: Lead; Writing - Review & Editing: Lead
M.P. Conceptualization: Supporting; Investigation: Lead; Writing - Original Draft: Lead
M.T. Investigation: Equal; Methodology: Equal
B.G. Data curation: Supporting; Formal analysis: Lead; Methodology: Lead; Supervision: Supporting; Validation: Supporting; Writing - Original Draft: Supporting
C.G. Investigation: Supporting
Y.M. Investigation: Supporting
L.S. Methodology: Equal
K.K. Methodology: Supporting
P.L. Investigation: Supporting; Methodology: Supporting
T.R. Methodology: Supporting
F.B. Methodology: Supporting
S.B. Methodology: Supporting
M.N. Methodology: Supporting
V.M. Methodology: Supporting
R.K. Investigation: Supporting
A.H. Conceptualization: Equal; Data curation: Lead; Investigation: Equal; Methodology: Equal; Project administration: Equal; Software: Equal; Supervision: Equal; Validation: Equal; Writing - Review & Editing: Equal
J.P. Conceptualization: Supporting; Supervision: Supporting; Writing - Review & Editing: Supporting
I.I. Methodology: Supporting; Supervision: Supporting; Writing - Review & Editing: Supporting
M.R. Conceptualization: Supporting; Funding acquisition: Supporting; Methodology: Supporting; Supervision: Equal; Writing - Review & Editing: Supporting.

Table of content

1. General Remarks 4

1.1. Instrumentation and Physical Methods 5

1.2. Raman Spectroscopy 6

1.3. X-ray Absorption Spectroscopy (XAS) 6

1.4. Computational Details 7

1.5. Crystallographic Data 7

2. Experimental Procedures 8

2.1. Synthesis of *N,N*-Dimethyl-(2-nitrophenyl)methanamine 8

2.2. Synthesis of 2-{(Dimethylamino)methyl}aniline 10

2.3. Synthesis of 2-{2-((dimethylamino)methyl)phenyl}-1,1,3,3-tetramethylguanidine (TMGbenza, **L1**) 11

2.4. Synthesis of [Cu(**L1**)(MeCN)]X ([**C1**]X) 13

2.4.1. Synthesis of [Cu(**L1**)(MeCN)]PF_6 ([**C1**]PF_6) 14

2.4.2. Synthesis of [Cu(**L1**)(MeCN)]BF_4 ([**C1**]BF_4) 16

2.4.3. Synthesis of [Cu(**L1**)(MeCN)]OTf ([**C1**]OTf) 17

2.4.4. Synthesis of [Cu(**L1**)(MeCN)]ClO_4 ([**C1**]ClO_4) 19

2.5. Synthesis of $[Cu_2(\mu\text{-}O)_2(\mathbf{L1})_2](X)_2$ ([**O1**]$(X)_2$) 20

2.5.1. Spectrophotometric Titration of [**O1**]$(PF_6)_2$ with FcCOOH 21

2.5.2. Cryo-UHR-ESI Mass Spectrometry of [**O1**]$(PF_6)_2$ 23

2.5.3. Thermal Decomposition Kinetics of [**O1**]$(PF_6)_2$ 24

2.5.4. Crystal Structure of Decomposition Products of [**O1**]$(X)_2$ 25

2.5.4.1. Synthesis of $[Cu_3(\mu\text{-O}\mathbf{L1})_2(\mu\text{-OH})_2](PF_6)_2 \cdot 2$ thf ([**H1**]$(PF_6)_2$) 25

2.5.4.2. Synthesis of $[Cu_3(\mu\text{-O}\mathbf{L1})_2(\mu\text{-OH})_2](BF_4)_2 \cdot 2$ thf ([**H1**]$(BF_4)_2$) 26

2.6. Catalytic Reactivity of [**O1**]$(PF_6)_2$ 28

2.6.1. Synthesis of Benzo[a]phenazine (**P1**) 29

2.6.2. Synthesis of Quinolino[3,4-b]quinoxaline (**P2**) 31

2.6.3. Synthesis of Pyrido[3,2-a]phenazine (**P3**) 33

2.6.4. Synthesis of Pyrrolo[3,2-a]phenazine (**P4**) 34

2.6.5. Synthesis of Pyrrolo[2,3-a]phenazine (**P5**) 36

2.6.6. Reaction of Phenols, Pyridinols and 1-Methyl 2-Naphthol with [**O1**]$(PF_6)_2$ 37

2.7. Control Experiments 39

2.7.1. Reaction of [**O1**]$(PF_6)_2$ with triethylamine 39

2.7.2. Reaction of [**O1**]$(PF_6)_2$ with 1,2-phenylenediamine 39

2.7.3. Reaction of 6-indolol with $[Cu(MeCN)_4]PF_6$ (1.0 mM) in the presence of O_2 40

2.8. UV/Vis Spectra and EPR Spectra of the Reaction of Phenolic Substrates with [**O1**]$(PF_6)_2$ 41

2.8.1. UV/Vis Spectra and EPR Spectra of the Reaction of Phenols with [**O1**]$(PF_6)_2$ 41

2.8.2. UV/Vis Spectra of the Reaction of Pyridinols with [**O1**]$(PF_6)_2$....44

2.8.3. UV/Vis Spectra of the Reaction of Naphthols with [**O1**]$(PF_6)_2$ 45

2.8.4. UV/Vis Spectra of the Reaction of Quinolinols with [**O1**]$(PF_6)_2$ 46

2.8.5. UV/Vis Spectra of the Reaction of Indolols with [**O1**]$(PF_6)_2$....49

2.9. Crystallographic Data of Phenazines....51

2.10. Reactivity of Tyrosinase 52

3. DFT Calculations....53

3.1. Energies, Geometric and Spectroscopic Parameters of the Active Species....53

3.2. Fukui Function of Phenolic Substrates 54

3.3. Fukui Function of Quinones of the Phenolic Substrates....55

References 56

1. General Remarks

All operations were performed under an inert atmosphere of nitrogen with the use of standard Schlenk or glovebox techniques. Pure nitrogen (nitrogen 5.0) was dried by a column of P_2O_5. THF, diethyl ether, *n*-hexane and *n*-pentane were distilled under nitrogen atmosphere from sodium/benzophenone ketyl radical before usage. Acetonitrile and DMSO were purified by distillation from CaH_2. Methanol was dried from magnesium. All chemicals were purchased commercially (Table S1) and used without further purification unless otherwise noted. Copper salts $[Cu(MeCN)_4]X$ (X = PF_6, OTf, BF_4, ClO_4) were synthesized by reaction of Cu_2O (Sigma Aldrich) and acid HX (Sigma Aldrich) in acetonitrile and recrystallized at least twice from acetonitrile/diethyl ether at -30 °C.[1] Vilsmeier salt chloro-*N,N,N',N'*-tetramethylformamidinium chloride was synthesized according to a literature procedure.[2–4] Ferrocene monocarboxylic acid was recrystallized twice from tetrahydrofuran. Thin layer chromatography sheets were purchased from *MACHEREY-NAGEL* (SiO_2, layer thickness 0.20 mm, fluorescent indicator). Column chromatography was performed on Geduran Si 60 (40-63 µm, Merck).

Table S1: Used chemicals.

chemicals	supplier
1-methyl 2-naphthol	abcr
1-naphthol	Fluka
1,2-phenylenediamine	Fluka
2-methyl 8-quinolinol	abcr
2-naphthol	Sigma-Aldrich
2-nitrobenzyl bromide	abcr
2,4-di-*tert*-butyl phenol	Sigma-Aldrich
3-pyridinol	abcr
3-quinolinol	abcr
4-indolol	abcr
4-methoxy phenol	Sigma-Aldrich
4-pyridinol	abcr
4-quinolinol	abcr
4-*tert*-butyl phenol	abcr
5-indolol	abcr
6-indolol	abcr
6-quinolinol	Sigma-Aldrich
7-indolol	abcr
8-quinolinol	Sigma-Aldrich
acetonitrile-d_3	Sigma-Aldrich
benzophenone	Alfa Aesar
calcium hydride (0-2 mm)	Acros Organics
charcoal	Acros Organics
chloroform-d	Sigma-Aldrich
dimethyl amine	Merck
dimethyl sulfoxide-d_6	Sigma-Aldrich

ethylenediaminetetraacetic acid (EDTA)	Fluka
ferrocene monocarboxylic acid (FcCOOH)	abcr
ferric chloride	Riedel-de Haën
hydrazine monohydrate	Tokyo Chemical Industry
hydrochloric acid	Fisher Scientific
phenol	Sigma-Aldrich
potassium hydroxide	Grüssing
sodium	Sigma-Aldrich
sodium chloride	Grüssing
sodium hydroxide	Grüssing
sodium sulfate	Grüssing
triethylamine	abcr

1.1. Instrumentation and Physical Methods

^{1}H, ^{13}C{^{1}H}, ^{19}F{^{1}H} and ^{31}P{^{1}H} NMR spectra were recorded on a *Bruker Avance II 400* and *Bruker Avance III HD 400* spectrometer at 25 °C in NMR tubes, respectively. Resonances were referenced to the residual solvent signal, relative to TMS. Chemical shifts were assigned with the use of two-dimensional NMR experiments (COSY, HSQC, HMBC). All NMR data were deposited as original data in Chemotion[5] Repository and are published under an Open Access model. The link to the original data is given in the analytical description. Elemental analyses were carried out on an *elementar vario EL* and an *elementar vario EL cube* instrument. EI mass spectrometry was performed with the use of a *Thermo Fisher Scientific Finnigan MAT 95* spectrometer with a source voltage of 5 kV and an electron energy of 70 eV. ESI mass spectra were recorded on a *Thermo Fisher Scientific LTQ Orbitrap XL* spectrometer at a source voltage of 4.49 kV and a capillary temperature of 299.54 °C. FT-IR spectra were recorded on a *Shimadzu IR Tracer 100* equipped with a CsI beam splitter in combination with an ATR unit (*Quest* model from *Specac* utilising a robust monolithic crystalline diamond) in a resolution of 2 cm^{-1} and on a *ThermoFisher Avatar^{TM} 360* spectrometer with the use of KBr pellets or NaCl plates in a resolution of 2 cm^{-1}. UV/Vis spectroscopy was carried out on a *Cary 60* spectrophotometer of *Agilent Technologies* connected *via* a Cary 50 fiber optic coupler and combined with a fiber-optic quartz glass immersion probe (*Hellma*, 1 mm) and a tailored Schlenk cell. EPR spectra were recorded on a *Magnettech MiniScope MS400* spectrometer with the use of a frozen 4 mM solution of [**O1**]$(PF_6)_2$ in the presence of 50 equivalents of 4-*tert*-butyl phenol and 100 equivalents of triethylamine in tetrahydrofuran at 77 K.

Cryospray-ionization mass spectrometry (CSI-MS) measurements, reported in section 2.5.2., were performed on an *UHR-TOF Bruker Daltonik maXis plus*, an ESI-quadrupole time-of-flight (qToF) mass spectrometer capable of a resolution of at least 60.000 FWHM, which was coupled to a *Bruker Daltonik* Cryospray unit. Detection was in positive ion mode; the source voltage was 3.8 kV. The flow rate was 4.0 µL/min. The drying gas (N_2), to achieve solvent removal, and the spray gas were both held at -80 °C. The mass spectrometer was calibrated prior to every experiment *via* direct infusion of *Agilent* ESI-TOF low concentration tuning mixture, which provided a m/z range of singly charged peaks up to 2700 Da in both ion modes.

Cryospray-ionization mass spectrometry (CSI-MS) measurements, reported in section 2.6.6. and 2.7.2., were performed on an *UHR-TOF Bruker Daltonik maXis II*, an ESI-quadrupole time-of-flight (qToF) mass spectrometer capable of a resolution of at least 80.000 FWHM, which was coupled to a *Bruker Daltonik* Cryospray unit. Detection was in positive ion mode; the source voltage was 3.5 kV. The flow rate was 3.0 µL/min. The drying gas (N_2), to achieve solvent removal, and the spray gas were both held at -80 °C. The mass spectrometer was calibrated prior to every experiment *via* direct infusion of *Agilent* ESI-TOF low concentration tuning mixture, which provided a m/z range of singly charged peaks up to 3000 Da in both ion modes.

1.2. Raman Spectroscopy

Raman measurements were performed with a UT-3 Raman spectrometer[6], combined with a frequency doubled Ti:sapphire laser (Tsunami model 3960C-15HP, *Spectra Physics Lasers Inc.*) to obtain an excitation wavelength of 420 nm with a pulse width of 2.3 ps. The cryostat was a slightly modified version of a setup described previously[7] with a 1.4 mL screw cap Suprasil® cuvette with septum (117104F-10-40, *Hellma*) for oxygenation, equipped with a Peltier element (QC-127-1.4-6.0MS, *QuickCool*) and a cooling copper block which encloses three sides of the cuvette. The laser beam was widened with a spatial filter and then focused on the cuvette inside the cryostat. The focus spot size was around 20 µm in diameter. With a micrometer screw, a focal depth of 30 µm inside the cuvette was adjusted. Raman scattered light was captured with the entrance optics of the UT-3 triple monochromator spectrometer.[6] The precursor [**C1**]PF_6 with a concentration of 20 mmol L^{-1} in tetrahydrofuran/acetonitrile (80:20) was cooled in the cuvette cryostat to below –90 °C. Dioxygen was added *via* a cannula through the septum (0.02 bar overpressure for 2 min) until a distinct color change from colorless to khaki was observed. The used laser power in front of the entrance optics was 37 mW. Data was accumulated for 3 x 120 s and corrected for the spectral sensitivity of the instrument.

1.3. X-ray Absorption Spectroscopy (XAS)

X-ray absorption spectroscopy data were collected in fluorescence mode using a Passivated Implanted Planar Silicon (PIPS) detector at beamline P64 (DESY, PETRA III, Hamburg, Germany).[8]

The precursor of complex [**O1**]$(PF_6)_2$ was prepared under inert conditions (oxygen and water free) and then transferred to a cuvette with septum. The cuvette was then cooled in a liquid ethanol bath of liquid ethanol based closed-cycle chiller (Proline RP890, *Lauda*) to below 183 K. Afterwards oxygen was added for 5 mins to form the complex. With a precooled syringe, the solution (~75 µL) was first transferred to the sample holder which was frozen directly after in a liquid nitrogen bath and then put into a closed cycle helium cryostat (SHI-950T, *Janis and SHI*) which was precooled to 150 K. The sample was kept at 150 K during the whole measurement.

The measurement time for a complete scan from 8780 eV to 9880 eV was 300 s. In total, the complex was measured for one hour. Copper foil was measured concomitantly, and the first inflection point energy set to 8979.0 eV and all measurements were calibrated to this shift afterwards. Data processing and analysis were performed with Athena and Artemis.[9]

Data reduction and Analysis:

For each spectrum, a second-order polynomial was fitted to the pre-edge region, extrapolated and then subtracted from the data using Athena. Normalization was performed starting 150 eV above the edge with a normalization order of 3. For background removal, Rbkg was set to 1.1 and the k-weight to 2. The spline range was 0 to 15.3 $Å^{-1}$ in k and 0 to 894 eV in energy above the edge. Low and high spline clamps were set to “None” and “Strong” respectively. For EXAFS fitting, the first shell and five additional carbon atoms, as they have a similar distance to the copper atom as the other copper atom, were used. Scattering paths were calculated using Demeter 0.9.26 with Ifeffit 1.2.12 [10] and a DFT-calculated structure of the complex.

Parameters:

ΔE_0	= 6.38404822	# +/-	2.02977590
σ^2 (for Cu-O, Cu-N, Cu-C)	= 0.00014048	# +/-	0.00074801
σ^2 (for Cu-Cu)	= 0.01341955	# +/-	0.00512504
delta (for Cu-N, Cu-O)	= 0.05059119	# +/-	0.00606741
delta2 (for Cu-Cu)	= -0.03150106	# +/-	0.01810690
delta3 (for Cu-C)	= 0.02573750	# +/-	0.01541418

Results:

Figure S1 shows the Cu K-edge with a position of 8987.0 eV indicative for Cu(III). From the fit which describes the data with the smallest χ^2 we obtain bond-lengths for Cu-O, Cu-N which are also between typical distances for Cu(III) and Cu(II).[11] The fit was capped at k = 10.5 as the remaining data from one measurement are too noisy. Combined with all the other measurements, the EXAFS measurements reveal the presence of Cu(III) in the complex, validating the assumption of a bis(μ-oxo) species.

Table S2: Cu-XX distances from the DFT model (R_{eff}) and the best fit results (R) from Artemis.

XX	N	S_0^2	σ^2	ΔE_0	Δr	R_{eff}	R
O	2.00000	0.94000	0.00014	6.38400	0.09116	1.80190	1.89306
N	1.00000	0.94000	0.00014	6.38400	0.09682	1.91380	2.01062
N	1.00000	0.94000	0.00014	6.38400	0.09939	1.96460	2.06399
Cu	1.00000	0.94000	0.01342	6.38400	-0.08663	2.75020	2.66357
C	1.00000	0.94000	0.00014	6.38400	0.06966	2.70640	2.77606
C	1.00000	0.94000	0.00014	6.38400	0.07117	2.76530	2.83647
C	1.00000	0.94000	0.00014	6.38400	0.07349	2.85550	2.92899
C	1.00000	0.94000	0.00014	6.38400	0.07433	2.88790	2.96223
C	1.00000	0.94000	0.00014	6.38400	0.07572	2.94190	3.01762

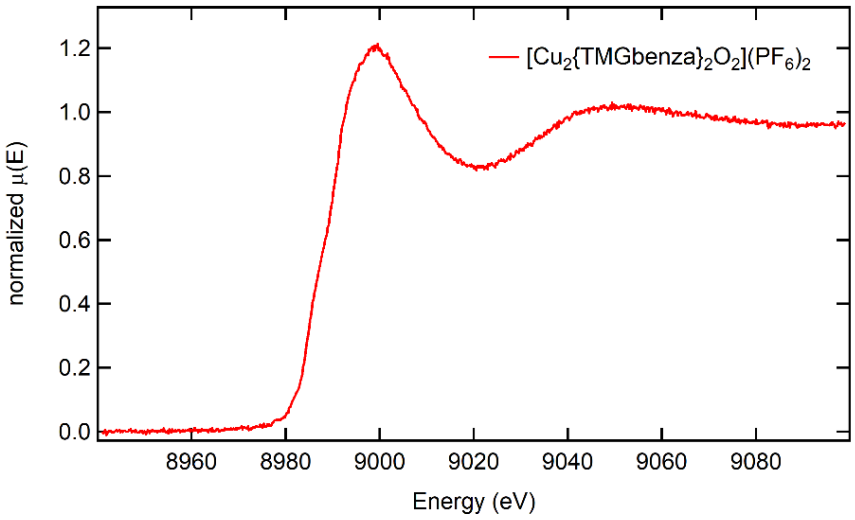

Figure S1: Normalized Cu-K absorption edge of [**O1**]$(PF_6)_2$. Integration time of the spectrum was 300 s. The edge position, defined as 50% of the edge jump, is determined as 8987.0 eV. The shoulders at 8987.3 eV and 8992.0 eV in the rising edge of [**O1**]$(PF_6)_2$ are similar to the ones reported for $[Cu(III)_2(\mu\text{-}O)_2(L_{ME})_2]^{2+}$ as 1s → 4p and 1s → 4p + shakedown transitions.[11]

1.4. Computational Details

Density functional theory (DFT) calculations were performed with the program suite Gaussian 16, revision B01.[12] The geometries of bis(μ-oxo) species were optimized (Figure 2) by using the nonlocal hybrid meta GGA TPSSh functional[13], the triple-zeta basis set def2-TZVP[14] as implemented in Gaussian on all atoms and the empirical dispersion correction with Becke-Johnson damping factors (GD3BJ).[15-16] In previous publications, we found this combination best for the calculation of bioinorganic copper complexes.[17-21] Furthermore, we used a PCM solvent model (tetrahydrofuran). Frequency calculations showed no imaginary values. The condensed Fukui function for an electrophilic attack was calculated using AOMix.[22]

1.5. Crystallographic Data

The single crystal diffraction data for [**H1**]$(PF_6)_2$, [**H1**]$(BF_4)_2$ and [**L1**H_2]$(BF_4)_2$ are presented in Table S6, data for **P3** and **P5** in Table S9. The data for [**H1**]$(PF_6)_2$, [**H1**]$(BF_4)_2$, [**L1**H_2]$(BF_4)_2$, **P3** and **P5** were collected with a four-circle goniometer *STOE Stadivari* with Dectris Pilatus3 R 200 K hybrid pixel detector with the use of GeniX 3D high flux Mo-Kα radiation (0.71073 Å) or Cu-Kα radiation (1.54186 Å) at 100 K. The temperature was controlled by using an *Oxford Cryostream 800*. Crystals were mounted with grease on glass fibers.

Data were collected with *X-Area Pilatus* and integrated with *X-Area Integrate* and *X-Area Recipe*. The absorption correction was performed by Gaussian integration with *X-Red32*. Scaling of reflections was carried out by using *X-Area LANA*.[23]

The structures were solved by direct and conventional Fourier methods and all non-hydrogen atoms were refined anisotropically with full-matrix least-squares based on F^2 (*XPREP*[24], *SHELXT*[25], *SHELXL*[26] and *ShelXle*[27]). Hydrogen atoms were derived from difference Fourier maps and placed at idealized positions, riding on their parent C atoms, with isotropic displacement parameters $U_{iso}(H) = 1.2\ U_{eq}(C)$ and $1.5\ U_{eq}$(C methyl). All methyl groups were allowed to rotate but not to tip.

Full crystallographic data have been deposited with the Cambridge Crystallographic Data Centre as supplementary no. CCDC – 1950654 for [**H1**]$(PF_6)_2$, CCDC – 1950655 for [**H1**]$(BF_4)_2$, CCDC – 1950656 for **P3,** CCDC – 1950657 for **P5** and CCDC - 1963147 for [**L1**H_2]$(BF_4)_2$. Copies of the data can be obtained free of charge on application to CCDC, 12 Union Road, Cambridge CB2 1EZ, UK (fax: (+44)1223-336-033; e-mail: deposit@ccdc.cam.ac.uk).

2. Experimental Procedures

2.1. Synthesis of *N,N*-Dimethyl-(2-nitrophenyl)methanamine

The synthesis of the title compound is based on a literature procedure.[28]

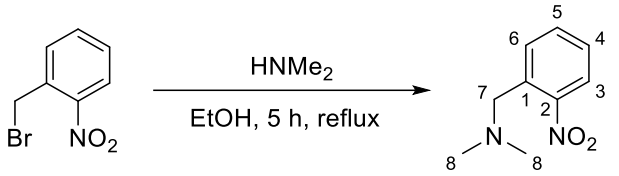

Scheme S1: Nucleophilic substitution of 2-nitrobenzyl bromide with dimethyl amine.

Dimethyl amine (40 wt% in H_2O, 102.6 mL, 510 mmol, 5.1 eq) was added dropwise to a stirred solution of 2-nitrobenzyl bromide (21.6 g, 100 mmol, 1.0 eq) in ethanol (480 mL). The mixture was refluxed for 5 h. The yellow solution was acidified to pH 1 by using concentrated hydrochloric acid. The solvent was removed under reduced pressure. The pH level of the resulting mixture was adjusted to 14 by using aqueous NaOH solution. The solution was extracted with diethyl ether (4 x 100 mL). The combined organic layers were washed with saturated aqueous NaCl solution, dried over Na_2SO_4 and evaporated to dryness. The product was isolated as a yellow oil (15.9 g, 88.3 mmol, 88%).

^{1}H NMR (400 MHz, Chloroform-d, 25 °C): δ [ppm] = 7.83 (dd, J = 8.1, 1.2 Hz, 1H, H3), 7.63 – 7.59 (m, 1H, H5), 7.54 (td, J = 7.5, 1.3 Hz, 1H, H4), 7.41 – 7.36 (m, 1H, H6), 3.71 (s, 2H, H7), 2.22 (s, 6H, H8).

^{13}C{^{1}H} NMR (101 MHz, Chloroform-d, 25 °C): δ [ppm] = 149.8 (C2), 134.6 (C1), 132.6 (C4), 131.1 (C5), 127.9 (C6), 124.5 (C3), 60.4 (C7), 45.8 (C8).

Analytical data matches those reported in literature.[28]

Additional information on the NMR spectra of the target compound including original data files is available via Chemotion Repository: https://dx.doi.org/10.14272/FCAMUPIRWKNASD-UHFFFAOYSA-N.1

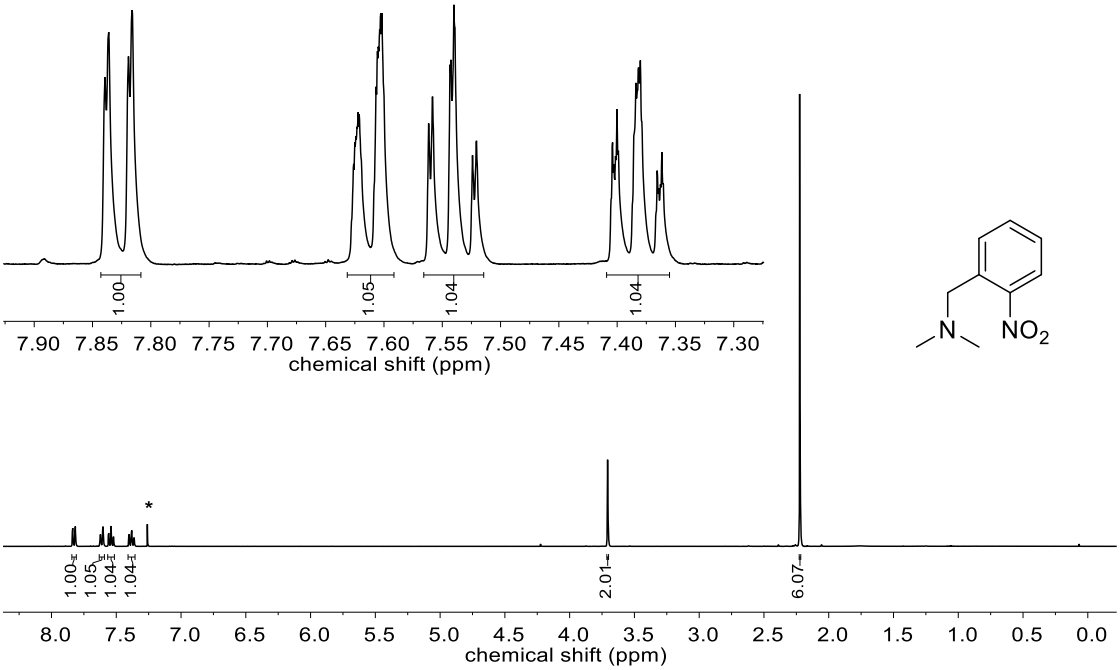

Figure S2: ^{1}H NMR spectrum of *N,N*-dimethyl-(2-nitrophenyl)methanamine (* = $CDCl_3$).

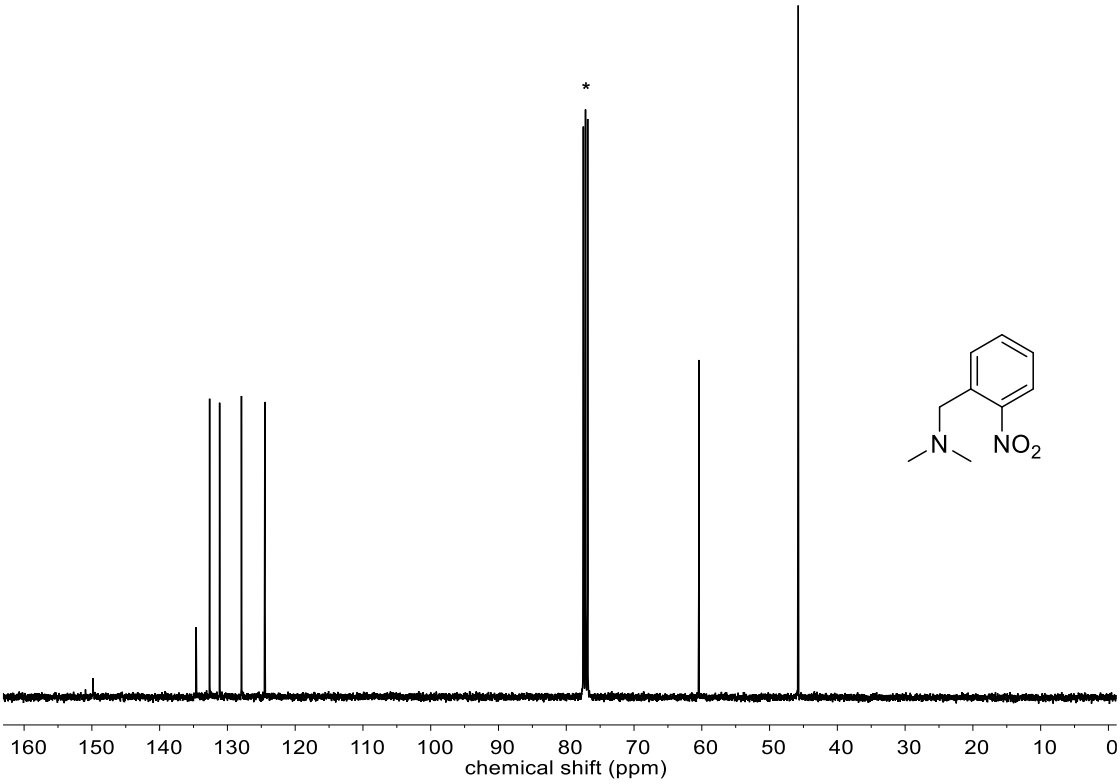

Figure S3: ^{13}C{^{1}H} NMR spectrum of *N,N*-dimethyl-(2-nitrophenyl)methanamine (* = $CDCl_3$).

2.2. Synthesis of 2-{(Dimethylamino)methyl}aniline

The synthesis of the title compound is based on a literature procedure.[28]

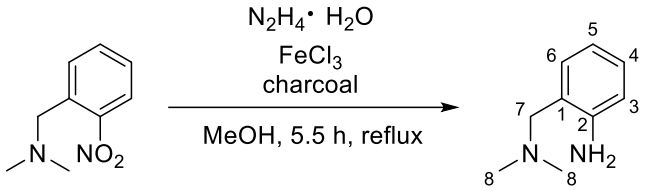

Scheme S2: Hydrogenation of *N,N*-dimethyl-(2-nitrophenyl)methanamine by using hydrazine monohydrate.

A solution of *N,N*-dimethyl-(2-nitrophenyl)methanamine (15.9 g, 88.3 mmol, 1.0 eq) in dried methanol (150 mL) was added to a suspension of $FeCl_3$ (720 mg, 4.4 mmol, 0.05 eq), charcoal (6.0 g) and hydrazine monohydrate (26.6 mL, 547 mmol, 6.2 eq) in two aliquots. The first portion was added dropwise initially. After stirring for 30 min at 65 °C, the remaining portion was added dropwise to the black suspension. The mixture was stirred at 65 °C for additional 5 h and then at room temperature overnight. The suspension was filtered, and the filtrate was evaporated to dryness. The residue was dissolved in dichloromethane, dried over Na_2SO_4 and dried under reduced pressure to give 2-{(dimethylamino)methyl}aniline as a colorless solid (10.9 g, 72.6 mmol, 82%).

^{1}H NMR (400 MHz, Chloroform-*d,* 25 °C): *δ* [ppm] = 7.10 (td, *J* = 7.6, 1.5 Hz, 1H, H4), 7.01 – 6.97 (m, 1H, H6), 6.70 – 6.63 (m, 2H, H3+5), 4.62 (br s, 2H, NH_2), 3.42 (s, 2H, H7), 2.20 (s, 6H, H8).

^{13}C{^{1}H} NMR (101 MHz, Chloroform-*d*, 25 °C): *δ* [ppm] = 147.0 (C2), 130.2 (C6), 128.3 (C4), 123.3 (C1), 117.5 (C5), 115.4 (C3), 63.4 (C7), 45.0 (C8).

Analytical data matches those reported in literature.[28-29]

Additional information on the NMR spectra of the target compound including original data files is available via Chemotion Repository: https://dx.doi.org/10.14272/XQWHZHODENELCJ-UHFFFAOYSA-N.1

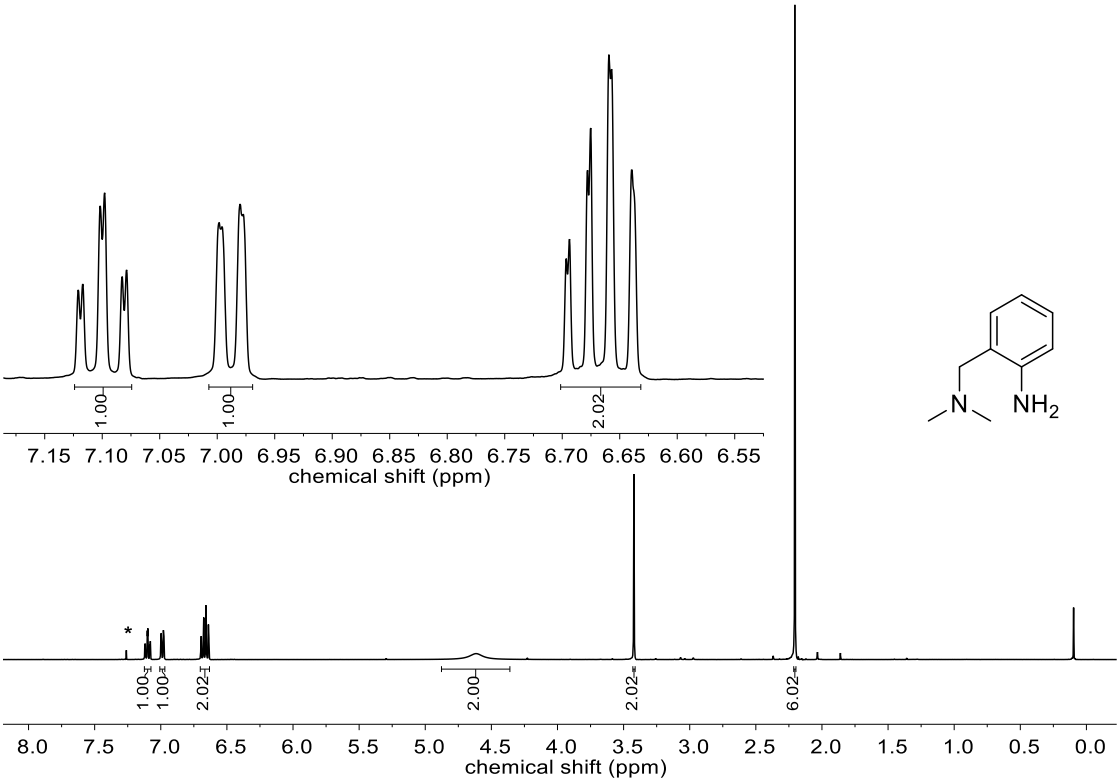

Figure S4: ^{1}H NMR spectrum of 2-{(dimethylamino)methyl}aniline (* = $CDCl_3$).

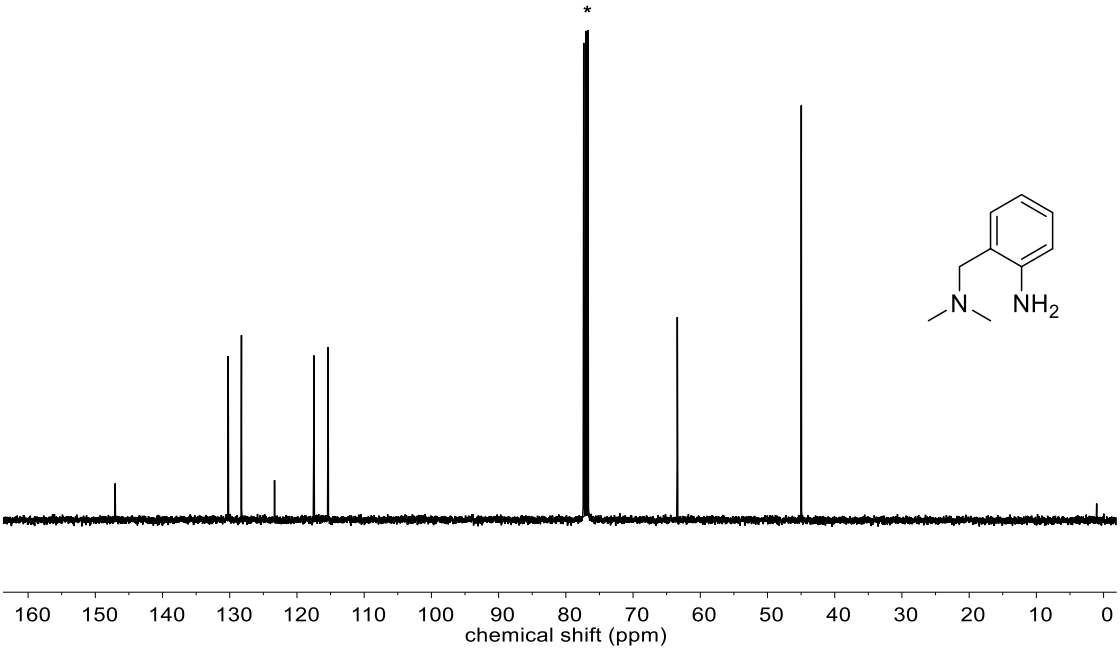

Figure S5: $^{13}C\{^1H\}$ NMR spectrum of 2-{(dimethylamino)methyl}aniline (* = $CDCl_3$).

2.3. Synthesis of 2-{2-((dimethylamino)methyl)phenyl}-1,1,3,3-tetramethylguanidine (TMGbenza, L1)

The synthesis of the title compound is based on a literature procedure.[3,4]

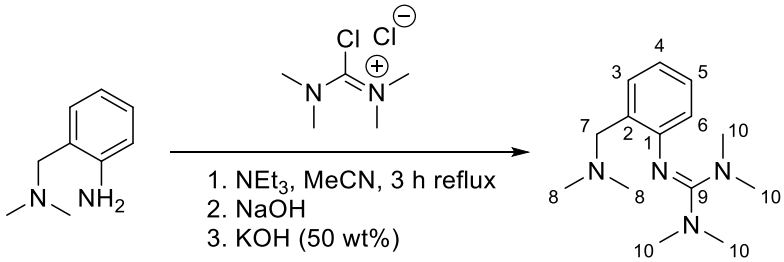

Scheme S3: Condensation of 2-{(dimethylamino)methyl}aniline with Vilsmeier salt chloro-*N,N,N',N'*-tetramethylformamidinium chloride.

To a stirring solution of 2-{(dimethylamino)methyl}aniline (10.9 g, 72.6 mmol, 1.0 eq) in dried acetonitrile (70 mL), triethyl amine (10.2 mL, 72.6 mmol, 1.0 eq) was added at room temperature. A solution of chloro-*N,N,N',N'*-tetramethylformamidinium chloride (12.4 g, 72.6 mmol, 1.0 eq) in dried acetonitrile (70 mL) was added dropwise to the reaction mixture. The slightly yellow solution was refluxed for 3 h. After cooling the reaction mixture down to room temperature, aqueous NaOH solution (3.11 g, 72.6 mmol, 1.0 eq, in 15 mL) was added. All volatiles were removed under reduced pressure. Aqueous KOH solution (50 wt%, 50 g in 50 mL) was added and the mixture was extracted with acetonitrile (4 x 50 mL). The combined organic layers were dried over Na_2SO_4 and charcoal, filtered and evaporated to dryness. The title compound was afforded as a yellow oil (17.3 g, 69.7 mmol, 96%). The product was purified by vacuum distillation (130-150 °C, 3 x 10^{-2} mbar) to give a light-yellow oil (15.9 g, 64.1 mmol, 88%).

^{1}H NMR (400 MHz, Acetonitrile-d_3, 25 °C): δ [ppm] = 7.24 (dd, J = 7.4, 1.6 Hz, 1H, H6), 7.04 (td, J = 7.5, 1.7 Hz, 1H, H4), 6.78 (td, J = 7.4, 1.3 Hz, 1H, H3), 6.41 (dd, J = 7.9, 1.3 Hz, 1H, H5), 3.30 (s, 2H, H7), 2.62 (s, 12H, H10), 2.16 (s, 6H, H8).

$^{13}C\{^1H\}$ NMR (101 MHz, Acetonitrile-d_3, 25 °C): δ [ppm] = 159.5 (C9), 151.8 (C1), 130.8 (C2), 130.0 (C6), 127.7 (C4), 122.1 (C5), 120.3 (C3), 60.6 (C7), 46.0 (C8), 39.8 (C10).

CHN anal. calc. for $C_{14}H_{24}N_4$: C 67.70%; H 9.74%; N 22.56%; found: C 67.58%; H 9.61%; N 23.31%.

MS-EI: m/z (%) = 248.3 (55) [M^+], 233.3 (30) [M^+-Me], 190.3 (24), 188.2 (100), 161.2 (74), 145.2 (20), 134.2 (21) [M^+-N=C(NMe_2)$_2$], 132.2 (26), 131.2 (25), 118.2 (35), 117.2 (33), 72.3 (39).

IR (NaCl plates): $\tilde{\nu}$ [cm^{-1}] = 3058 (w, C-H_{arom}), 2937 (m, C-H_{arom}), 2885 (m, C-H_{aliph}), 2850 (m, C-H_{aliph}), 2811 (m), 2766 (m), 1606 (vs, C=N), 1587 (vs, C=N), 1566 (s), 1502 (m), 1481 (m), 1451 (m), 1426 (m), 1376 (s), 1261 (m), 1234 (m), 1209 (m), 1138 (s), 1098 (m), 1061 (m), 1018 (s), 923 (w), 866 (w), 842 (m), 782 (m), 742 (m), 700 (w), 628 (w).

Additional information on the NMR spectra of the target compound including original data files is available via Chemotion Repository: https://dx.doi.org/10.14272/WYPRQDLUGJFJCG-UHFFFAOYSA-N.1

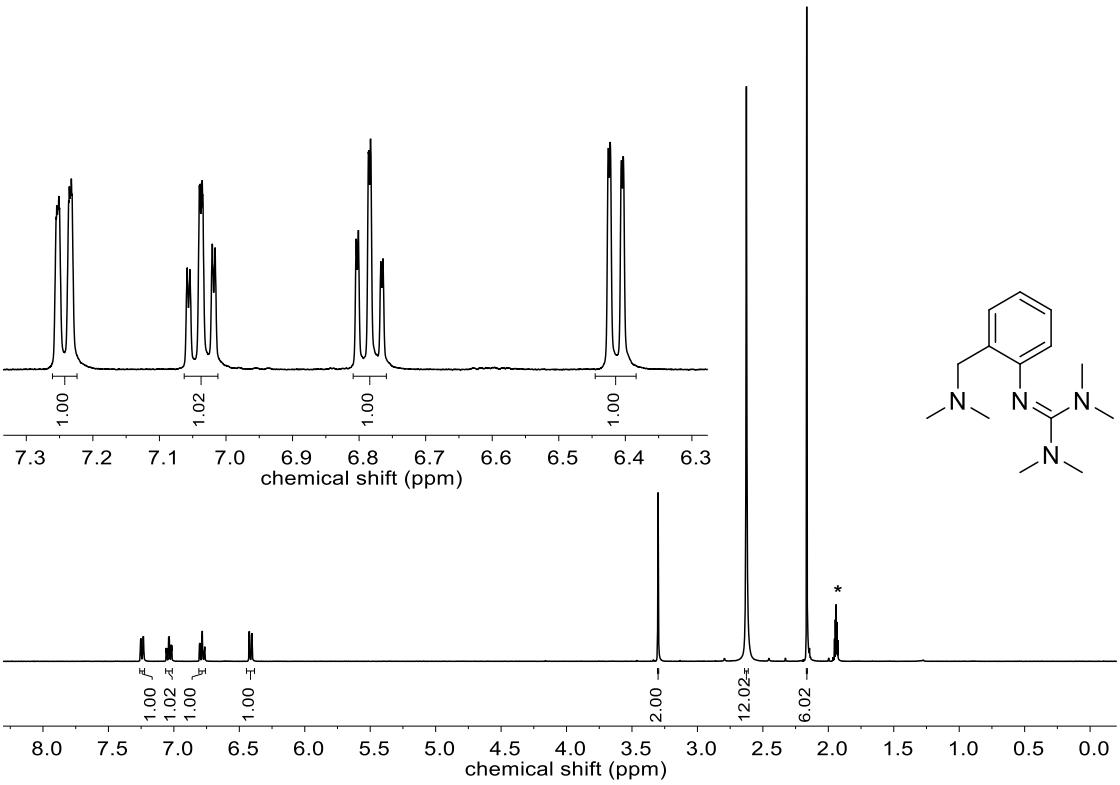

Figure S6: ^{1}H NMR spectrum of 2-{2-((dimethylamino)methyl)phenyl}-1,1,3,3-tetramethylguanidine (**L1**) (* = CD_3CN).

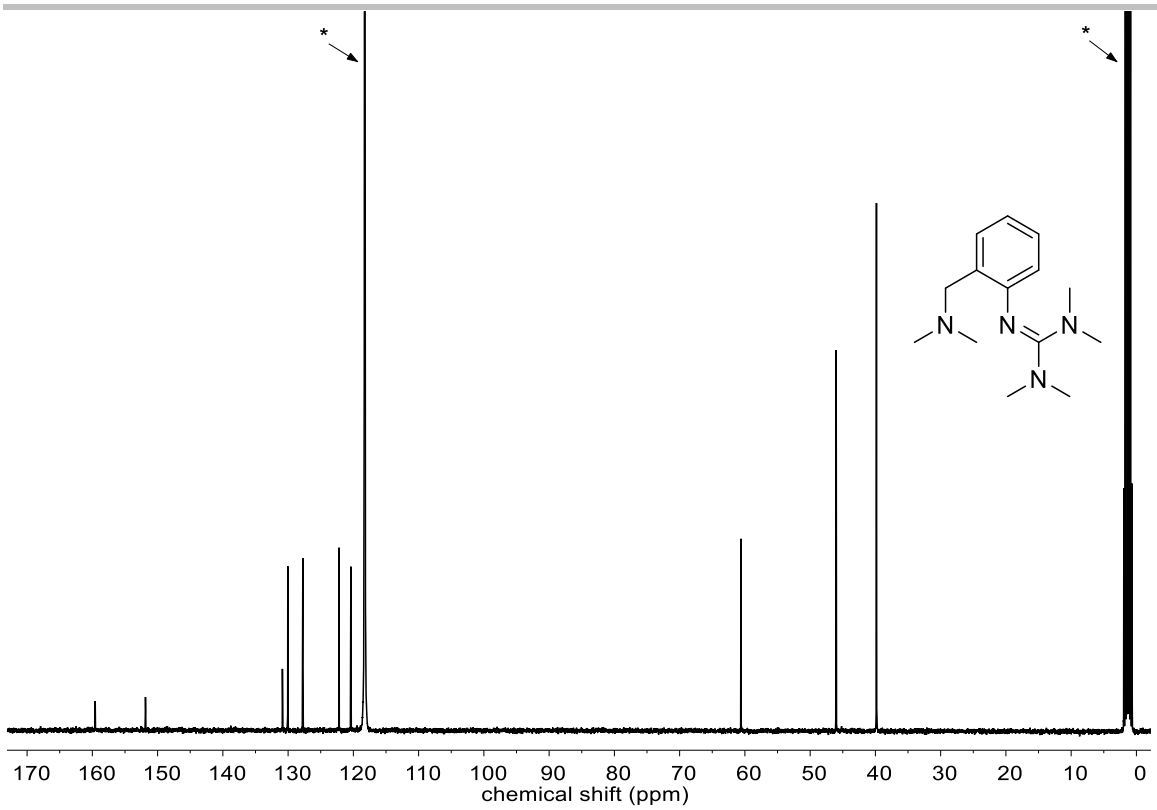

Figure S7: $^{13}C\{^{1}H\}$ NMR spectrum of 2-{2-((dimethylamino)methyl)phenyl}-1,1,3,3-tetramethylguanidine (**L1**) (* = CD_3CN).

2.4. Synthesis of [Cu(L1)(MeCN)]X ([C1]X)

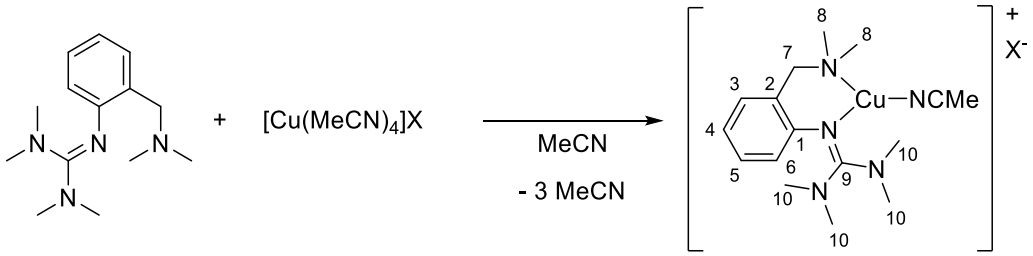

Scheme S4: Synthesis of precursor species [Cu(**L1**)(MeCN)]X ([**C1**]X, X = PF_6, OTf, BF_4, ClO_4).

Ligand and copper salt are recommended to be highly diluted in acetonitrile in order to suppress the formation of a bischelate complex originating from high concentration of the ligand.

A solution of **L1** (24.8 mg, 0.1 mmol, 1.0 eq) in dried acetonitrile (2.0 mL) was added dropwise to a stirring solution of $[Cu(MeCN)_4]X$ (0.10 mmol, 1.0 eq) in dried acetonitrile (3.0 mL) during a period of 10 min. The colorless solution was stirred for 2 h and evaporated to dryness (Caution! The complex is very sensitive to oxygen which is indicated by partial coloration of the precipitate or oil to light-green). The residue was washed with dried pentane (3 x 1.0 mL) and dried *in vacuo*.

2.4.1. Synthesis of [Cu(L1)(MeCN)]PF_6 ([C1]PF_6)

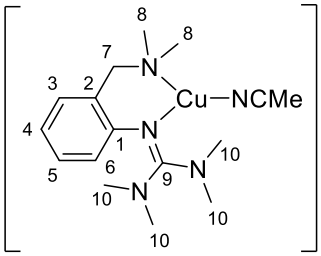

The title compound was isolated as a colorless solid (49 mg, 0.098 mmol, 98%).

^{1}H NMR (400 MHz, Acetonitrile-d_3, 25 °C): δ [ppm] = 7.22 (td, J = 7.7, 1.6 Hz, 1H, H4), 7.14 (dd, J = 7.5, 1.3 Hz, 1H, H6), 6.91 (td, J = 7.4, 1.2 Hz, 1H, H3), 6.48 – 6.42 (dd, J = 7.8, 1.3 Hz, 1H, H5), 3.44 (s, 2H, H7), 2.71 (br, 12H, H10), 2.31 (s, 6H, H8).

^{13}C{^{1}H} NMR (101 MHz, Acetonitrile-d_3, 25 °C): δ [ppm] = 164.7 (C9), 151.7 (C1), 133.3 (C6), 130.3 (C4), 129.1 (C2), 123.3 (C5), 122.3 (C3), 65.3 (C7), 48.1 (C8), 40.1 (C10).

^{19}F{^{1}H} NMR (377 MHz, Acetonitrile-d_3, 25 °C): δ [ppm] = -72.94 (d, J = 706.3 Hz, PF_6).

^{31}P{^{1}H} NMR (162 MHz, Acetonitrile-d_3, 25 °C): δ [ppm] = -144.60 (hept, J = 706.3 Hz, PF_6).

HRMS-ESI+ (MeCN): m/z calc. for $[(C_{14}H_{24}N_4)Cu]^+$: 311.1297, found: 311.1291, calc. for $[(C_{14}H_{24}N_4)Cu(CH_3CN)]^+$: 352.1562, found: 352.1557.

IR (NaCl plates): $\tilde{\nu}$ [cm^{-1}] = 3201 (w, C-H_{arom}), 3164 (m, C-H_{arom}), 3004 (m, C-H_{aliph}), 2945 (m, C-H_{aliph}), 1538 (s, C=N), 1424 (s), 1272 (vw), 1215 (vw), 1193 (vw), 1174 (vw), 1156 (w), 1030 (s), 999 (m), 920 (s), 877 (m), 842 (vs, PF_6), 792 (w), 749 (vs, PF_6), 688 (vw), 660 (vw), 635 (vw), 611 (vw), 586 (vw), 559 (s), 509 (m).

Additional information on the NMR spectra of the target compound including original data files is available via Chemotion Repository: https://dx.doi.org/10.14272/SXYROFUQPFOADI-UHFFFAOYSA-N.1

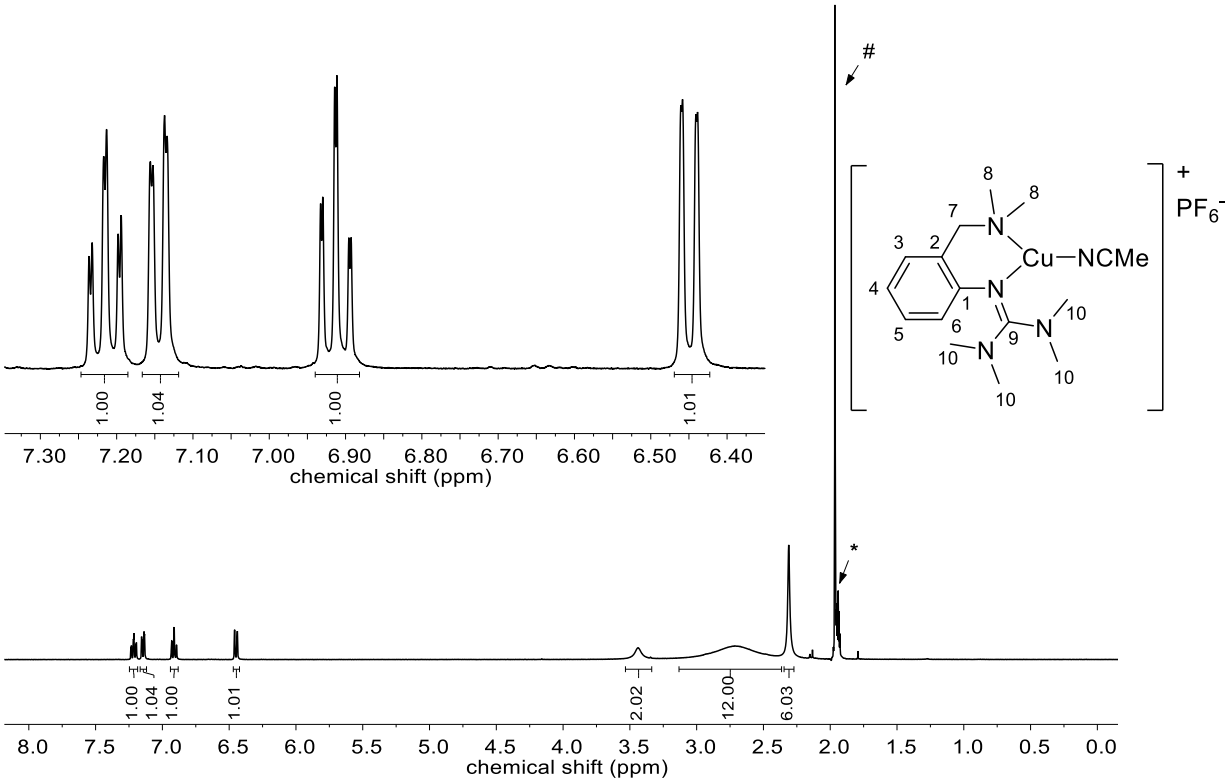

Figure S8: ^{1}H NMR spectrum of [Cu(**L1**)(MeCN)]PF_6 ([**C1**]PF_6) (* = CD_3CN, # = CH_3CN).

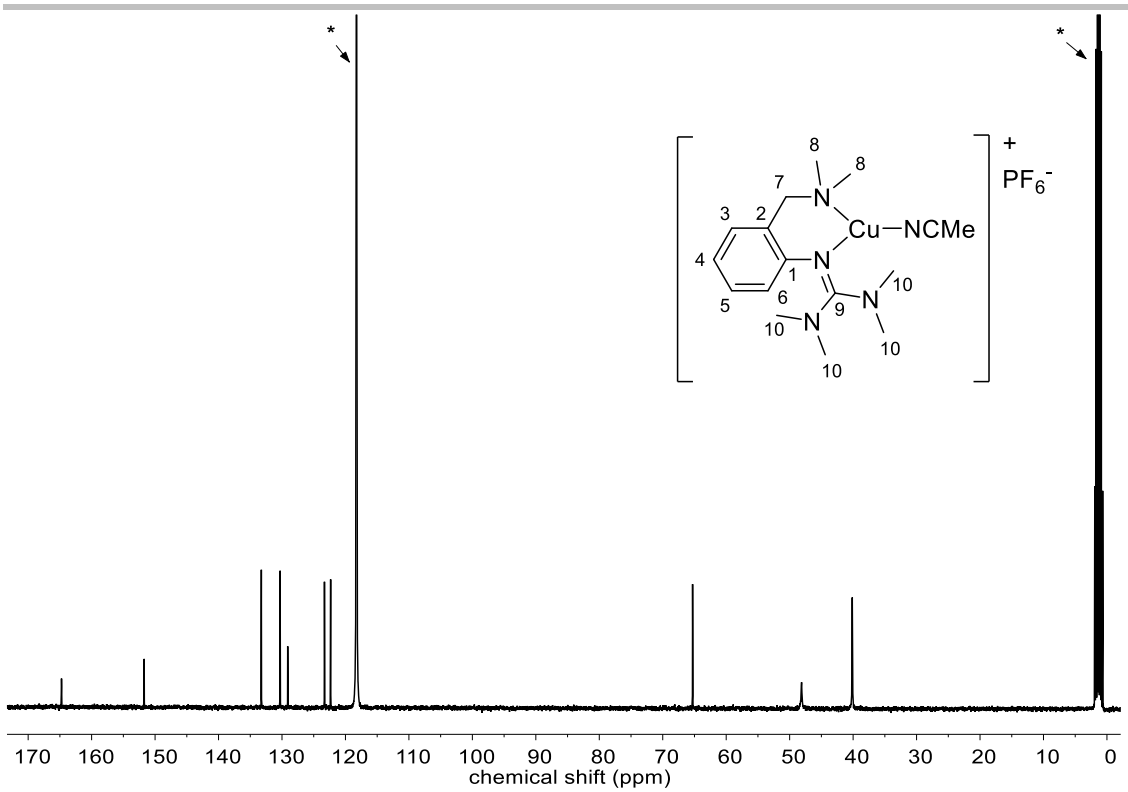

Figure S9: $^{13}C\{^{1}H\}$ NMR spectrum of [Cu(**L1**)(MeCN)]PF_6 ([**C1**]PF_6) (* = CD_3CN and CH_3CN).

Spectral features of [**C1**]PF_6 were analyzed via UV/Vis spectroscopy. For this purpose, [**C1**]PF_6 (5.0 mg, 0.010 mmol) in dried and degassed acetonitrile (0.5 mL) was injected into dried and degassed tetrahydrofuran (9.5 mL) at room temperature. The colorless solution turned slightly yellow within 20 min.

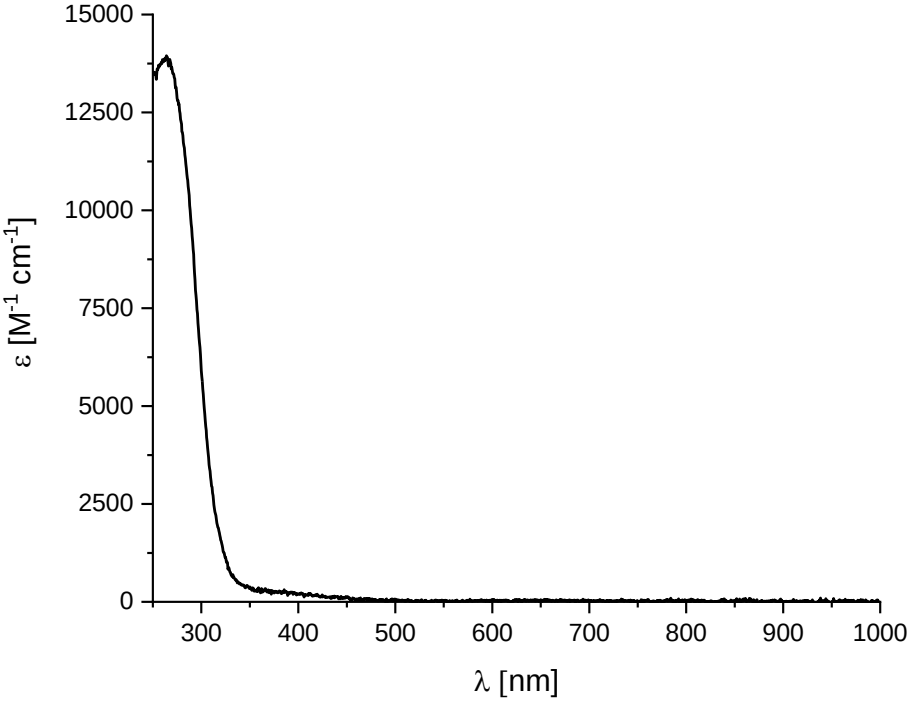

Figure S10: UV/Vis spectrum of [**C1**](PF_6) (1.0 mM) in tetrahydrofuran at room temperature.

2.4.2. Synthesis of [Cu(L1)(MeCN)]BF_4 ([C1]BF_4)

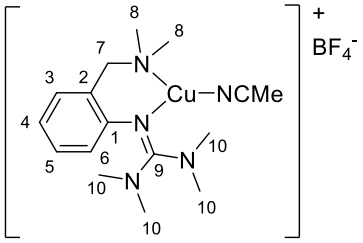

The title compound was generated *in-situ*.

^{1}H NMR (400 MHz, Acetonitrile-d_3, 25 °C): δ [ppm] = 7.20 (td, J = 7.7, 1.6 Hz, 1H, H4), 7.16 (dd, J = 7.5, 1.3 Hz, 1H, H6), 6.91 (td, J = 7.4, 1.2 Hz, 1H, H3), 6.47 (d, J = 7.8 Hz, 1H, H5), 3.44 (s, 2H, H7), 2.70 (br, 12H, H10), 2.28 (s, 6H, H8).

^{13}C{^{1}H} NMR (101 MHz, Acetonitrile-d_3, 25 °C): δ [ppm] = 164.6 (C9), 151.6 (C1), 133.0 (C6), 130.1 (C4), 129.3 (C2), 123.4 (C5), 122.3 (C3), 64.9 (C7), 47.9 (C8), 40.1 (C10).

^{19}F{^{1}H} NMR (377 MHz, Acetonitrile-d_3, 25 °C): δ [ppm] = -151.78 (s, BF_4).

Additional information on the NMR spectra of the target compound including original data files is available via Chemotion Repository: https://dx.doi.org/10.14272/NLACLAPNGFWSTA-UHFFFAOYSA-N.1

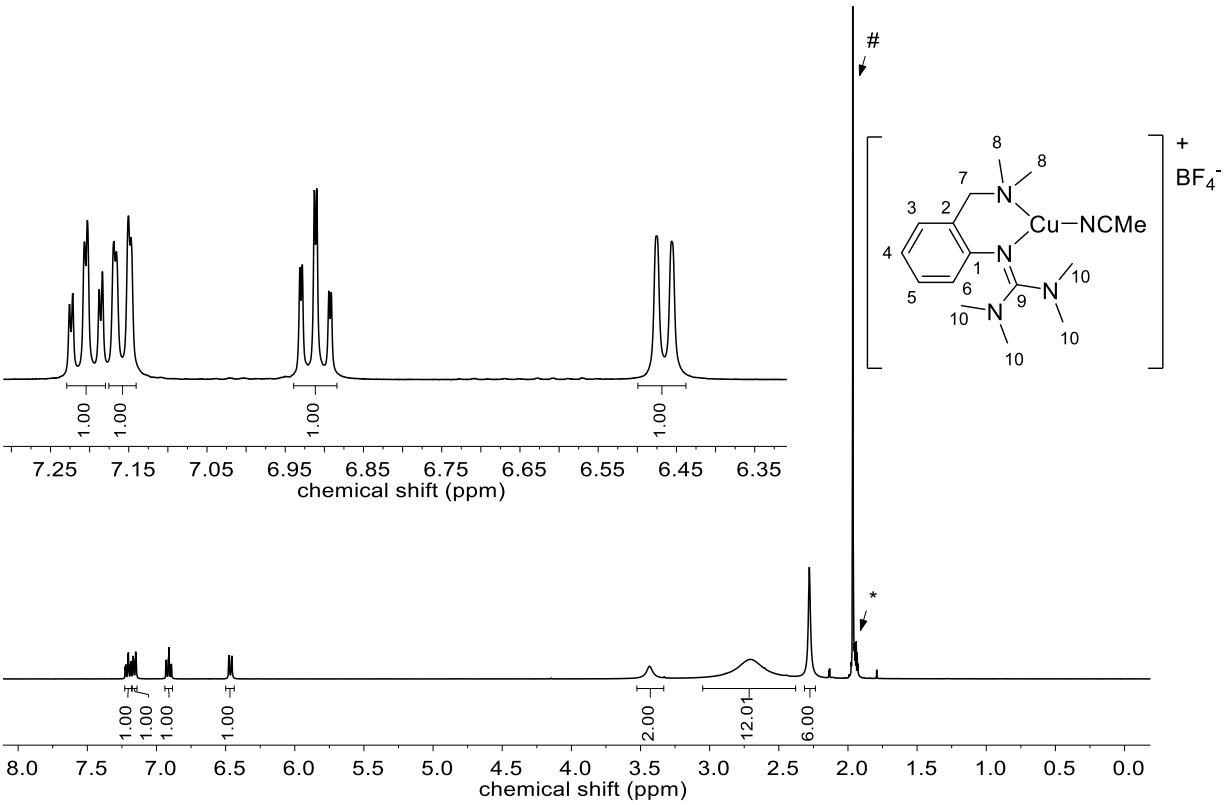

Figure S11: ^{1}H NMR spectrum of [Cu(**L1**)(MeCN)]BF_4 ([**C1**]BF_4) (* = CD_3CN, # = CH_3CN).

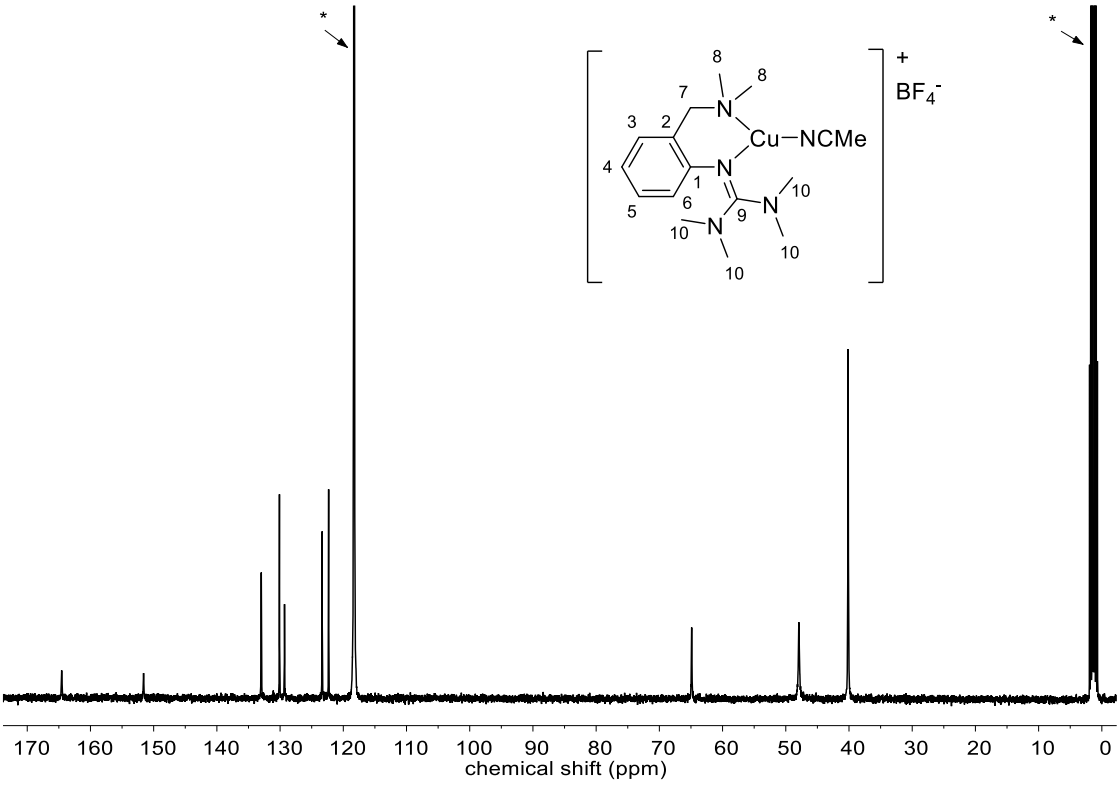

Figure S12: $^{13}C\{^1H\}$ NMR spectrum of [Cu(**L1**)(MeCN)]BF_4 ([**C1**]BF_4) (* = CD_3CN and CH_3CN).

2.4.3. Synthesis of [Cu(L1)(MeCN)]OTf ([C1]OTf)

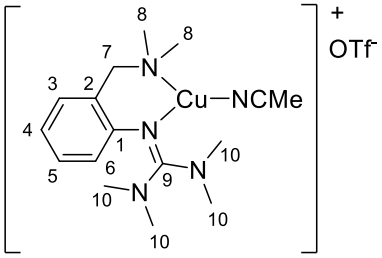

The title compound was generated *in-situ*.

^{1}H NMR (400 MHz, Acetonitrile-d_3, 25 °C): δ [ppm] = 7.21 (td, J = 7.6, 1.6 Hz, 1H, H4), 7.14 (dd, J = 7.5, 1.6 Hz, 1H, H6), 6.91 (td, J = 7.4, 1.3 Hz, 1H, H3), 6.45 (dd, J = 7.9, 1.3 Hz, 1H, H5), 3.44 (s, 2H, H7), 2.71 (br, 12H, H10), 2.31 (s, 6H, H8).

$^{13}C\{^1H\}$ NMR (101 MHz, Acetonitrile-d_3, 25 °C): δ [ppm] = 164.7 (C9), 151.7 (C1), 133.2 (C6), 130.3 (C4), 129.1 (C2), 123.3 (C5), 122.3 (C3), 65.3 (C7), 48.1 (C8), 40.1 (C10).

$^{19}F\{^1H\}$ NMR (377 MHz, Acetonitrile-d_3, 25 °C): δ [ppm] = -79.24 (s, OTf).

Additional information on the NMR spectra of the target compound including original data files is available via Chemotion Repository: https://dx.doi.org/10.14272/WOMQOOHUINDJRV-UHFFFAOYSA-M.1

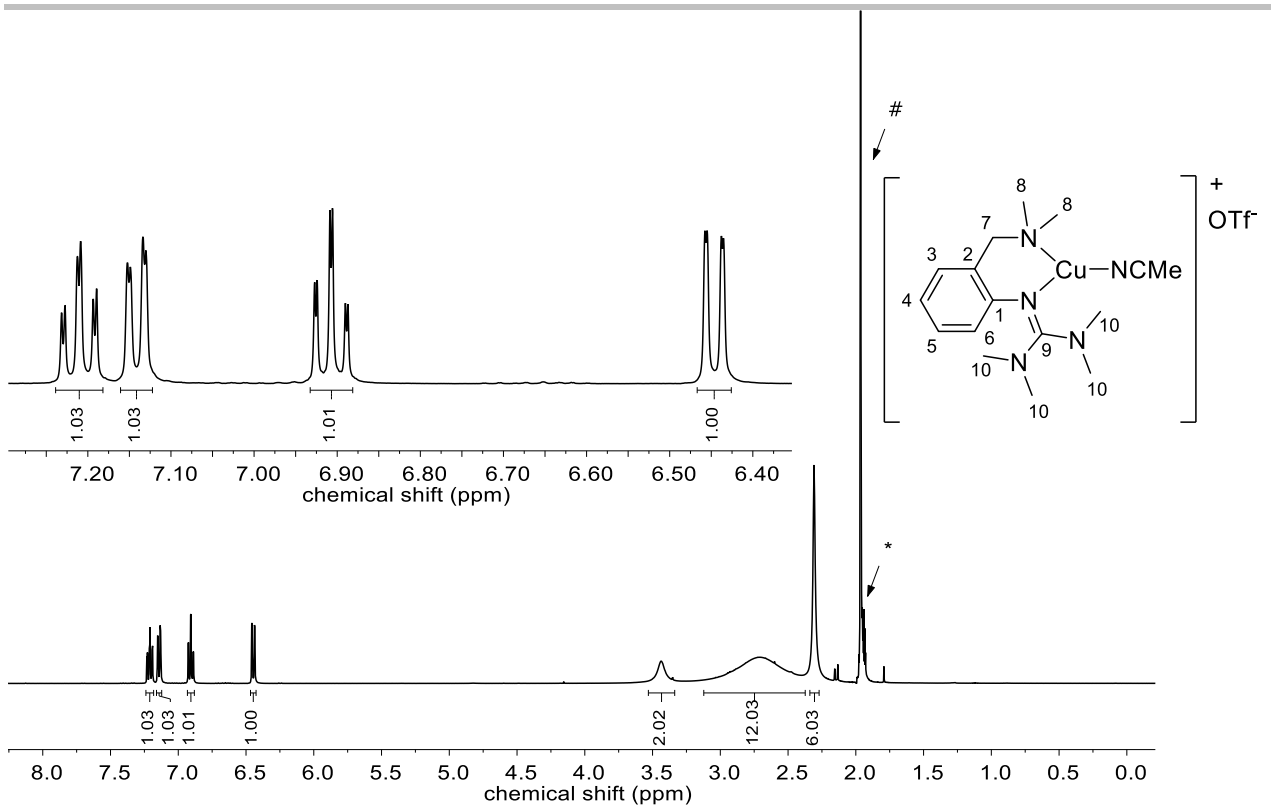

Figure S13: ^{1}H NMR spectrum of [Cu(**L1**)(MeCN)]OTf ([**C1**]OTf) (* = CD_3CN, # = CH_3CN).

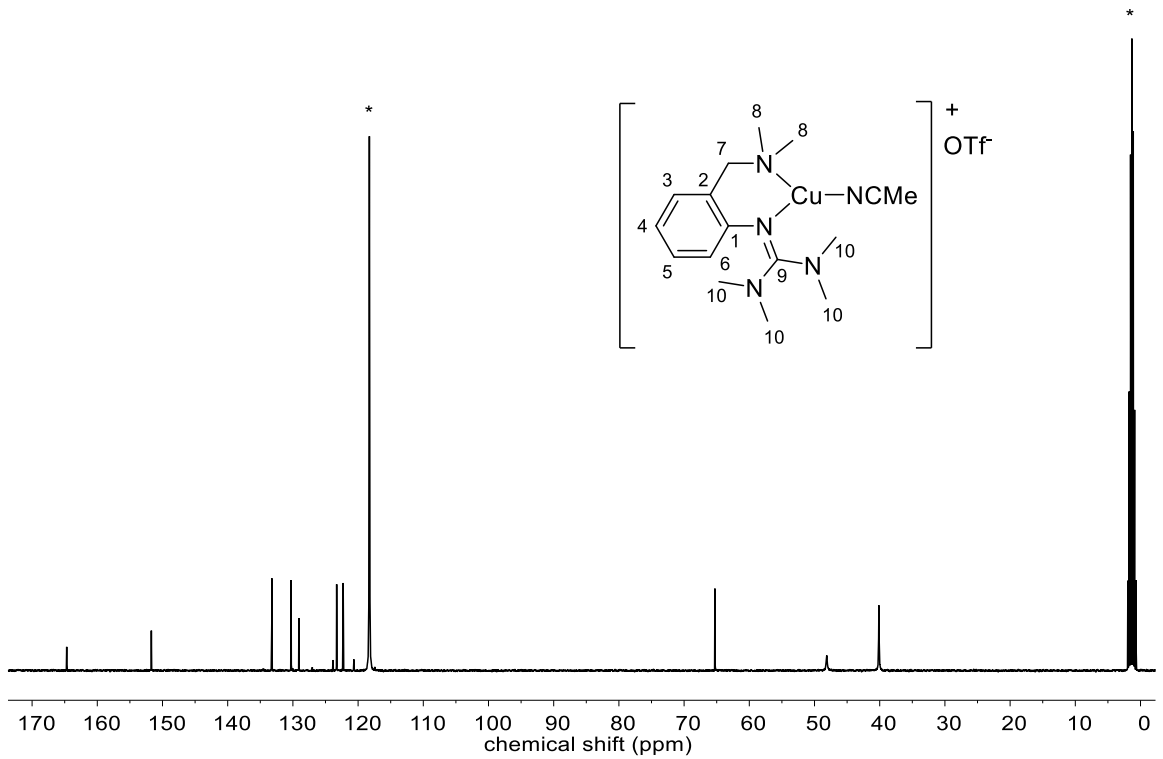

Figure S14: ^{13}C{^{1}H} NMR spectrum of [Cu(**L1**)(MeCN)]OTf ([**C1**]OTf) (* = CD_3CN and CH_3CN).

2.4.4. Synthesis of [Cu(L1)(MeCN)]ClO_4 ([C1]ClO_4)

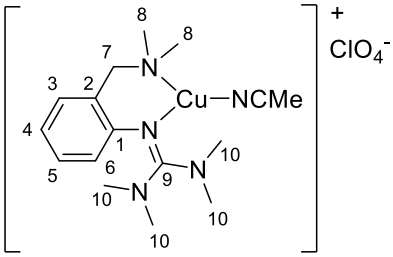

The title compound was generated *in-situ*.

^{1}H NMR (400 MHz, Acetonitrile-d_3, 25 °C): δ [ppm] = 7.21 (td, J = 7.7, 1.6 Hz, 1H, H4), 7.15 (dd, J = 7.5, 1.4 Hz, 1H, H6), 6.91 (td, J = 7.4, 1.2 Hz, 1H, H3), 6.45 (dd, J = 7.9, 1.4 Hz, 1H, H5), 3.44 (s, 2H, H7), 2.71 (br s, 12H, H10), 2.30 (s, 6H, H8).

^{13}C{^{1}H} NMR (101 MHz, Acetonitrile-d_3, 25 °C): δ [ppm] = 164.6 (C9), 151.7 (C1), 133.1 (C6), 130.2 (C4), 129.1 (C2), 123.3 (C5), 122.3 (C3), 65.1 (C7), 48.1 (C8), 40.1 (C10).

Additional information on the NMR spectra of the target compound including original data files is available via Chemotion Repository: https://dx.doi.org/10.14272/SQELSYLGCLCOLU-UHFFFAOYSA-M.1

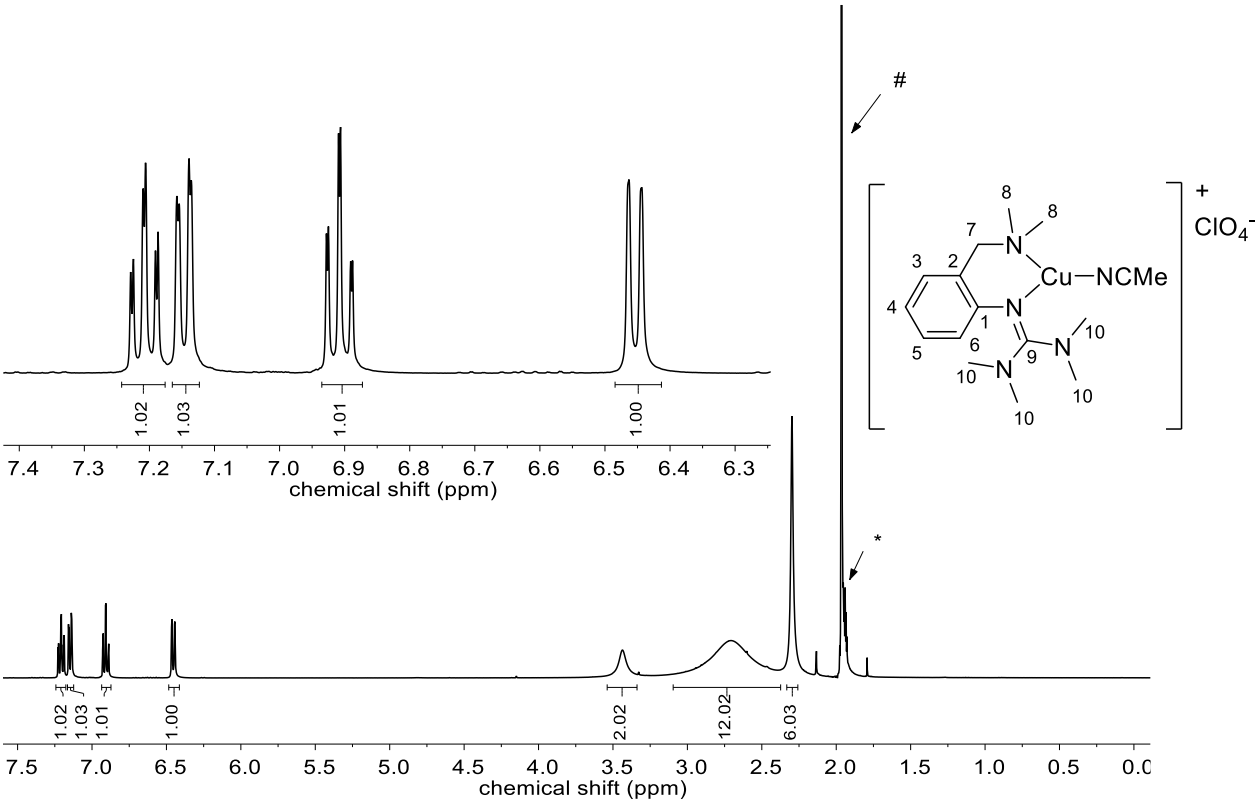

Figure S15: ^{1}H NMR spectrum of [Cu(**L1**)(MeCN)]ClO_4 ([**C1**]ClO_4) (* = CD_3CN, # = CH_3CN).

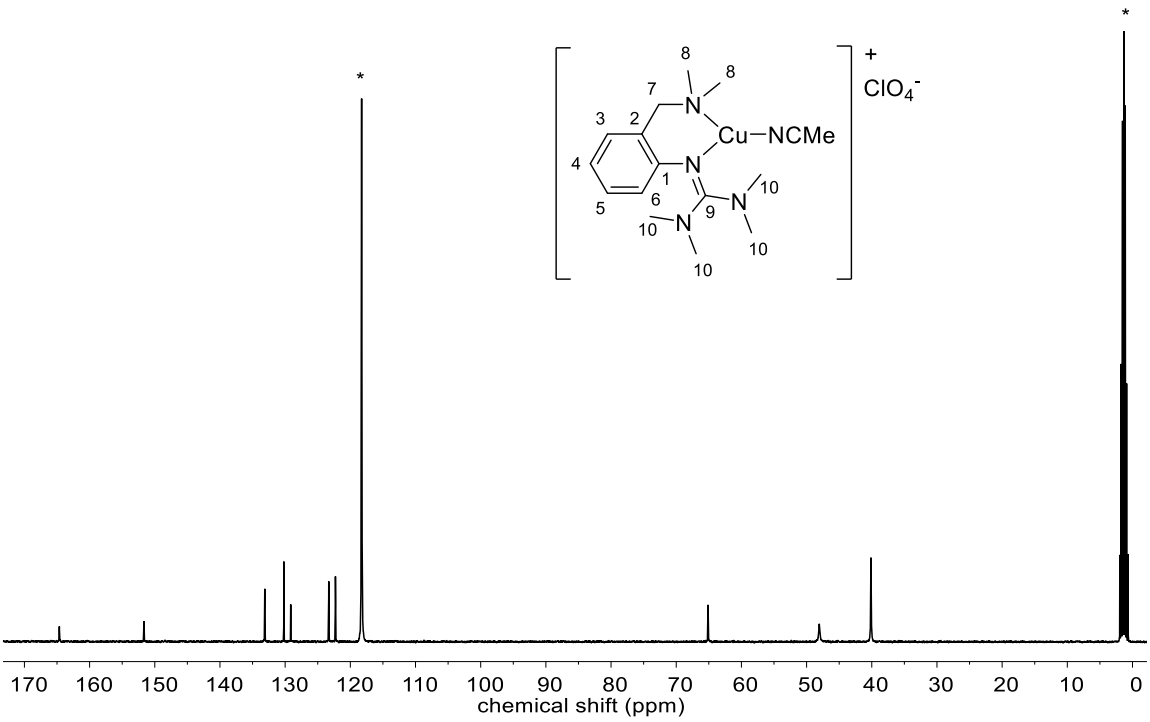

Figure S16: $^{13}C\{^1H\}$ NMR spectrum of [Cu(**L1**)(MeCN)]ClO_4 ([**C1**]ClO_4) (* = CD_3CN and CH_3CN).

2.5. Synthesis of [Cu_2(μ-O)$_2$(L1)$_2$](X)$_2$ ([O1](X)$_2$)

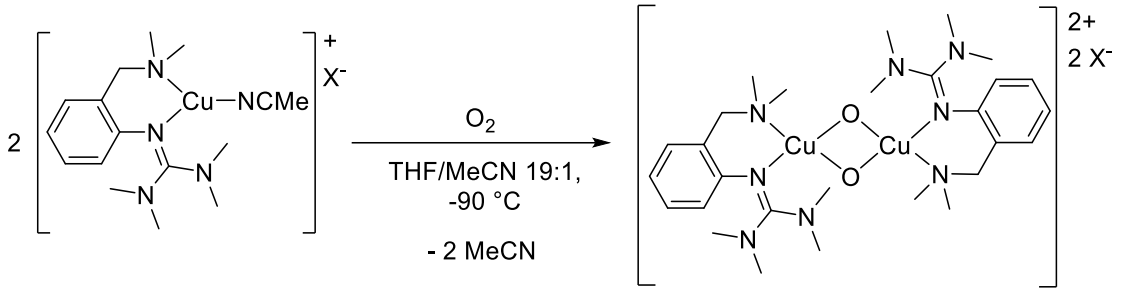

Scheme S5: Oxygenation of copper(I) species [Cu(**L1**)(MeCN)]X (X = PF_6, OTf, BF_4, ClO_4) with molecular dioxygen.

For the generation of the bis(μ-oxo) species [**O1**]$(PF_6)_2$ (0.005 mmol, 1.0 eq) dried and degassed tetrahydrofuran (9.5 mL) was saturated with molecular dioxygen at –90 °C and the colorless precursor complex [**C1**]PF_6 (0.010 mmol, 2.0 eq) in acetonitrile (0.5 mL) was added rapidly *via* a Hamilton syringe. The solution turned khaki immediately. The formation of [**O1**]$(PF_6)_2$ (0.5 mM) was followed by UV/Vis spectroscopy.

Similar oxygenation of [**C1**]X (X = OTf, BF_4, ClO_4) was performed leading to a khaki-colored solution of [**O1**]$(BF_4)_2$ and [**O1**]$(ClO_4)_2$ and an orange-colored solution of [**O1**]$(OTf)_2$. [**O1**]$(X)_2$ was formed within 3 min in all cases.

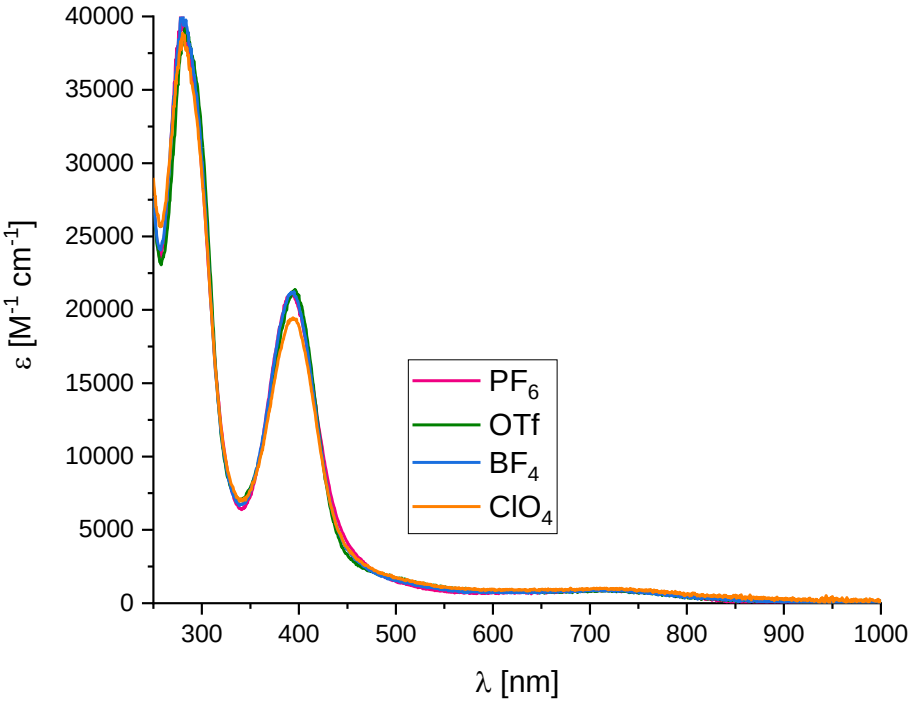

Figure S17: UV/Vis spectra of [**O1**]$(X)_2$ (X = PF_6, OTf, BF_4, ClO_4; 0.5 mM) in tetrahydrofuran at –90 °C.

Table S3: UV/Vis Transitions of [**O1**]$(X)_2$ (X = PF_6, OTf, BF_4, ClO_4) in tetrahydrofuran at –90 °C.

X	λ [nm]	ε [M^{-1} cm^{-1}]	λ [nm]	ε [M^{-1} cm^{-1}]	color
PF_6	280	40000	392	21000	khaki
BF_4	280	40000	392	21000	khaki
ClO_4	281	38000	393	19000	khaki
OTf	284	39000	396	21000	orange

2.5.1. Spectrophotometric Titration of [O1]$(PF_6)_2$ with FcCOOH

The titration experiment was conducted according to a literature procedure.[30]

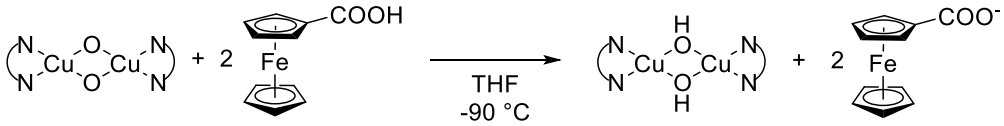

Scheme S6: Spectrophotometric titration of [**O1**]$(PF_6)_2$ with ferrocene monocarboxylic acid.

[**O1**]$(PF_6)_2$ (0.5 mM) was synthesized according to protocol 2.5. Excess of O_2 was removed by three cycles of evacuation and purging with N_2. A tenfold stock solution of the required amount of ferrocene monocarboxylic acid (2.8 mg, 0.012 mmol, 2.4 eq) in tetrahydrofuran (1.2 mL) was prepared and one-tenth of it positioned in a Hamilton syringe. The titrant was added stepwise in 0.1 mL (0.2 eq) steps. The titration experiment was followed by UV/Vis spectroscopy. After stabilization of the optical spectrum the next aliquot of FcCOOH was injected.

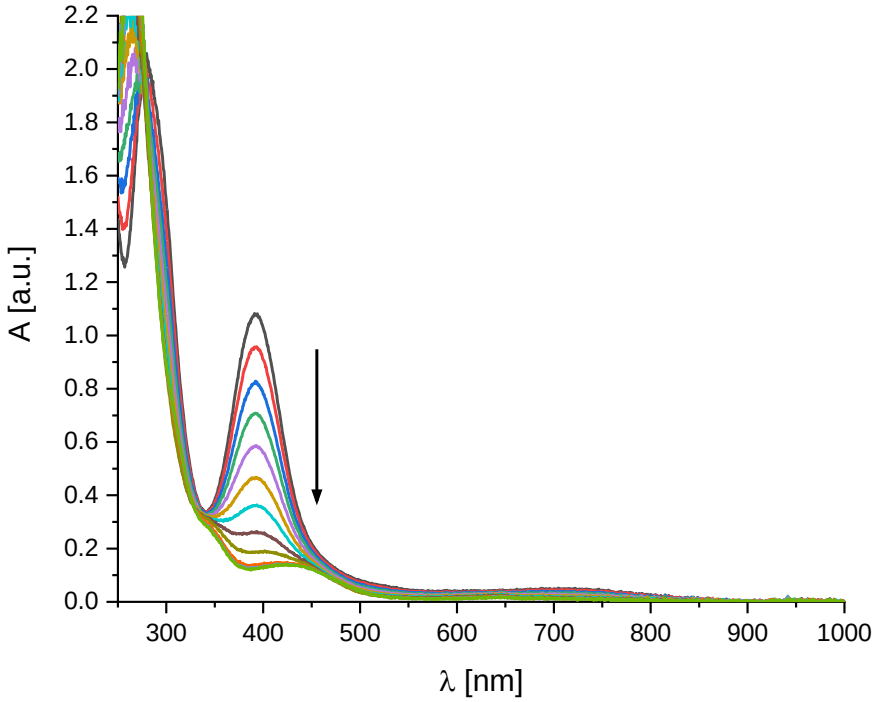

Figure S18: UV/Vis spectra of the titration of [**O1**]$(PF_6)_2$ (0.5 mM) with ferrocene monocarboxylic acid in tetrahydrofuran at –90 °C.

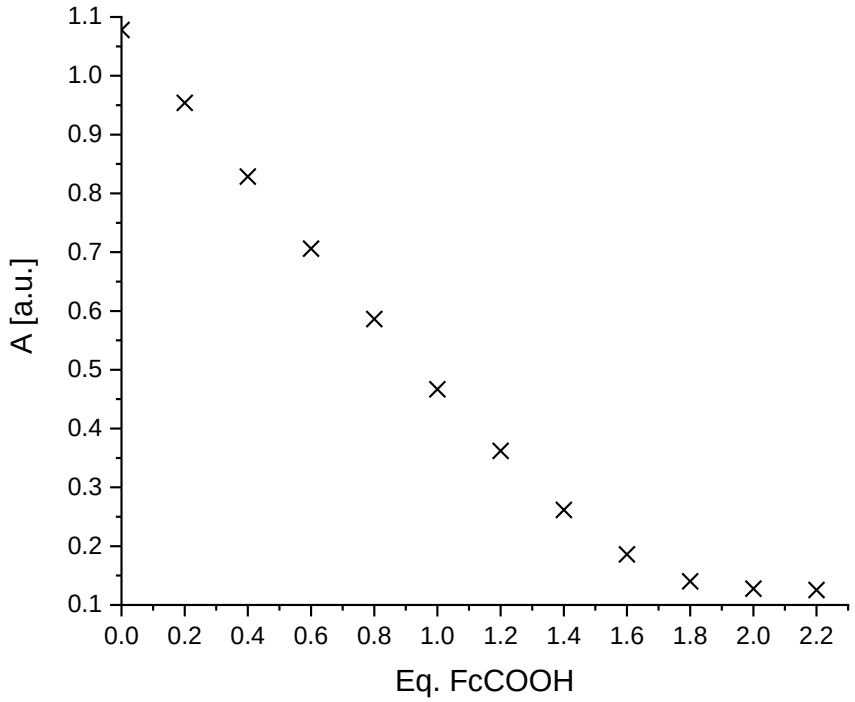

Figure S19: Absorbance of [**O1**]$(PF_6)_2$ during titration of [**O1**]$(PF_6)_2$ with FcCOOH (0 to 2.2 equivalents) in tetrahydrofuran at –90 °C monitored at 392.00 nm.

2.5.2. Cryo-UHR-ESI Mass Spectrometry of [O1](PF$_6$)$_2$

[**O1**](PF$_6$)$_2$ (0.5 mM) was synthesized according to protocol 2.5. and analyzed *via* Cryo-UHR-ESI mass spectrometry.

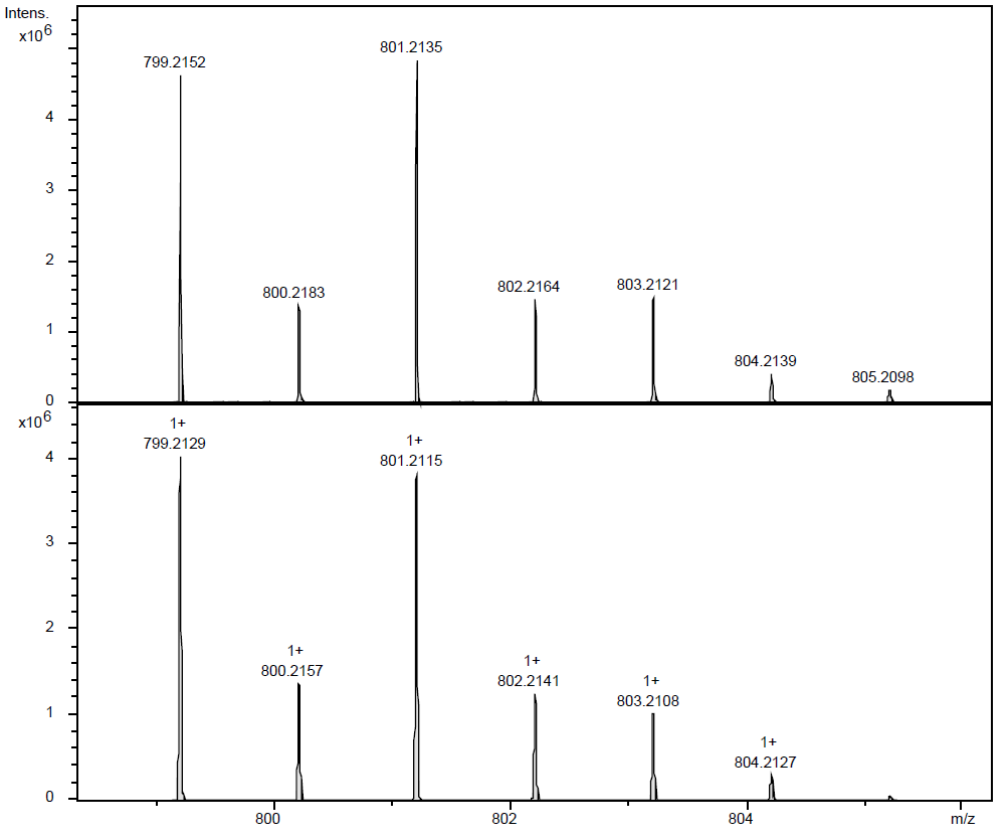

Figure S20: Cryo-UHR-ESI mass spectrometry of [**O1**](PF$_6$)$^+$ in tetrahydrofuran at –80 °C (top: experimental, bottom: calculated). The isotopic pattern and corresponding m/z value resemble the mass spectrum of the monocationic species [**O1**](PF$_6$)$^+$.

2.5.3. Thermal Decomposition Kinetics of [O1]$(PF_6)_2$

[**O1**]$(PF_6)_2$ (0.5 mM) was synthesized according to protocol 2.5. at the respective temperature. Excess of O_2 was removed by three cycles of evacuation and purging with N_2. The decomposition kinetics were followed by UV/Vis spectroscopy at constant temperature.

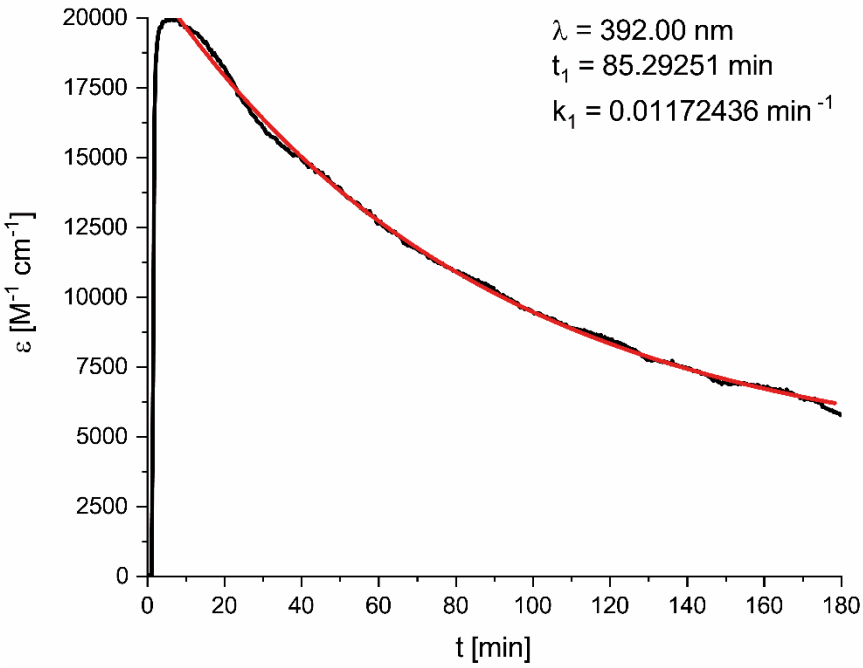

Figure S21: Thermal decay of [**O1**]$(PF_6)_2$ in tetrahydrofuran at –80 °C monitored at 392 nm.

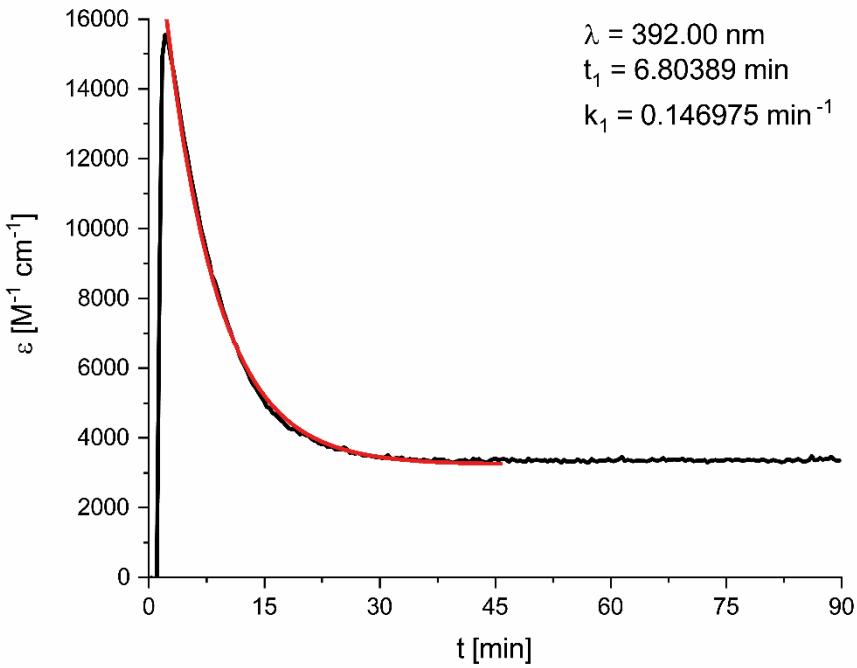

Figure S22: Thermal decay of [**O1**]$(PF_6)_2$ in tetrahydrofuran at –74 °C monitored at 392 nm.

Table S4: Thermal decay parameters of [**O1**]$(PF_6)_2$ in tetrahydrofuran at –80 °C and –74 °C.

T [°C]	$t_{1/2}$ [min]	k_1 [s^{-1}]
–80	59.1	$1.95 \cdot 10^{-4}$
–74	4.72	$2.45 \cdot 10^{-3}$

2.5.4. Crystal Structure of Decomposition Products of [O1](X)$_2$

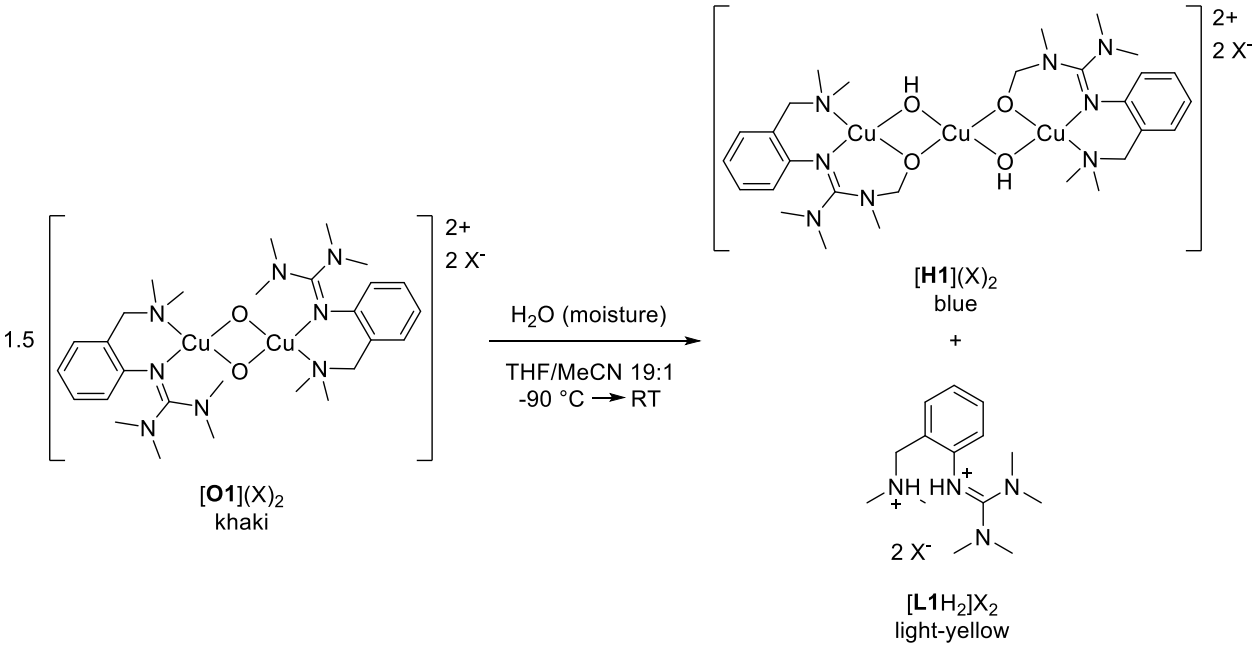

Scheme S7: Decomposition of [**O1**]$(X)_2$ and formation of tricopper μ-alkoxo μ-hydroxo complex [**H1**]$(X)_2$ and protonated ligand [**L1**H_2]X_2 (X = PF_6, BF_4).

[**O1**]$(X)_2$ was synthesized according to protocol 2.5. The solution was warmed up to room temperature and evaporated to dryness. The green residue was dissolved in acetonitrile and filtered afterwards. Single crystals of [**H1**]$(X)_2$ (X = PF_6, BF_4) suitable for X-ray diffraction were grown by slow diffusion of diethyl ether into the acetonitrile solution or by slow diffusion of acetonitrile out into toluene. Crystallization of blue and light-yellow blocks in a greenish solution was observed. Concomitantly, crystals of protonated ligand [**L1**H_2]$(BF_4)_2$ were obtained (see Table S6 for crystallographic details).

2.5.4.1. Synthesis of [Cu_3(μ-OL1)$_2$(μ-OH)$_2$]$(PF_6)_2$ · 2 thf ([H1]$(PF_6)_2$)

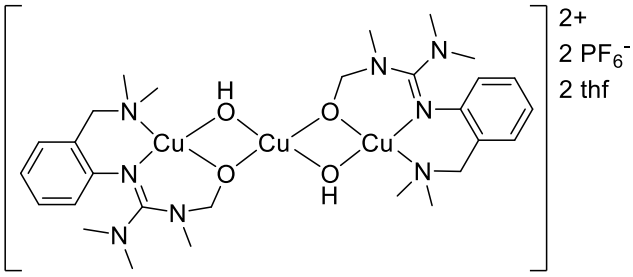

The title compound was isolated as blue crystalline blocks (19 mg, 16.1 µmol, 48%).

HRMS-ESI+ (MeCN): m/z calc. for ½{[$C_{28}H_{48}O_4N_8{}^{63}Cu_2{}^{65}Cu]^{2+}$}: 375.5834, found: 375.5823.

IR (ATR): $\tilde{\nu}$ [cm^{-1}] = 2957 (vw, C-H_{arom}), 2923 (vw, C-H_{aliph}), 2862 (vw, C-H_{aliph}), 1554 (w, C=N), 1514 (w), 1489 (w), 1457 (w), 1423 (w), 1399 (w), 1381 (m), 1344 (vw), 1277 (vw), 1231 (vw), 1183 (w), 1077 (m), 1038 (m), 983 (w), 908 (vw), 873 (vw), 830 (vs, PF_6), 760 (m), 708 (m), 556 (s), 504 (w), 462 (w).

2.5.4.2. Synthesis of $[Cu_3(\mu\text{-}OL1)_2(\mu\text{-}OH)_2](BF_4)_2 \cdot 2$ thf ($[H1](BF_4)_2$)

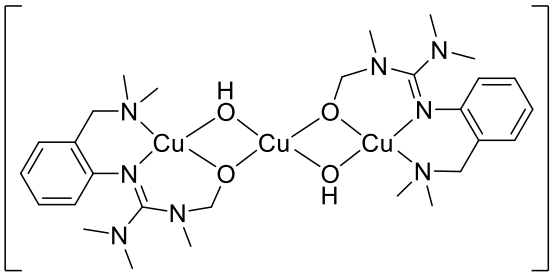

The title compound was isolated as blue crystalline blocks (16 mg, 15.1 µmol, 45%).

HRMS-ESI+ (MeCN): m/z calc. for $[(C_{28}H_{48}O_4N_8{}^{63}Cu_2{}^{65}Cu)(BF_4)]^+$: 838.16921, found: 838.16938.

IR (ATR): $\tilde{\nu}$ [cm^{-1}] = 2960 (vw, C-H$_{arom}$), 2927 (w, C-H$_{aliph}$), 2858 (vw, C-H$_{aliph}$), 1763 (m), 1654 (m), 1648 (m), 1637 (m), 1624 (m), 1594 (m, C=N), 1555 (m, C=N), 1490 (w), 1473 (w), 1458 (w), 1453 (w), 1424 (w), 1405 (w), 1378 (w), 1170 (m), 1056 (s, BF$_4$), 1033 (vs, BF$_4$), 989 (m), 930 (w), 870 (w), 839 (vw), 797 (w), 762 (m, BF$_4$).

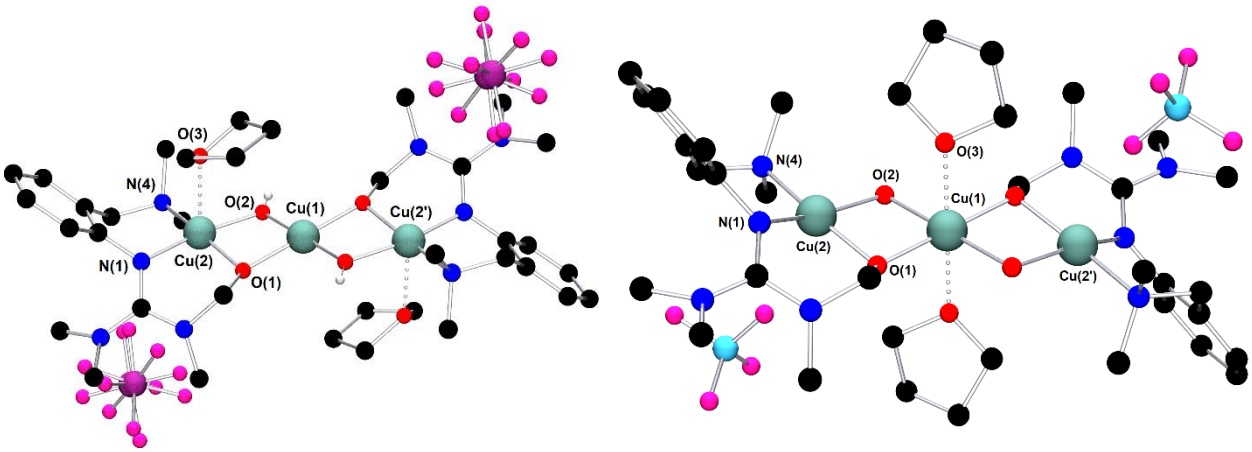

Figure S23: Molecular structures of [**H1**]$(PF_6)_2$ (left) and [**H1**]$(BF_4)_2$ (right) in the solid state. Hydrogen atoms, expect for hydroxy moieties if available, were omitted for clarity. It was not possible to find the hydrogen atom of the hydroxy group in [**H1**]$(BF_4)_2$.

The tetrahydrofuran orientation is reproducible as found in the molecular structures of [**H1**]$(PF_6)_2$ and [**H1**]$(BF_4)_2$, shown in Figure S23.

Table S5: Selected bond lengths [Å] and angles [°] of [**H1**]$(PF_6)_2$ and [**H1**]$(BF_4)_2$.

	[H1]$(PF_6)_2$	**[H1]$(BF_4)_2$**
Cu(1)-O(1)	1.912(2)	1.904(4)
Cu(1)-O(2)	1.893(2)	1.961(4)
Cu(1)-O(3)	-	2.253(4)
Cu(2)-O(1)	1.923(2)	1.902(5)
Cu(2)-O(2)	1.932(2)	1.961(4)
Cu(2)-O(3)	2.556(2)	-
Cu(1)···Cu(2)	2.953(1)	2.919(2)
Cu(2)-N(1)	1.986(2)	1.953(5)
Cu(2)-N(4)	2.019(3)	2.007(6)
N(1)-Cu(2)-N(4)	94.9(1)	96.1(2)
O(1)-Cu(1)-O(2)	78.0(1)	80.3(2)
O(1)-Cu(2)-O(2)	76.8(1)	80.4(2)
Cu(2)-O(1)-Cu(1)	100.7(1)	100.2(2)
Cu(2)-O(2)-Cu(1)	101.1(2)	96.2(2)
Cu(2)-Cu(1)-Cu(2')	180.0	180.0

Table S6: Crystallographic data and parameters of decomposition products [**H1**]$(PF_6)_2$, [**H1**]$(BF_4)_2$ and [**L1**H_2]$(BF_4)_2$.

	[H1]$(PF_6)_2$	**[H1]$(BF_4)_2$**	**[L1H_2]$(BF_4)_2$**
Empirical formula	$C_{36}H_{64}Cu_3F_{12}N_8O_6P_2$	$C_{36}H_{62}B_2Cu_3F_8N_8O_6$	$C_{28}H_{52}B_3F_{13}N_8$
Formula weight [g mol^{-1}]	1185.51	1067.17	780.20
T [K]	100	100	100
λ [Å]	0.71073	1.54186	0.71073
Crystal system	Monoclinic	Triclinic	Tetragonal
Space group	$P2_1/n$	$P\bar{1}$	$P4_32_12$
a [Å]	9.2369(18)	8.5995(17)	12.3090(17)
b [Å]	10.105(2)	8.8545(18)	12.3090(17)
c [Å]	26.392(5)	16.097(3)	24.986(5)
α [°]	90	75.67(3)	90
β [°]	97.65(3)	81.55(3)	90
γ [°]	90	73.08(3)	90
V [Å^3]	2441.4(9)	1132.4(5)	3785.6(13)

Z	2	1	4
ρ_{calc} [g cm^{-3}]	1.613	1.565	1.369
μ [mm^{-1}]	1.457	2.381	0.127
F(000)	1218	551	1632
Crystal size [mm]	0.190 x 0.150 x 0.110	0.090 x 0.070 x 0.050	0.220 x 0.190 x 0.130
hkl range	–9 ≤ h ≤ 13, ±15, –36 ≤ l ≤ 39	–8 ≤ h ≤ 10, –10 ≤ k ≤ 9, –16 ≤ l ≤ 18	±14, ±14, ±30
Reflections collected	23367	9014	44583
Independent reflections	8772	3685	3523
R_{int}	0.0419	0.0594	0.0410
Number of parameters	371	291	251
R_1 [I≥2σ(I)]	0.0568	0.0699	0.0622
wR_2 (all data)	0.1598	0.1955	0.1394
Goodness-of-fit	1.137	0.944	1.108
Largest diff. peak hole [eÅ^{-3}]	1.199, –1.199	0.851, –0.531	0.675, –0.605
CCDC	1950654	1950655	1963147

2.6. Catalytic Reactivity of [O1](PF$_6$)$_2$

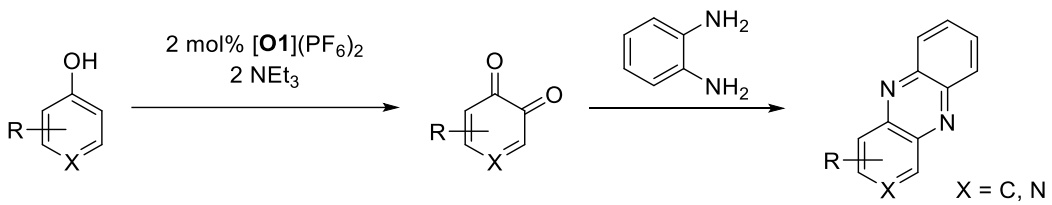

Scheme S8: Oxygenation of phenolic substrates mediated by [**O1**](PF$_6$)$_2$ and subsequent condensation with 1,2-phenylenediamine.

Reactivity studies of [**O1**](PF$_6$)$_2$ were performed in two scales: in small scale to obtain UV/Vis spectra within Lambert-Beer limitations and in larger scale to isolate a possible phenazine by the use of column chromatography.

[**O1**](PF$_6$)$_2$ (0.005 mmol, 1.0 eq) was synthesized according to protocol 2.5. Substrate solutions were prepared by dissolving the respective substrate (0.125 mmol, 25.0 eq) in either dried tetrahydrofuran or dried methanol, followed by the addition of triethylamine (0.035 mL, 0.250 mmol, 50.0 eq). The amount of solvent varied due to solubility limitations (Table S7). 1,2-Phenylenediamine (54.1 mg, 0.250 mmol, 50.0 eq) was dissolved in dried tetrahydrofuran (0.4 mL).

After stabilization of the optical spectrum of [**O1**](PF$_6$)$_2$, the substrate solution was injected into the Schlenk cell at -90 °C. A significant color change was observed. The reaction was monitored by UV/Vis spectroscopy until no further spectral change occurred (approx. 1 h). 1,2-Phenylenediamine solution was added at -90 °C and the reaction was followed by UV/Vis spectroscopy. After stabilization of the optical spectrum, the cooling bath was removed. The reaction mixture was warmed up to room temperature and stirred for 1 h. Aqueous hydrochloric acid (0.5 M, 5.0 mL) was added to the solution and the solvents were removed under reduced pressure. The aqueous phase was extracted with dichloromethane (4 x 10 mL). The combined organic layers were dried over Na_2SO_4 and evaporated to dryness.[30]

This procedure was upscaled by a factor of ten for quantification in case of substrate conversion indicated by UV/Vis spectra and NMR spectroscopy. Flame-dried molecular sieves (3 Å, 400 mg) were placed into the flask prior to the formation of [**O1**]$(PF_6)_2$. The crude product was purified *via* column chromatography on Geduran Si 60 and/or via sublimation to isolate the respective phenazine.

Table S7: Substrate solutions used for oxygenation of phenolic substrates mediated by [**O1**]$(PF_6)_2$.

substrate	solvent	volume [mL]
1-methyl 2-naphthol	tetrahydrofuran	0.1
1-naphthol	tetrahydrofuran	0.2
2-methyl 8-quinolinol	tetrahydrofuran	0.1
2-naphthol	tetrahydrofuran	0.2
2,4-di-*tert*-butyl phenol	tetrahydrofuran	0.1
3-pyridinol	methanol	0.1
3-quinolinol	methanol	1.0
4-indolol	tetrahydrofuran	0.2
4-methoxy phenol	tetrahydrofuran	0.1
4-pyridinol	methanol	0.1
4-quinolinol	methanol	0.3
4-*tert*-butyl phenol	tetrahydrofuran	0.1
5-indolol	tetrahydrofuran	0.2
6-indolol	tetrahydrofuran	0.4
6-quinolinol	methanol	0.8
7-indolol	tetrahydrofuran	0.5
8-quinolinol	tetrahydrofuran	0.1
phenol	tetrahydrofuran	0.1

2.6.1. Synthesis of Benzo[a]phenazine (P1)

All reactions were conducted according to protocol 2.6.

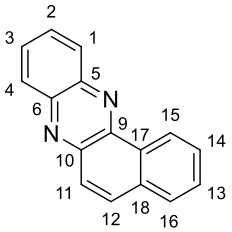

Chemical Formula: $C_{16}H_{10}N_2$
Molecular Weight: 230.27 g mol^{-1}

Benzo[a]phenazine was isolated as a yellow solid. It was generated starting from both 1-naphthol (126.6 mg, 0.550 mmol, 22% yield referred to the amount of substrate, 11 eq per equivalent catalyst [**O1**]$(PF_6)_2$) and 2-naphthol (178.4 mg, 0.775 mmol, 31% yield referred to the amount of substrate, 16 eq per equivalent catalyst [**O1**]$(PF_6)_2$).

R_f = 0.44 (ethyl acetate/hexane 5:95)

R_f = 0.62 (ethyl acetate/hexane 15:85)

^{1}H NMR (400 MHz, DMSO-d_6, 25 °C): δ [ppm] = 9.29 – 9.23 (m, 1H, H15), 8.38 – 8.31 (m, 1H, H1), 8.30 – 8.25 (m, 1H, H4), 8.20 (d, J = 9.3 Hz, 1H, H11), 8.11 – 8.06 (m, 1H, H16), 8.02 – 7.93 (m, 3H, H2+H3+H12), 7.90 – 7.82 (m, 2H, H13+H14).

^{13}C{^{1}H} NMR (101 MHz, DMSO-d_6, 25 °C): δ [ppm] = 143.1 (C10), 142.2 (C9), 141.7 (C6), 141.1 (C5), 133.4 (C11), 132.9 (C17), 130.5 (C2), 130.5 (C3), 130.2 (C18), 130.1 (C13), 129.2 (C1), 128.9 (C4), 128.5 (C16), 128.1 (C14), 126.8 (C12), 124.6 (C15).

HRMS-EI: m/z calc. for $C_{16}H_{10}N_2$: 230.0838, found: 230.0837.

IR (ATR): $\tilde{\nu}$ [cm^{-1}] = 2960 (w), 2923 (m), 2851 (w), 1735 (w), 1536 (w), 1494 (w), 1472 (w), 1355 (m), 1260 (m), 1220 (vw), 1198 (vw), 1136 (w), 1118 (w), 1101 (m), 1010 (m), 974 (w), 959 (m), 909 (w), 877 (m), 836 (m), 806 (m), 795 (m), 776 (m), 764 (m), 759 (vs), 753 (vs), 697 (m), 650 (m), 607 (m), 570 (m), 551 (vs), 536 (m), 503 (m), 485 (w), 404 (s).

Analytical data matches those reported in literature.[32]

Additional information on the NMR spectra of the target compound including original data files is available via Chemotion Repository: https://dx.doi.org/10.14272/SEXRCKWGFSXUOO-UHFFFAOYSA-N.1

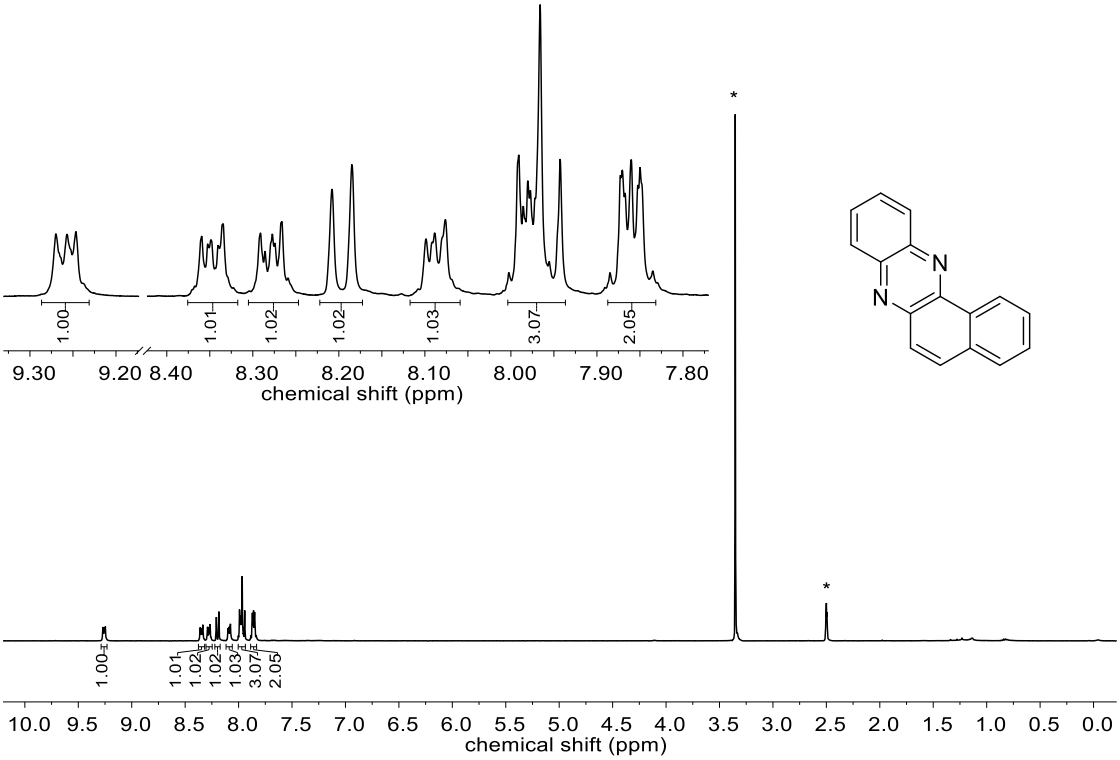

Figure S24: ^{1}H NMR spectrum of benzo[a]phenazine resulting from oxygenation of 1-naphthol and 2-naphthol, respectively, mediated by [**O1**]$(PF_6)_2$ (0.5 mM) in tetrahydrofuran at -90 °C and subsequent condensation by using 1,2-phenylenediamine (* = DMSO-d_6).

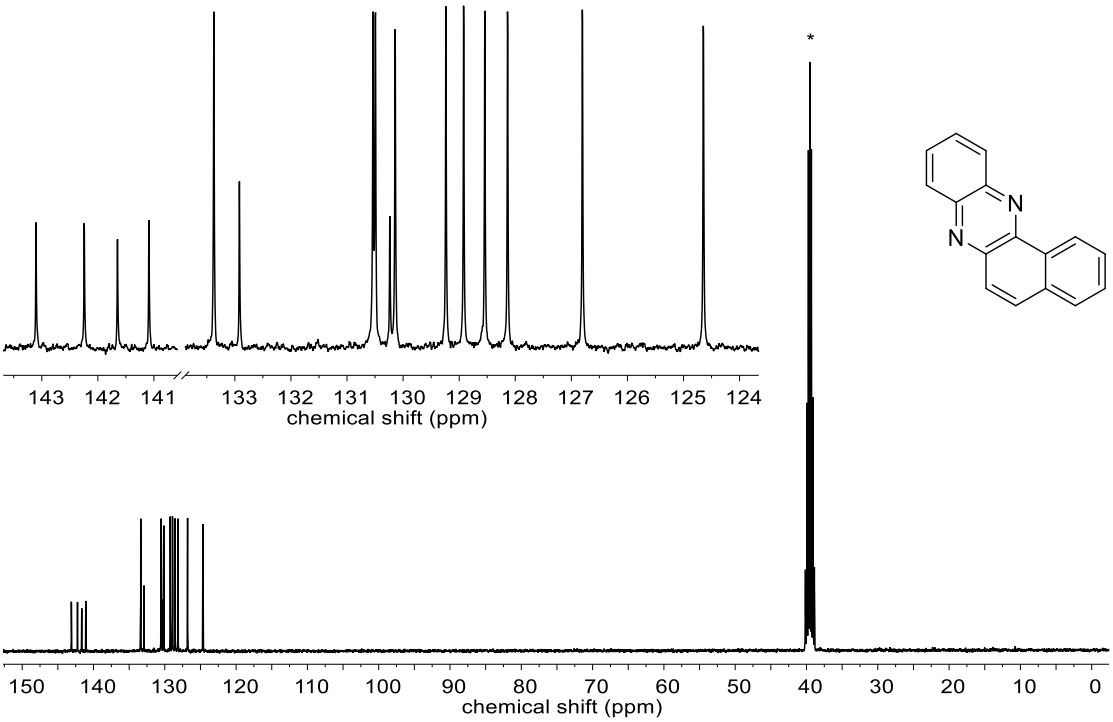

Figure S25: $^{13}C\{^1H\}$ NMR spectrum of benzo[a]phenazine resulting from oxygenation of 1-naphthol and 2-naphthol, respectively, mediated by [**O1**]$(PF_6)_2$ (0.5 mM) in tetrahydrofuran at -90 °C and subsequent condensation by using 1,2-phenylenediamine (* = DMSO-d_6).

2.6.2. Synthesis of Quinolino[3,4-b]quinoxaline (P2)

All reactions were conducted according to protocol 2.6.

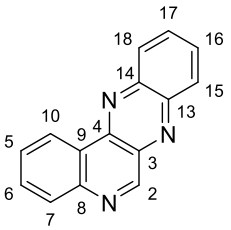

Chemical Formula: $C_{15}H_9N_3$
Molecular Weight: 231.26 g mol^{-1}

Quinolino[3,4-b]quinoxaline was isolated as a yellow solid. It was generated starting from both 3-quinolinol (185.0 mg, 0.800 mmol, 30% yield referred to the amount of substrate, 16 eq per equivalent catalyst [**O1**]$(PF_6)_2$) and 4-quinolinol (121.4 mg, 0.525 mmol, 21% yield referred to the amount of substrate, 11 eq per equivalent catalyst [**O1**]$(PF_6)_2$).

R_f = 0.50 (ethyl acetate/hexane 20:80)

^{1}H NMR (400 MHz, DMSO-d_6; 25 °C): δ [ppm] = 9.60 (s, 1H, H2), 9.16 (ddd, J = 8.0, 1.6, 0.6 Hz, 1H, H10), 8.44 – 8.40 (m, 2H, H15+H18), 8.26 – 8.19 (m, 1H, H7), 8.17 – 8.06 (m, 2H, H16+H17), 8.01 (ddd, J = 8.1, 7.2, 1.6 Hz, 1H, H6), 7.94 – 7.89 (m, 1H, H5).

$^{13}C\{^1H\}$ NMR (101 MHz, DMSO-d_6, 25 °C): δ [ppm] = 155.5 (C2), 145.0 (C8), 143.8 (C13), 142.9 (C14), 142.2 (C4), 136.6 (C3), 133.0 (C17), 131.7 (C6), 131.5 (C16), 129.9 (C18), 129.7 (C7), 129.3 (C15), 128.6 (C5), 124.0 (C10), 123.9 (C9).

HRMS-EI: m/z calc. for $C_{15}H_9N_3$: 231.0791, found: 231.0795.

IR (ATR): $\tilde{\nu}$ [cm^{-1}] = 2963 (w), 2921 (w), 2852 (vw), 1585 (w), 1534 (w), 1487 (w), 1464 (w), 1363 (w), 1258 (m), 1085 (m), 1011 (vs), 921(w), 881 (m), 794 (s), 777 (s), 769 (s), 704 (m), 649 (m), 611 (m), 592 (w), 571 (m), 550 (m), 511 (w), 410 (s).

Additional information on the NMR spectra of the target compound including original data files is available via Chemotion Repository: https://dx.doi.org/10.14272/JJGCDLVZJZGHBZ-UHFFFAOYSA-N.1

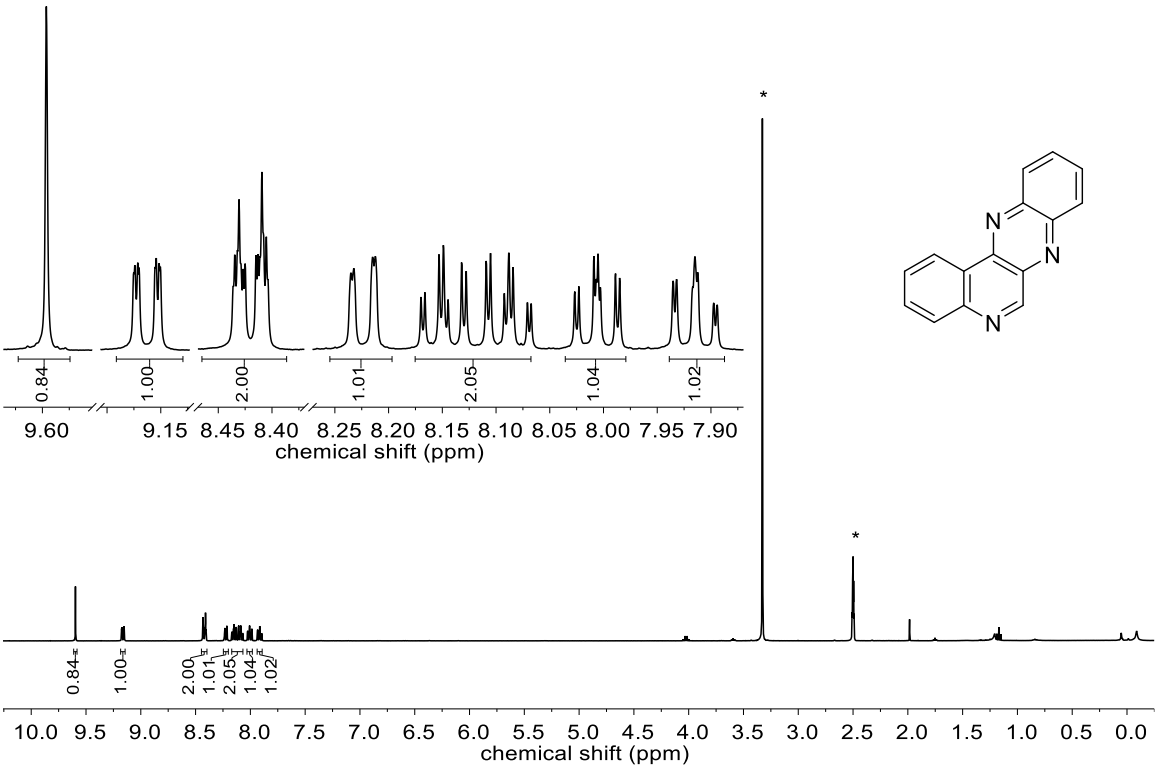

Figure S26: ^{1}H NMR spectrum of quinolino[3,4-b]quinoxaline resulting from oxygenation of 3-quinolinol and 4-quinolinol, respectively, mediated by [**O1**]$(PF_6)_2$ (0.5 mM) in tetrahydrofuran at -90 °C and subsequent condensation by using 1,2-phenylenediamine (* = DMSO-d_6).

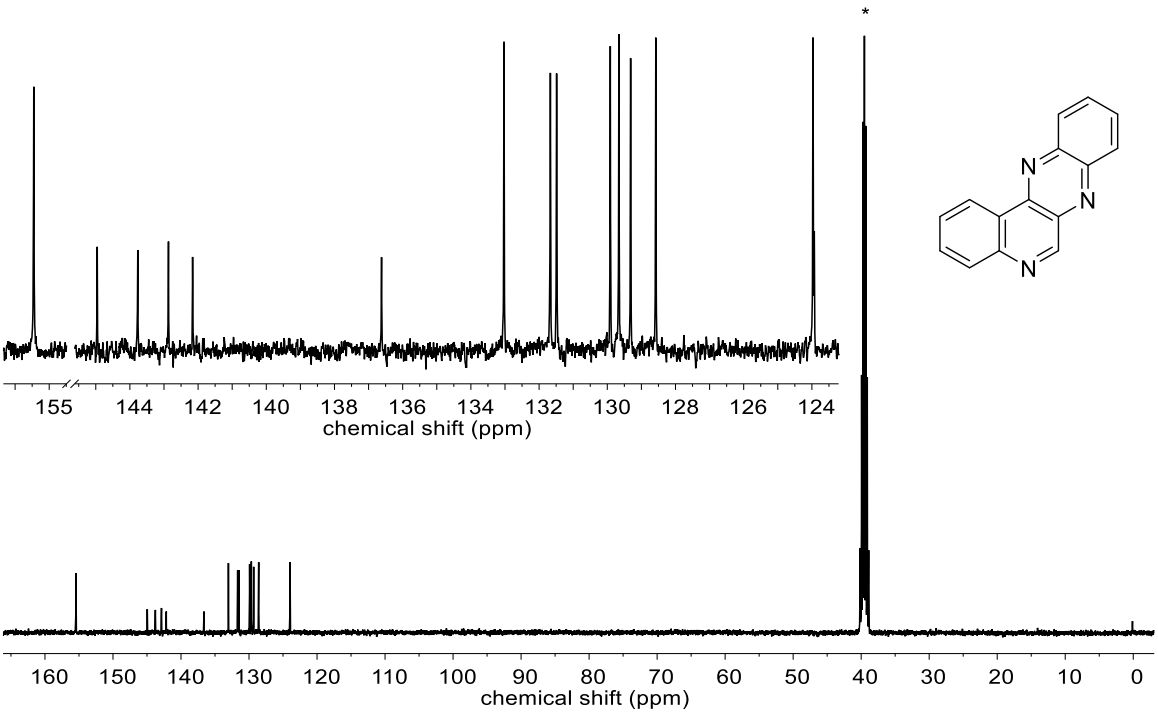

Figure S27: ^{13}C{^{1}H} NMR spectrum of quinolino[3,4-b]quinoxaline resulting from oxygenation of 3-quinolinol and 4-quinolinol, respectively, mediated by [**O1**]$(PF_6)_2$ (0.5 mM) in tetrahydrofuran at -90 °C and subsequent condensation by using 1,2-phenylenediamine (* = DMSO-d_6).

2.6.3. Synthesis of Pyrido[3,2-a]phenazine (P3)

All reactions were conducted according to protocol 2.6.

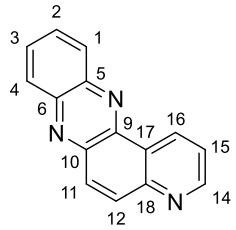

Chemical Formula: $C_{15}H_9N_3$
Molecular Weight: 231.26 g mol^{-1}

Pyrido[3,2-a]phenazine was isolated as a yellow solid starting from 6-quinolinol (173.4 mg, 0.750 mmol, 30% yield referred to the amount of substrate, 15 eq per equivalent catalyst [**O1**]$(PF_6)_2$). Single crystals of **P3** suitable for X-ray diffraction were grown from a concentrated DMSO solution.

R$_f$ = 0.26 (ethyl acetate/hexane 20:80)

^{1}H NMR (400 MHz, DMSO-d_6, 25 °C): δ [ppm] = 9.51 (dd, J = 8.2, 1.7 Hz, 1H, H14), 9.12 (dd, J = 4.5, 1.7 Hz, 1H, H16), 8.39 – 8.29 (m, 2H, H1+H4), 8.23 (s, 2H, H11+H12), 8.05 – 8.00 (m, 2H, H2+H3), 7.86 (dd, J = 8.2, 4.5 Hz, 1H, H15).

^{13}C{^{1}H} NMR (101 MHz, DMSO-d_6, 25 °C): δ [ppm] = 152.3 (C16), 149.3 (C18), 142.5 (C9), 142.5 (C10), 141.3 (C6), 140.9 (C5), 134.2 (C12), 132.5 (C14), 131.2 (C2), 131.1 (C3), 130.8 (C11), 129.3 (C1), 129.2 (C4), 126.0 (C17), 123.1 (C15).

HRMS-EI: m/z calc. for $C_{15}H_9N_3$: 231.0791, found: 231.0792.

IR (ATR): $\tilde{\nu}$ [cm^{-1}] = 2962 (w), 1585 (w), 1484 (w), 1434 (w), 1355 (w), 1258 (m), 1086 (m), 1006 (vs), 848 (m), 792 (vs), 774 (s), 760 (s), 650 (w), 610 (w), 574 (w), 553 (w), 502 (w), 486 (w), 476 (w), 423 (w).

Additional information on the NMR spectra of the target compound including original data files is available via Chemotion Repository: https://dx.doi.org/10.14272/ODJOHIWKLOPSFF-UHFFFAOYSA-N.1

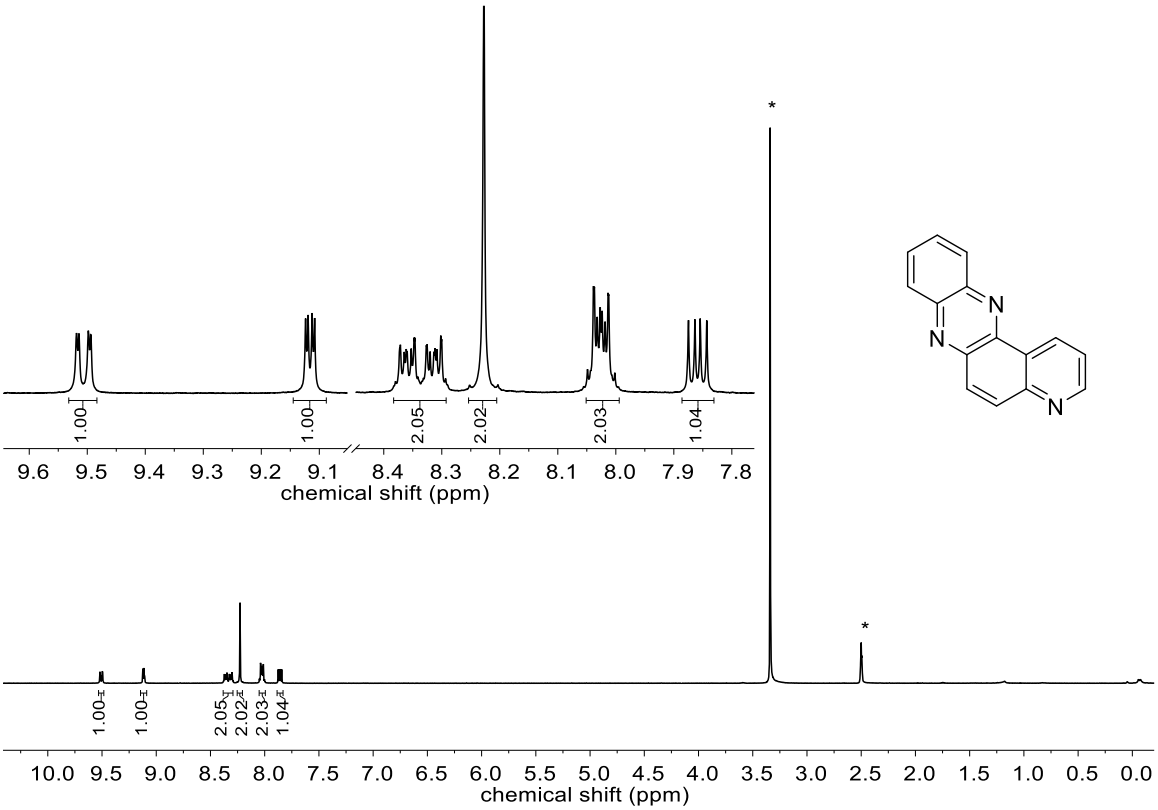

Figure S28: ^{1}H NMR spectrum of pyrido[3,2-a]phenazine resulting from oxygenation of 6-quinolinol mediated by [**O1**]$(PF_6)_2$ (0.5 mM) in tetrahydrofuran at -90 °C and subsequent condensation by using 1,2-phenylenediamine (* = DMSO-d_6).

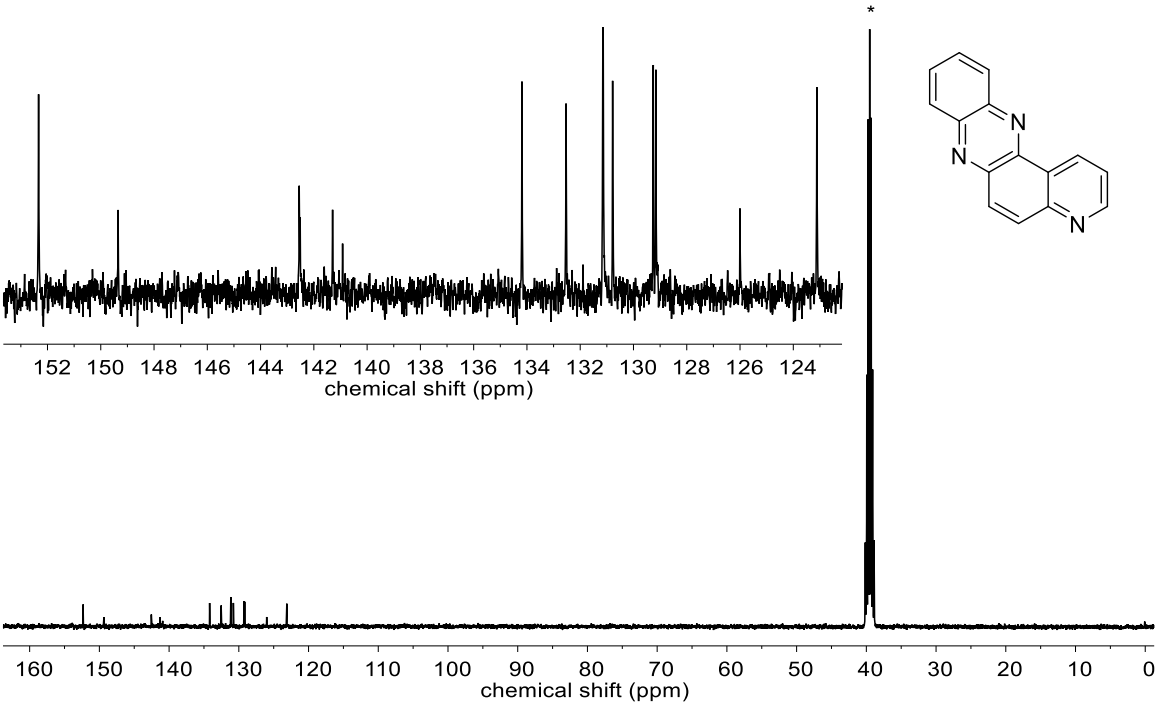

Figure S29: $^{13}C\{^1H\}$ NMR spectrum of pyrido[3,2-a]phenazine resulting from oxygenation of 6-quinolinol mediated by [**O1**]$(PF_6)_2$ (0.5 mM) in tetrahydrofuran at -90 °C and subsequent condensation by using 1,2-phenylenediamine (* = DMSO-d_6).

2.6.4. Synthesis of Pyrrolo[3,2-a]phenazine (P4)

All reactions were conducted according to protocol 2.6.

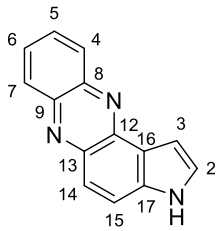

Chemical Formula: $C_{14}H_9N_3$
Molecular Weight: 219.25 g mol^{-1}

Pyrrolo[3,2-a]phenazine was isolated as a yellow solid. It was generated starting from both 4-indolol (104.1 mg, 0.475 mmol, 19% yield referred to the amount of substrate, 10 eq per equivalent catalyst [**O1**]$(PF_6)_2$) and 5-indolol (142.5 mg, 0.650 mmol, 26% yield referred to the amount of substrate, 13 eq per equivalent catalyst [**O1**]$(PF_6)_2$).

R_f = 0.64 (ethyl acetate/hexane 75:25)

^{1}H NMR (400 MHz, DMSO-d_6, 25 °C): δ [ppm] = 12.08 (s, 1H, NH), 8.30 – 8.22 (m, 2H, H4+H7), 8.06 (dd, J = 9.2, 0.9 Hz, 1H, H14), 7.93 – 7.84 (m, 2H, H5+H6), 7.79 (dd, J = 9.2, 0.4 Hz, 1H, H15), 7.58 – 7.55 (m, 1H, H2), 7.34 (ddd, J = 3.0, 2.1, 0.9 Hz, 1H, H3).

$^{13}C\{^1H\}$ NMR (101 MHz, DMSO-d_6, 25 °C): δ [ppm] = 141.8 (C12), 141.3 (C8), 140.7 (C9), 140.0 (C13), 133.8 (C17), 129.8 (C6), 129.2 (C4), 128.6 (C5), 128.6 (C7), 124.4 (C2), 122.2 (C15), 121.4 (C16), 121.4 (C14), 103.9 (C3).

HRMS-ESI+: m/z (%) calc. for $C_{14}H_9N_3$: 220.07965, found: 220.08656 (100).

IR (ATR): $\tilde{\nu}$ [cm^{-1}] = 3170 (w), 3133 (w), 3113 (w), 3093 (w), 3056 (w), 3002 (w), 2914 (vw), 2840 (vw), 1586 (m), 1541 (m), 1436 (m), 1353 (m), 1339 (m), 1136 (m), 1022 (m), 999 (vs), 893 (m), 828 (m), 729 (vs), 671 (w), 615 (w), 589 (s), 529 (s), 517 (m), 473 (m), 420 (s).

Additional information on the NMR spectra of the target compound including original data files is available via Chemotion Repository: https://dx.doi.org/10.14272/AEFJLSGXOWZNJZ-UHFFFAOYSA-N.1

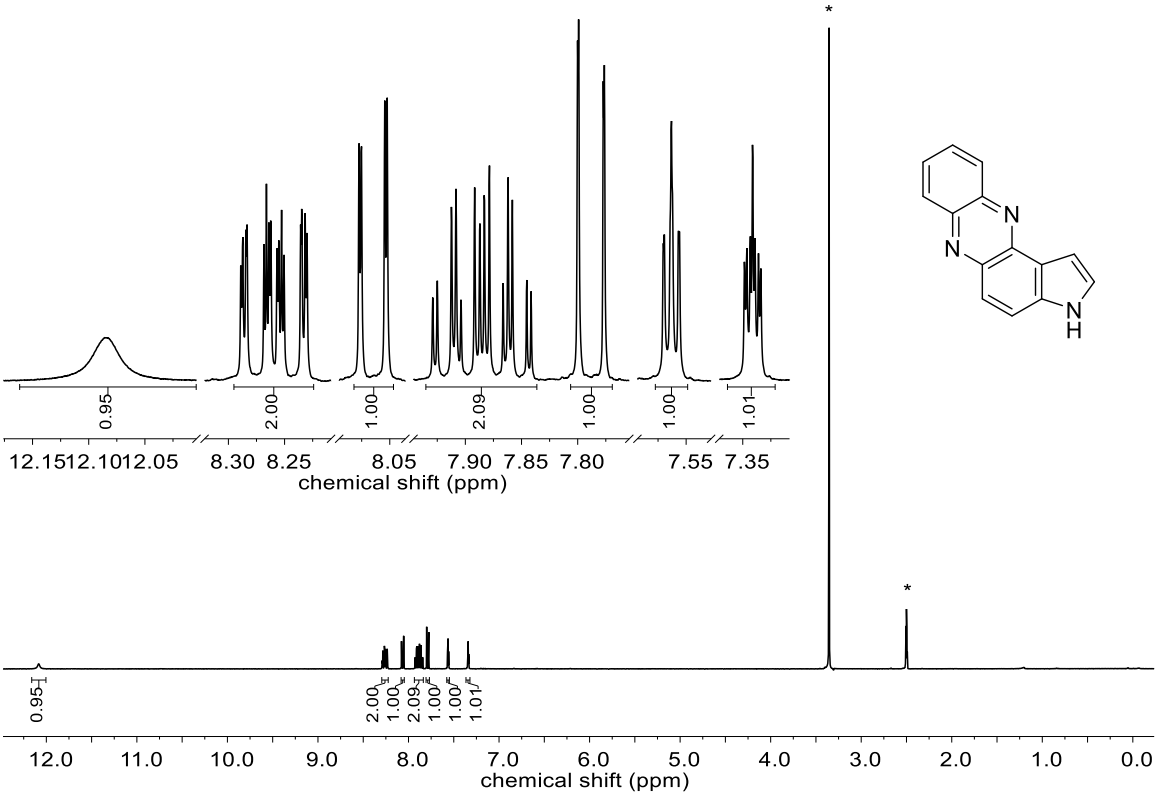

Figure S30: ^{1}H NMR spectrum of pyrrolo[3,2-a]phenazine resulting from oxygenation of 4-indolol and 5-indolol, respectively, mediated by [**O1**]$(PF_6)_2$ (0.5 mM) in tetrahydrofuran at -90 °C and subsequent condensation by using 1,2-phenylenediamine (* = DMSO-d_6).

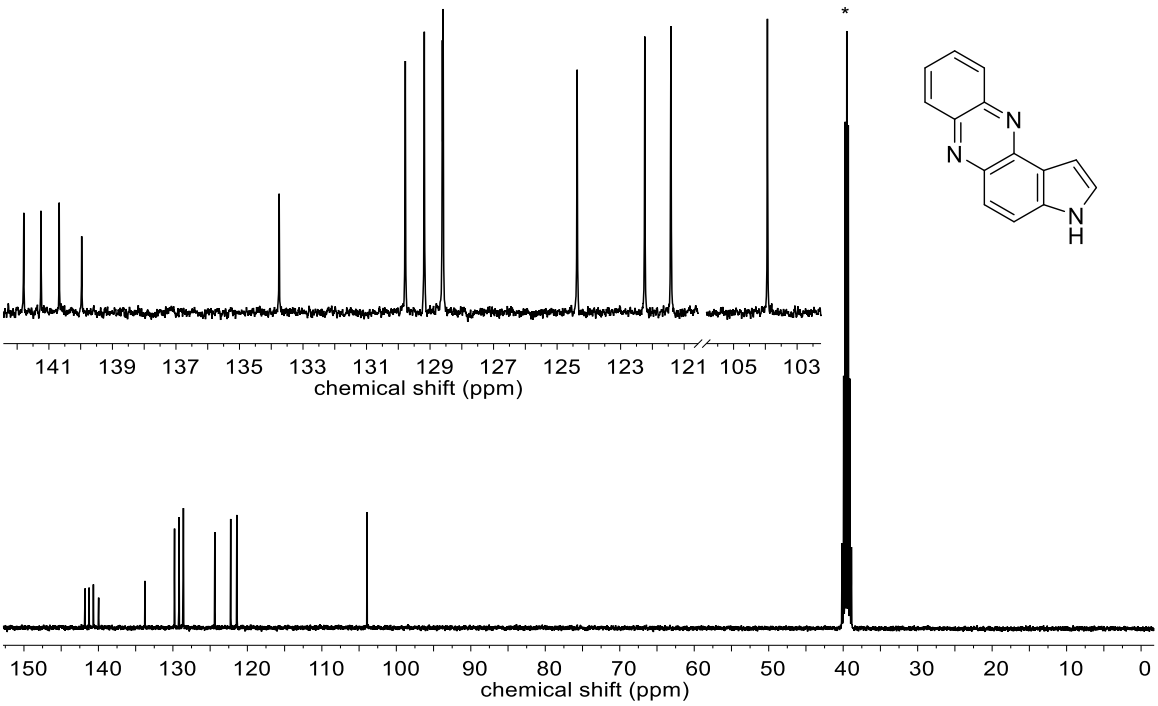

Figure S31: ^{13}C{^{1}H} NMR spectrum of pyrrolo[3,2-a]phenazine resulting from oxygenation of 4-indolol and 5-indolol, respectively, mediated by [**O1**]$(PF_6)_2$ (0.5 mM) in tetrahydrofuran at -90 °C and subsequent condensation by using 1,2-phenylenediamine (* = DMSO-d_6).

2.6.5. Synthesis of Pyrrolo[2,3-a]phenazine (P5)

All reactions were conducted according to protocol 2.6.

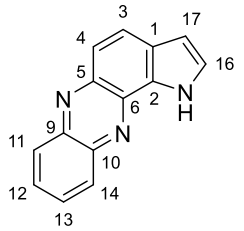

Chemical Formula: $C_{14}H_9N_3$
Molecular Weight: 219.25 g mol^{-1}

Pyrrolo[2,3-a]phenazine was isolated as a yellow solid. It was generated starting from both 6-indolol (148.0 mg, 0.675 mmol, 27% yield referred to the amount of substrate, 14 eq per equivalent catalyst [**O1**]$(PF_6)_2$) and 7-indolol (169.9 mg, 0.775 mmol, 31% yield referred to the amount of substrate, 16 eq per equivalent catalyst [**O1**]$(PF_6)_2$). Single crystals of **P5** suitable for X-ray diffraction were grown from a concentrated hexane solution.

R$_f$ = 0.46 (ethyl acetate/hexane 50:50)

^{1}H NMR (400 MHz, DMSO-d_6, 25 °C): δ [ppm] = 12.88 (s, 1H, NH), 8.30 – 8.23 (m, 2H, H11+H14), 8.13 (d, J = 9.1 Hz, 1H, H4), 7.91 (m, 2H, H12+H13), 7.70 (d, J = 9.0 Hz, 1H, H3), 7.57 (t, J = 2.7 Hz, 1H, H16), 6.80 – 6.77 (m, 1H, H17).

^{13}C{^{1}H} NMR (101 MHz, DMSO-d_6, 25 °C): δ [ppm] = 142.2 (C6), 140.9 (C10), 140.8 (C9), 134.8 (C2), 130.0 (C13), 129.3 (C11), 128.7 (C12), 128.2 (C14), 128.1 (C5), 128.0 (C4), 126.1 (C16), 126.0 (C1), 120.5 (C3), 104.9 (C17).

HRMS-EI: m/z calc. for $C_{14}H_9N_3$: 219.0791, found: 219.0799.

IR (ATR): $\tilde{\nu}$ [cm^{-1}] = 2962 (w), 2923 (w), 2854 (vw), 1400 (w), 1359 (w), 1259 (m), 1086 (m), 1011 (s), 896 (w), 866 (m), 790 (vs), 751 (m), 717 (m), 661 (m), 621 (w), 592 (w), 556 (w), 527 (m), 470 (m), 400 (m).

Additional information on the NMR spectra of the target compound including original data files is available via Chemotion Repository: https://dx.doi.org/10.14272/BMNLXKVRGRRHKW-UHFFFAOYSA-N.1

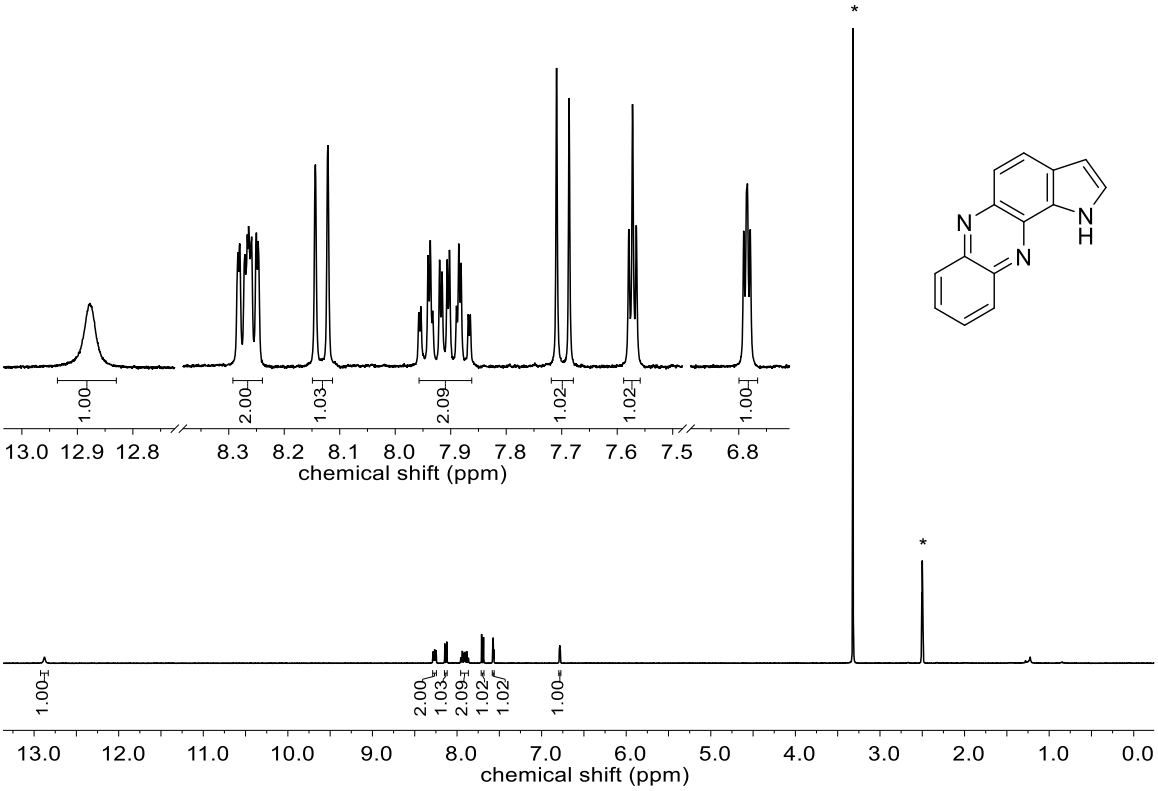

Figure S32: ^{1}H NMR spectrum of pyrrolo[2,3-a]phenazine resulting from oxygenation of 6-indolol and 7-indolol, respectively, mediated by [**O1**]$(PF_6)_2$ (0.5 mM) in tetrahydrofuran at -90 °C and subsequent condensation by using 1,2-phenylenediamine (* = DMSO-d_6).

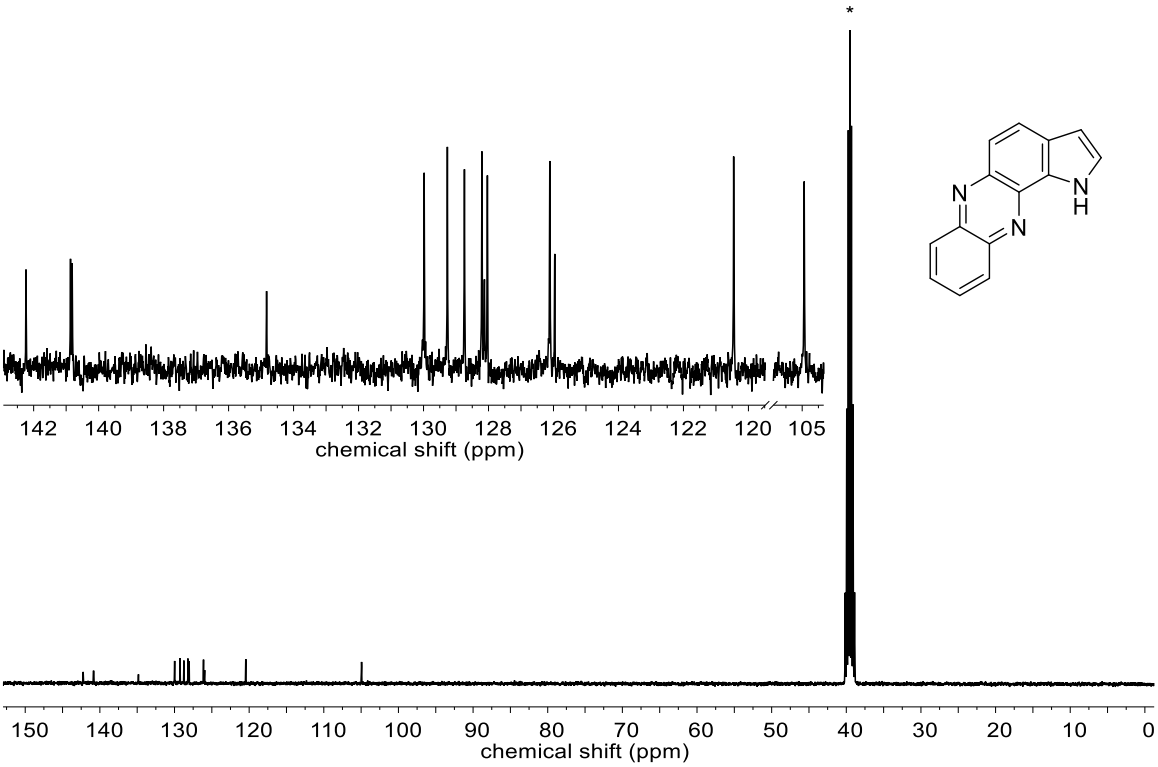

Figure S33: $^{13}C\{^{1}H\}$ NMR spectrum of pyrrolo[2,3-a]phenazine resulting from oxygenation of 6-indolol and 7-indolol, respectively, mediated by [**O1**]$(PF_6)_2$ (0.5 mM) in tetrahydrofuran at -90 °C and subsequent condensation by using 1,2-phenylenediamine (* = DMSO-d_6).

2.6.6. Reaction of Phenols, Pyridinols and 1-Methyl 2-Naphthol with [O1]$(PF_6)_2$

All reactions were conducted according to protocol 2.6.

Reaction of phenol and 2,4-di-*tert*-butyl phenol (Table S8, entry 1-2) with [**O1**]$(PF_6)_2$ led to an immediate color change of the solution to reddish-brown and a decrease of the absorption band at 392 nm. However, no formation of a new absorption band was observed in case of 2,4-di-*tert*-butyl phenol, neither at -90 °C nor at room temperature (Figure S38). In case of phenol, a broad shoulder between 350 nm and 550 nm was observed at -90 °C, which decreased upon warming up to room temperature. Cryo-UHR-ESI measurements of the reaction solution using phenol revealed a m/z value of 201.0885 (calculated 201.0546), which was attributed to the C-O coupled quinone $[M+H]^+$ (Table S8, entry 1), 223.1690 (calculated 223.0366) for $[M+Na]^+$. Reaction of 4-*tert*-butyl phenol and 4-methoxy phenol (Table S8, entry 3-4) with [**O1**]$(PF_6)_2$ revealed likewise a reddish-brown solution. A new absorption band was observed at 530 nm by using 4-methoxy phenol (Figure S39) and at 510 nm by using 4-*tert*-butyl phenol (Figure S40). Cryo-UHR-ESI measurements of the reaction solution using 4-*tert*-butyl phenol revealed a m/z value of 313.1276 (calculated 313.1325) which was attributed to the C-O coupled quinone $[M+H]^+$ (Table S8, entry 4), 414.3005 (calculated 414.3003) for $[M+HNEt_3]^+$. Using 4-methoxy phenol, a m/z value of 161.1072 (calculated 161.0209) was found which was assigned to the quinone $[M+Na]^+$ (Table S8, entry 3), 283.1440 (calculated 283.0577) for the C-O coupled quinone $[M+Na]^+$, 364.2704 (calculated 364.2118) for the C-O coupled quinone $[M+HNEt_3]^+$.

Reaction of pyridinols (Table S8, entries 5-6) with [**O1**]$(PF_6)_2$ led to an immediate color change to greyish-brown. After addition of the substrate solution, an absorption band at 375 nm was observed immediately in both cases, which decayed quickly afterwards, indicating a highly reactive quinone intermediate formed (Figure S42-43). Cryo-UHR-ESI measurements of the reaction solution using 3-pyridinol revealed a m/z value of 205.1530 (calculated 205.0608), which was attributed to the C-O coupled catechol $[M+H]^+$, 306.2537 (calculated 306.1812) for $[M+HNEt_3]^+$. Using 4-pyridinol, a likewise m/z value of 205.1529 for the C-O coupled catechol $[M+H]^+$ was found.

Considering the immediate color change of the reaction solution and the detected coupling products in cryo-UHR-ESI measurements by the use of a phenol and the shown reactivity of [**O1**]$(PF_6)_2$ towards more complex substrate classes (e.g. quinolinols, naphthols and

indolols), these findings underline a significant oxidative strength of [**O1**]$(PF_6)_2$ leading to very fast undesired side reactions even at low temperatures.

Reaction of 1-methyl 2-naphthol (Table S8, entry 7; Figure S46) with [**O1**]$(PF_6)_2$ led to a decrease of the absorption band at 392 nm. UV/Vis spectra revealed no new absorption band around 400 nm as expected, showing no product formation as the 1-position is occupied by the methyl substituent, thus inhibiting the oxygenation process.

Table S8: Reaction of phenolic substrates with [**O1**]$(PF_6)_2$ and consecutive reaction with 1,2-phenylenediamine according to scheme S8.

entry	substrate	product
1		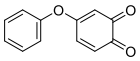
2	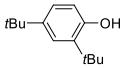	-
3	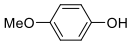	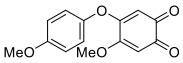
4	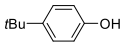	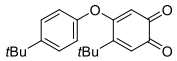
5		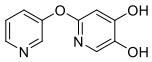
6		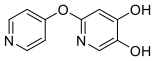
7	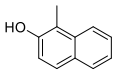	-

2.7. Control Experiments

2.7.1. Reaction of [O1]$(PF_6)_2$ with triethylamine

[**O1**]$(PF_6)_2$ was prepared according to protocol 2.5. After addition of triethylamine (0.07 mL) no immediate color change was observed. The reaction was followed by UV/Vis spectroscopy. At -90 °C, the decrease of the absorption band at 392 nm was observed over time (Figure S34). After 90 min the reaction solution discolored to light green.

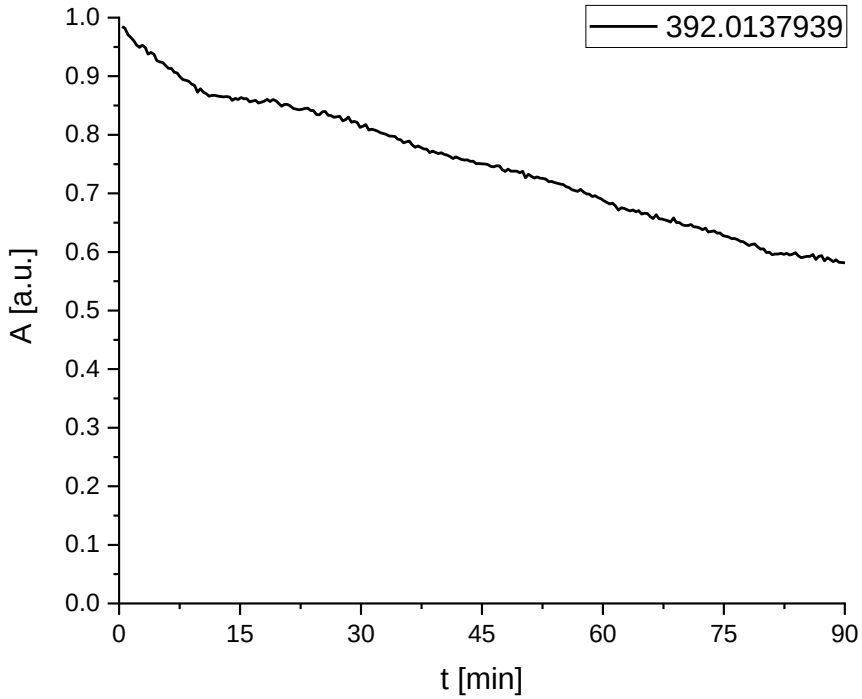

Figure S34: UV/Vis spectrum of the reaction of [**O1**]$(PF_6)_2$ (0.5 mM) with triethylamine in tetrahydrofuran at -90 °C monitored at 392 nm..

2.7.2. Reaction of [O1]$(PF_6)_2$ with 1,2-phenylenediamine

The control experiment was conducted according to protocol 2.6 without adding a substrate solution. Reaction of [**O1**]$(PF_6)_2$ with 1,2-phenylenediamine led to an immediate color change to violet. The reaction was followed by UV/Vis spectroscopy. At -90 °C, the decrease of the absorption band at 392 nm and simultaneously the formation of absorption bands at 520, 665 and 950 nm were observed (Figure S35). Upon warming to room temperature, absorption bands at 550 and 900 nm were formed. Cryo-UHR-ESI measurements of the reaction solution revealed a m/z value of 417.1832 (calculated to 417.1828 and attributed to [Cu(**L1**)(1,2-NH-NH-Ph)]$^+$), a m/z value of 418.1855 (calculated to 418.1906 and attributed to [Cu(**L1**)(1,2-NH-NH_2-Ph)]$^+$) and a m/z value of 419.1811 (calculated to 419.1984 and attributed to [Cu(**L1**)(1,2-NH_2-NH_2-Ph)]$^+$. Upon warming of the reaction solution to room temperature, UHR-ESI measurements of the reaction solution exhibited, in addition to those values mentioned above, a m/z value of 275.0356 (calculated 275.0358), which was assigned to [Cu(1,2-NH-NH-Ph)$_2$]$^+$.

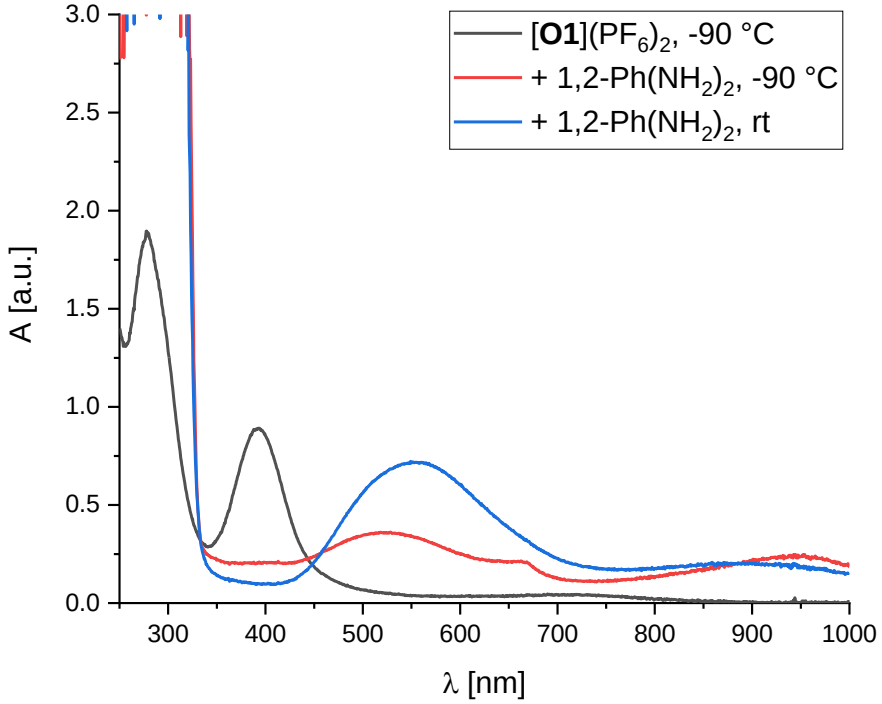

Figure S35: UV/Vis spectra of the reaction of 1,2-phenylenediamine with [**O1**]$(PF_6)_2$ (0.5 mM) in tetrahydrofuran at -90 °C and room temperature.

2.7.3. Reaction of 6-indolol with $[Cu(MeCN)_4]PF_6$ (1.0 mM) in the presence of O_2

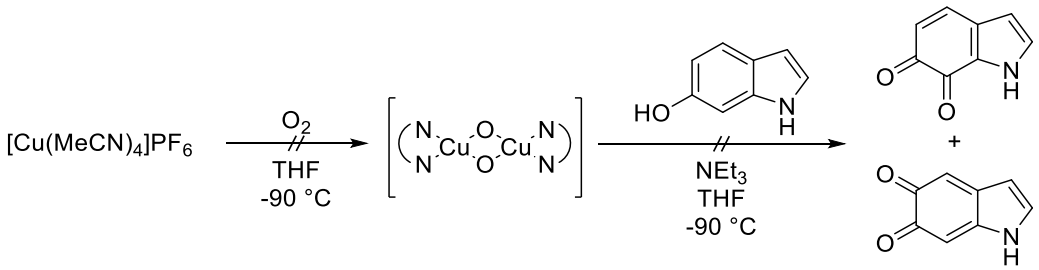

Scheme S9: Reaction of 6-indolol with $[Cu(MeCN)_4]PF_6$ (1.0 mM) in the presence of O_2 in tetrahydrofuran at -90 °C.

The control experiment was conducted according to protocol 2.6 without the ligand to proof the necessity of a stabilizing ligand system for the catalyst. Reaction of copper salt with molecular dioxygen revealed no visible absorbance in the UV/Vis spectrum within 20 min, indicating no formation of bis(μ-oxo) dicopper(III) species. Addition of a 6-indolol solution only led to the formation of a shoulder at 330 nm, which was referred to the substrate itself (Figure S36).

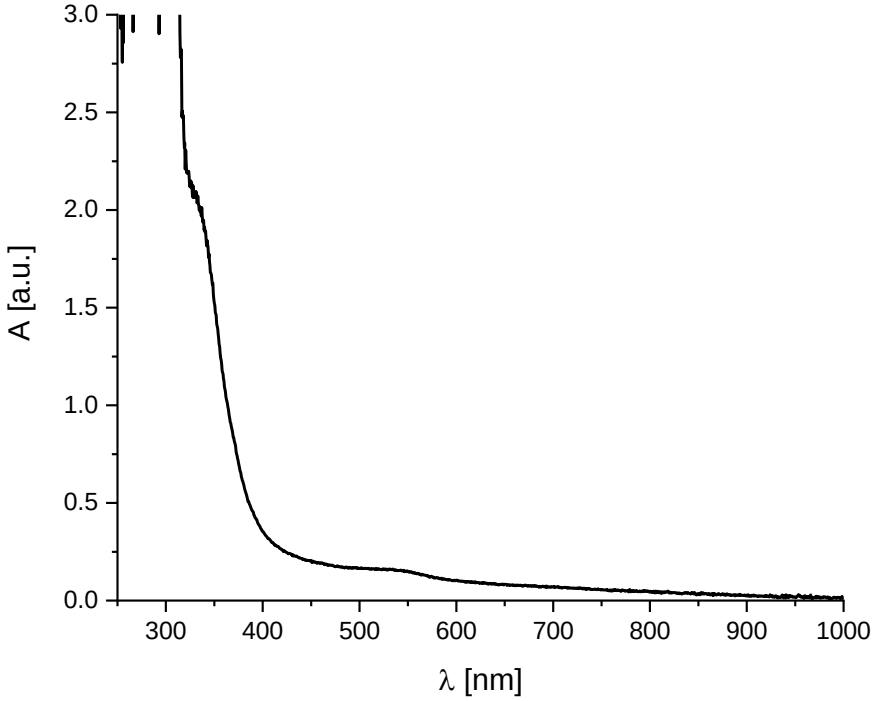

Figure S36: UV/Vis spectra of the reaction of 6-indolol with $[Cu(MeCN)_4]PF_6$ (0.5 mM) in the presence of O_2 in tetrahydrofuran at -90 °C.

2.8. UV/Vis Spectra and EPR Spectra of the Reaction of Phenolic Substrates with $[O1](PF_6)_2$

2.8.1. UV/Vis Spectra and EPR Spectra of the Reaction of Phenols with $[O1](PF_6)_2$

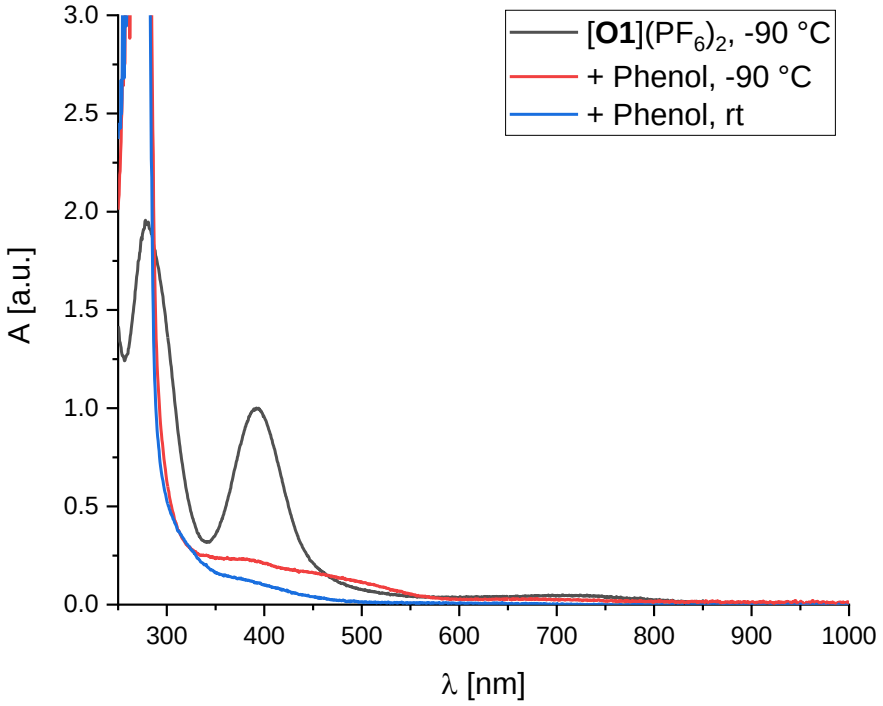

Figure S37: UV/Vis spectra of the reaction of phenol with **[O1]**$(PF_6)_2$ (0.5 mM) in tetrahydrofuran at -90 °C and room temperature.

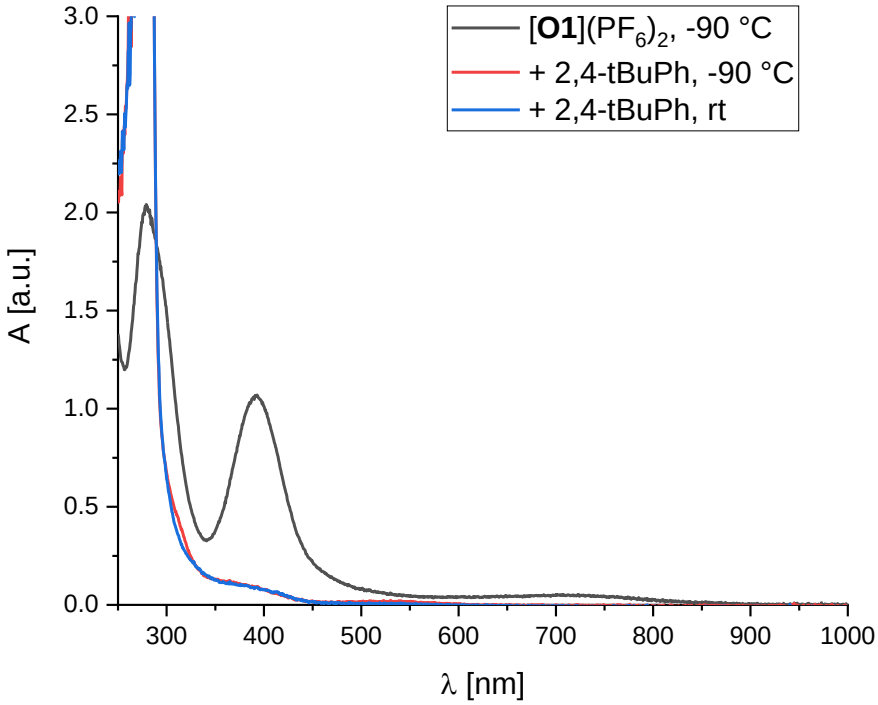

Figure S38: UV/Vis spectra of the reaction of 2,4-di-*tert*-butyl phenol with [**O1**]$(PF_6)_2$ (0.5 mM) in tetrahydrofuran at -90 °C and room temperature.

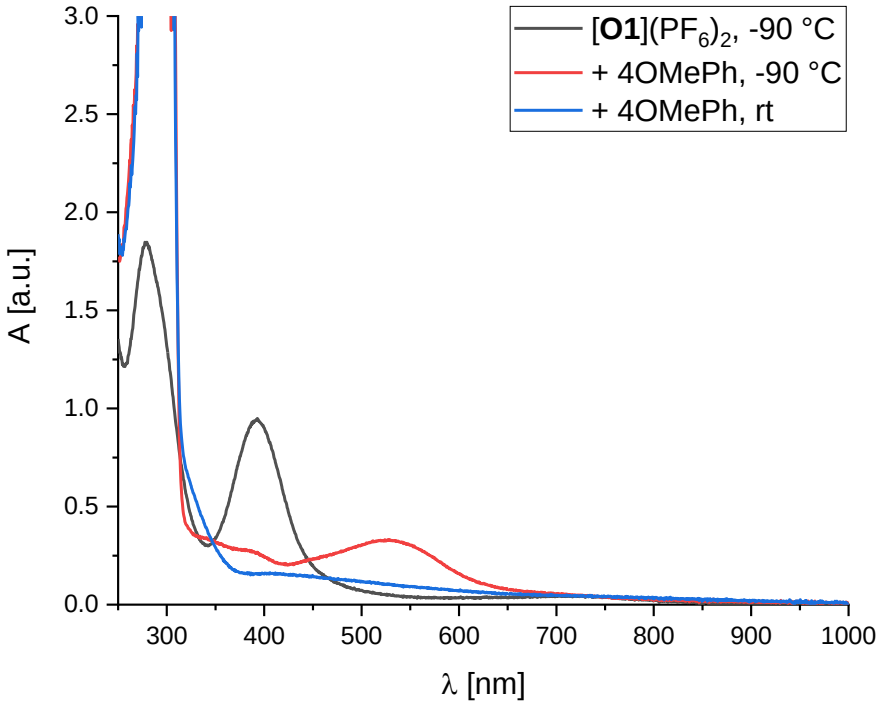

Figure S39: UV/Vis spectra of the reaction of 4-methoxy phenol with [**O1**]$(PF_6)_2$ (0.5 mM) in tetrahydrofuran at -90 °C and room temperature.

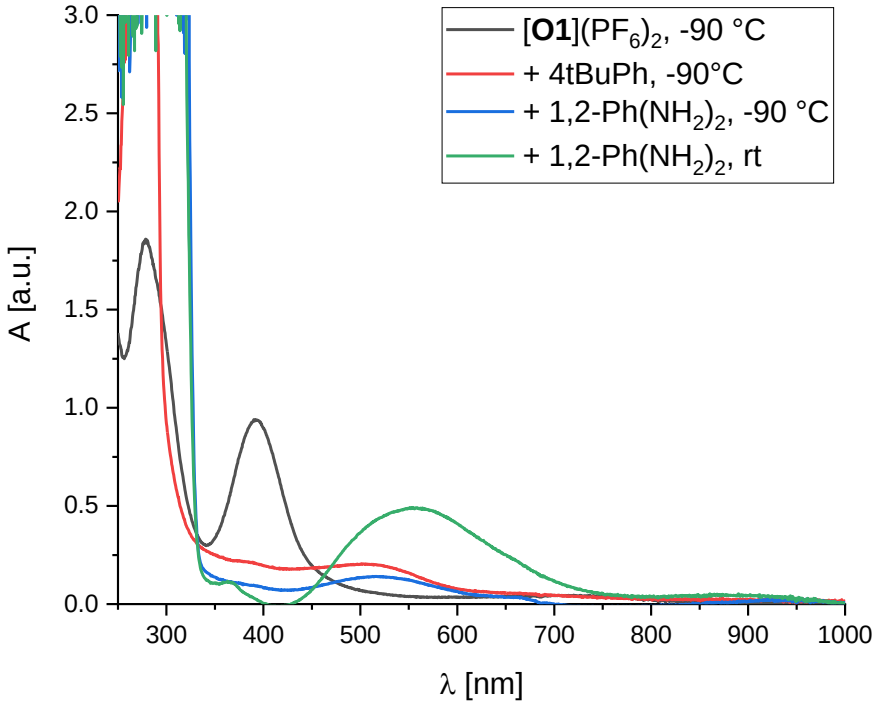

Figure S40: UV/Vis spectra of the reaction of 4-*tert*-butyl phenol with [**O1**]$(PF_6)_2$ (0.5 mM) in tetrahydrofuran at -90 °C and subsequent reaction with 1,2-phenylenediamine.

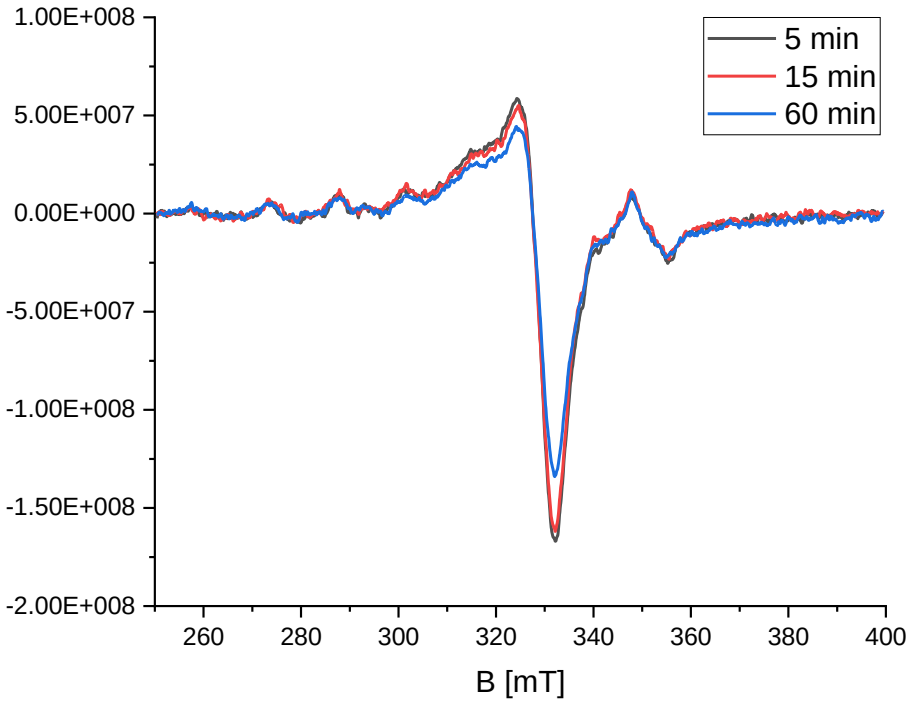

Figure S41: X-Band EPR spectra of the reaction of 4-*tert*-butyl phenol with [**O1**]$(PF_6)_2$ (4.0 mM) in tetrahydrofuran (experimental parameters: temperature 77 K, microwave frequency 9.427 GHz, B_0 field 324.9581 mT, modulation 0.2000 mT, the signal at 351 mT was referred to the Duran® glass capillary containing iron(III) impurities).

2.8.2. UV/Vis Spectra of the Reaction of Pyridinols with [O1](PF$_6$)$_2$

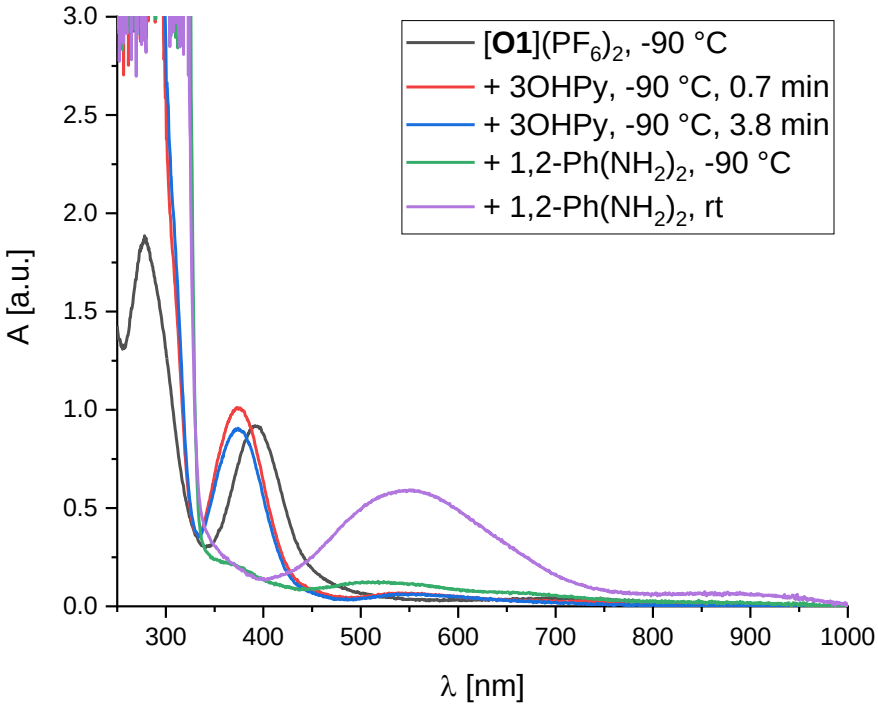

Figure S42: UV/Vis spectra of the reaction of 3-pyridinol with [**O1**](PF$_6$)$_2$ (0.5 mM) in tetrahydrofuran at -90 °C and subsequent reaction with 1,2-phenylenediamine.

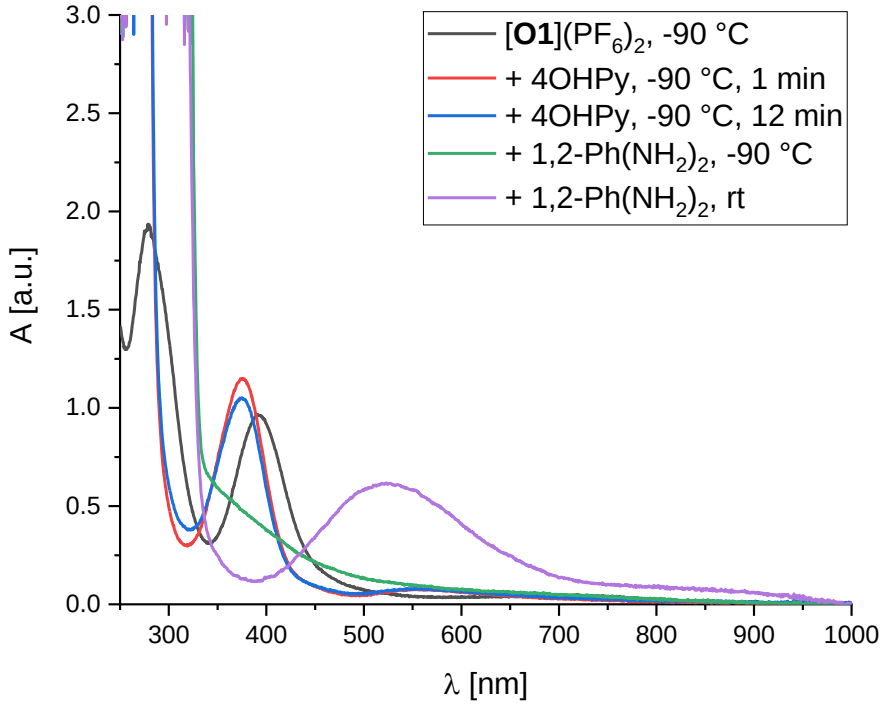

Figure S43: UV/Vis spectra of the reaction of 4-pyridinol with [**O1**](PF$_6$)$_2$ (0.5 mM) in tetrahydrofuran at -90 °C and subsequent reaction with 1,2-phenylenediamine.

2.8.3. UV/Vis Spectra of the Reaction of Naphthols with [O1](PF$_6$)$_2$

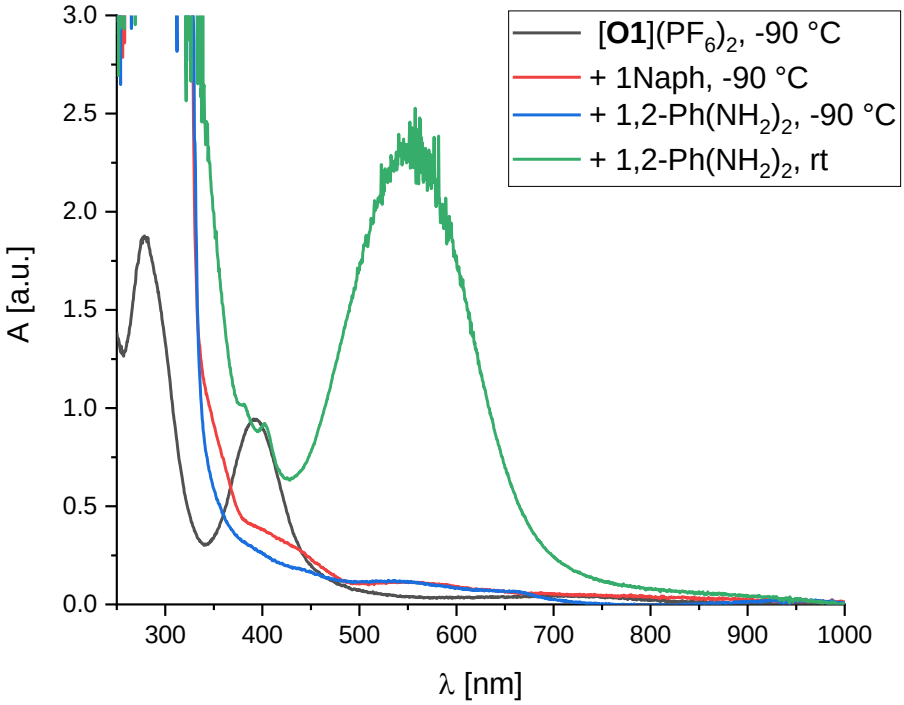

Figure S44: UV/Vis spectra of the reaction of 1-naphthol with [**O1**](PF$_6$)$_2$ (0.5 mM) in tetrahydrofuran at -90 °C and subsequent reaction with 1,2-phenylenediamine.

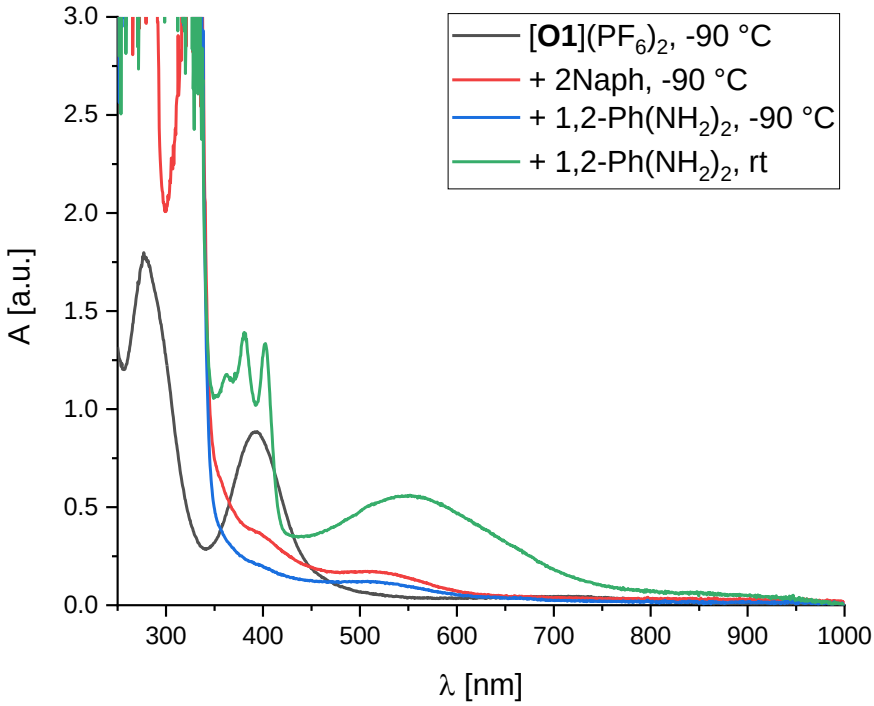

Figure S45: UV/Vis spectra of the reaction of 2-naphthol with [**O1**](PF$_6$)$_2$ (0.5 mM) in tetrahydrofuran at -90 °C and subsequent reaction with 1,2-phenylenediamine.

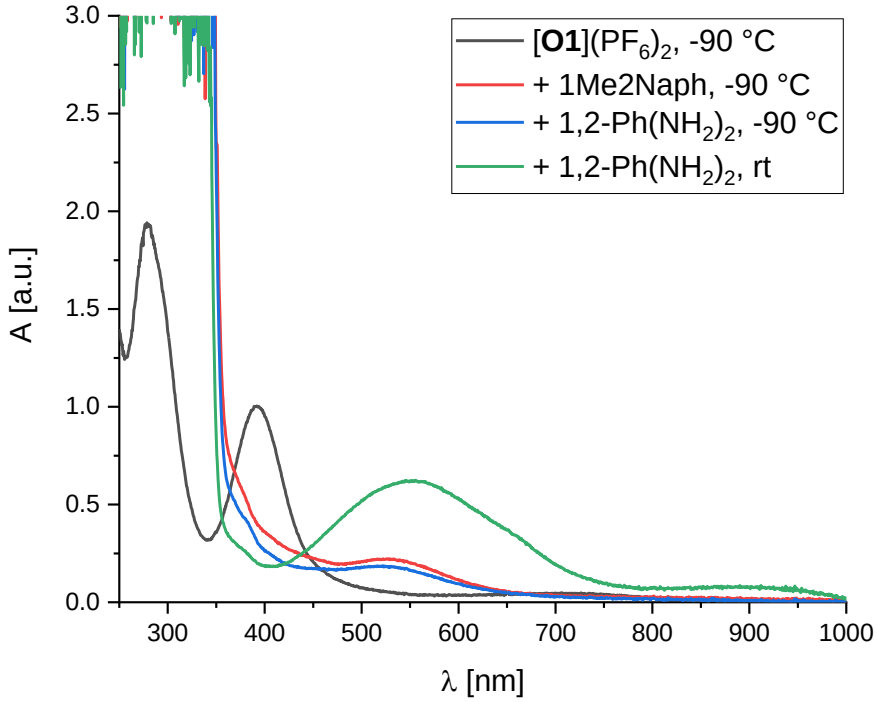

Figure S46: UV/Vis spectra of the reaction of 1-methyl 2-naphthol with [**O1**]$(PF_6)_2$ (0.5 mM) in tetrahydrofuran at -90 °C and subsequent reaction with 1,2-phenylenediamine.

2.8.4. UV/Vis Spectra of the Reaction of Quinolinols with [O1]$(PF_6)_2$

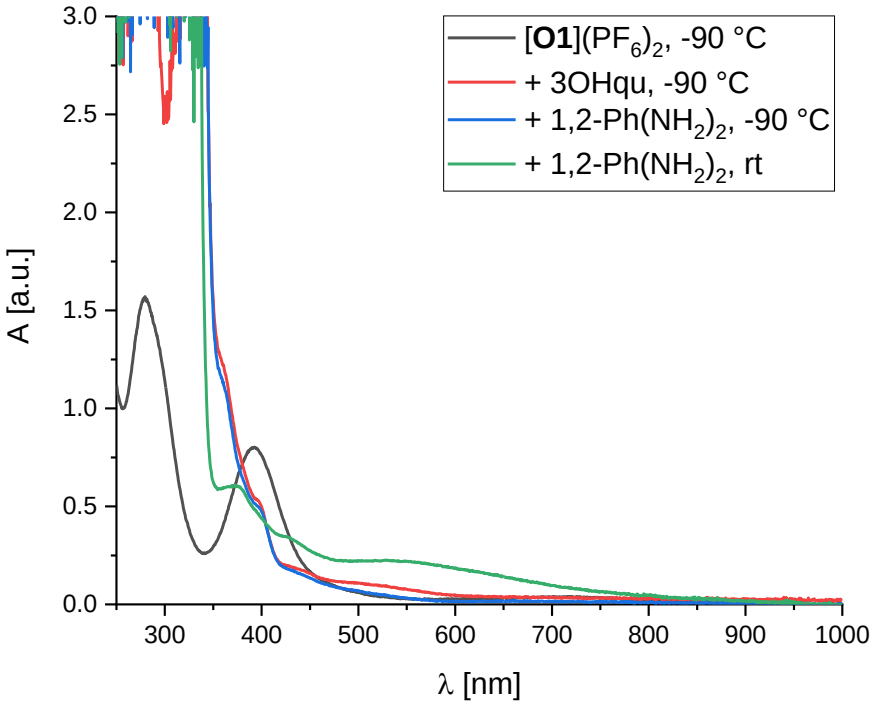

Figure S47: UV/Vis spectra of the reaction of 3-quinolinol with [**O1**]$(PF_6)_2$ (0.5 mM) in tetrahydrofuran at -90 °C and subsequent reaction with 1,2-phenylenediamine.

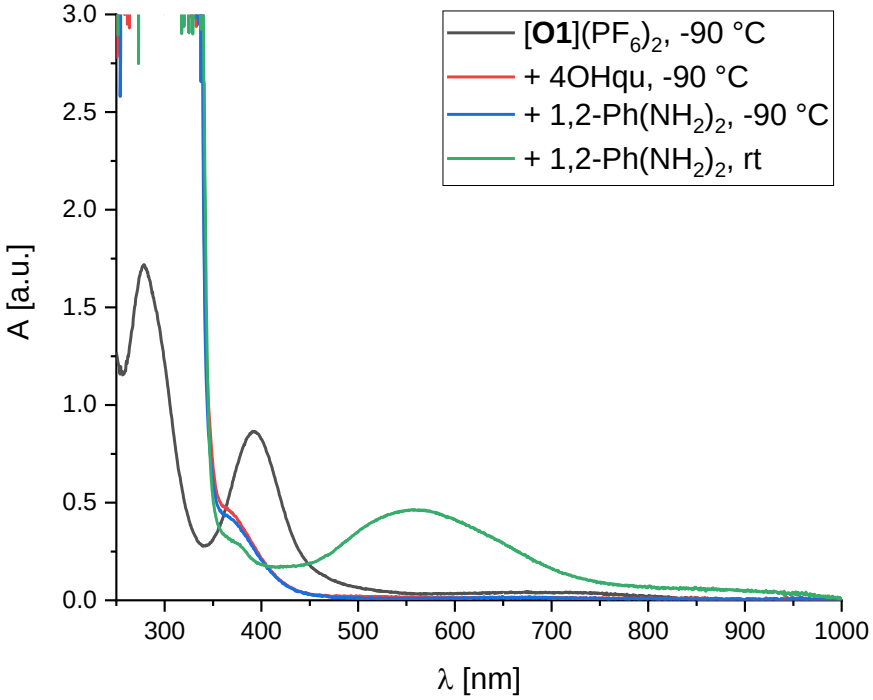

Figure S48: UV/Vis spectra of the reaction of 4-quinolinol with [**O1**]$(PF_6)_2$ (0.5 mM) in tetrahydrofuran at -90 °C and subsequent reaction with 1,2-phenylenediamine.

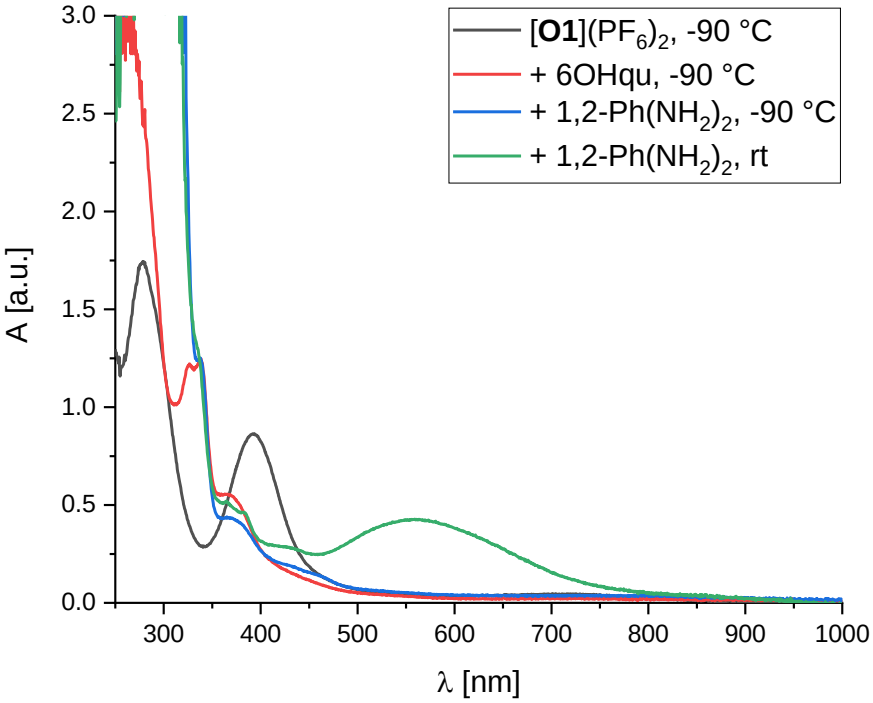

Figure S49: UV/Vis spectra of the reaction of 6-quinolinol with [**O1**]$(PF_6)_2$ (0.5 mM) in tetrahydrofuran at -90 °C and subsequent reaction with 1,2-phenylenediamine.

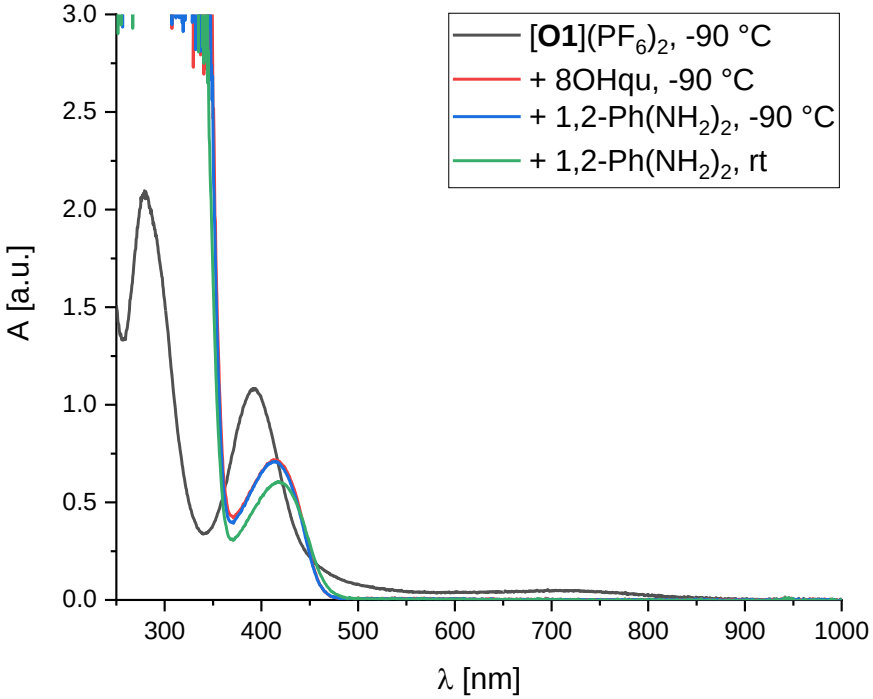

Figure S50: UV/Vis spectra of the reaction of 8-quinolinol with [**O1**]$(PF_6)_2$ (0.5 mM) in tetrahydrofuran at -90 °C and subsequent reaction with 1,2-phenylenediamine.

Oxygenation of 8-quinolinol by the use of [**O1**]$(PF_6)_2$ led to an intense absorption band at 416 nm in the UV/Vis spectrum (Figure S50), indicating the formation of 7,8-quinolinedione (TON = 12 after 1.4 min, TON = 14 after 12 min).[31] Similarly, oxygenation of 2-methyl 8-quinolinol revealed an absorption band at 402 nm in the UV/Vis spectrum (Figure S51), indicating the formation of 2-methyl 7,8-quinolinedione (TON = 12 after 22 min).[31] However, condensation of the quinone with 1,2-phenylenediamine led to no formation of the corresponding phenazine product.

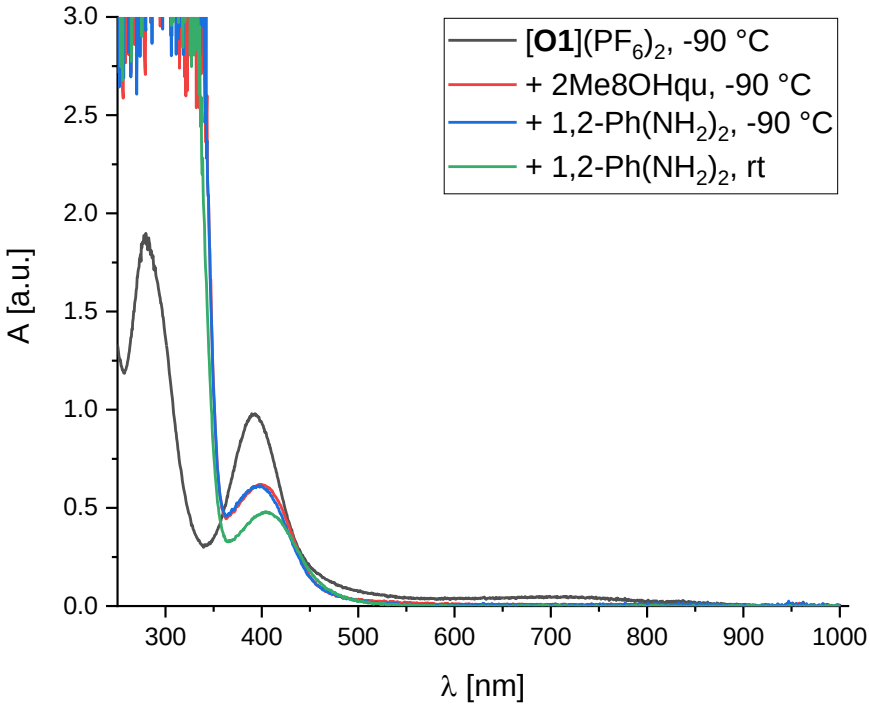

Figure S51: UV/Vis spectra of the reaction of 2-methyl-8-quinolinol with [**O1**]$(PF_6)_2$ (0.5 mM) in tetrahydrofuran at -90 °C and subsequent reaction with 1,2-phenylenediamine.

2.8.5. UV/Vis Spectra of the Reaction of Indolols with [O1](PF$_6$)$_2$

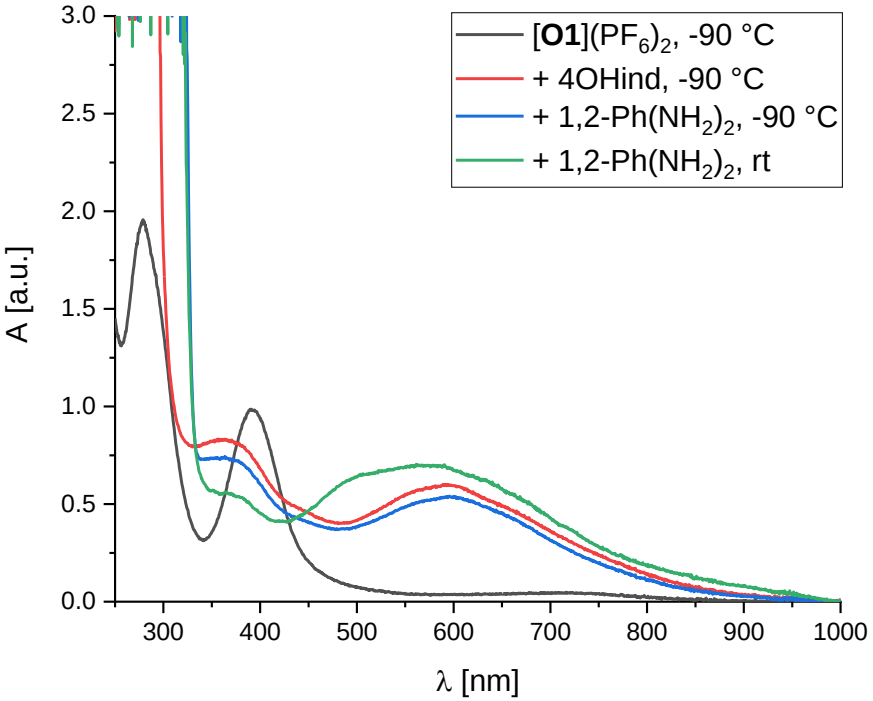

Figure S52: UV/Vis spectra of the reaction of 4-indolol with [**O1**](PF$_6$)$_2$ (0.5 mM) in tetrahydrofuran at -90 °C and subsequent reaction with 1,2-phenylenediamine.

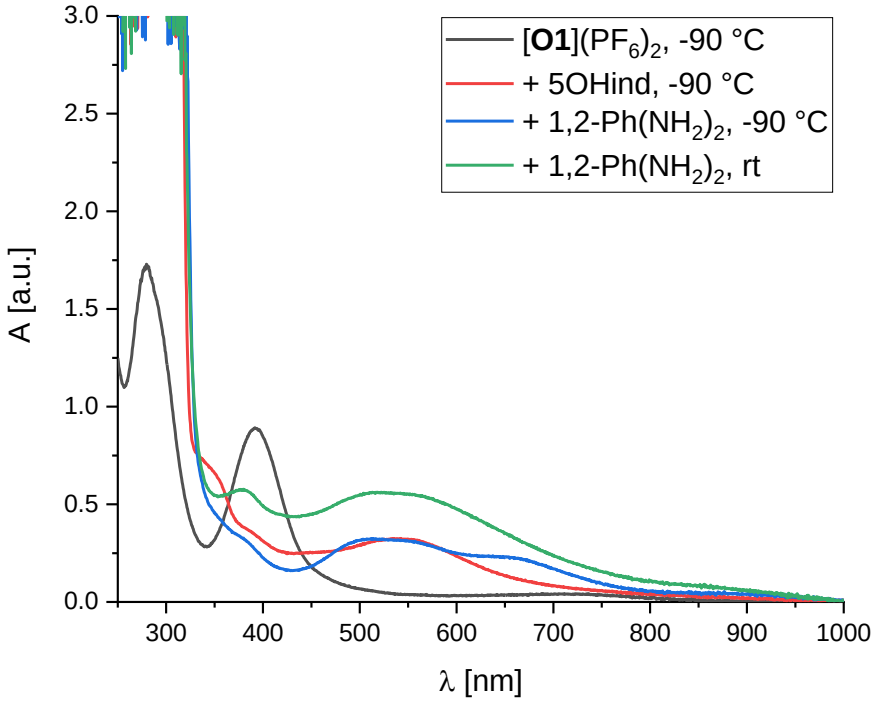

Figure S53: UV/Vis spectra of the reaction of 5-indolol with [**O1**](PF$_6$)$_2$ (0.5 mM) in tetrahydrofuran at -90 °C and subsequent reaction with 1,2-phenylenediamine.

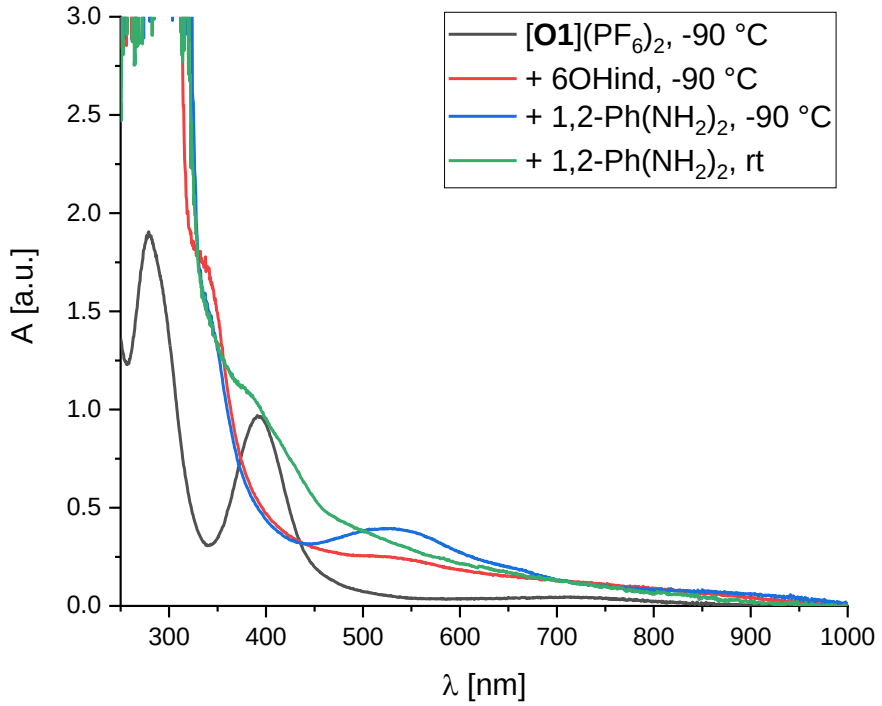

Figure S54: UV/Vis spectra of the reaction of 6-indolol with [**O1**]$(PF_6)_2$ (0.5 mM) in tetrahydrofuran at -90 °C and subsequent reaction with 1,2-phenylenediamine.

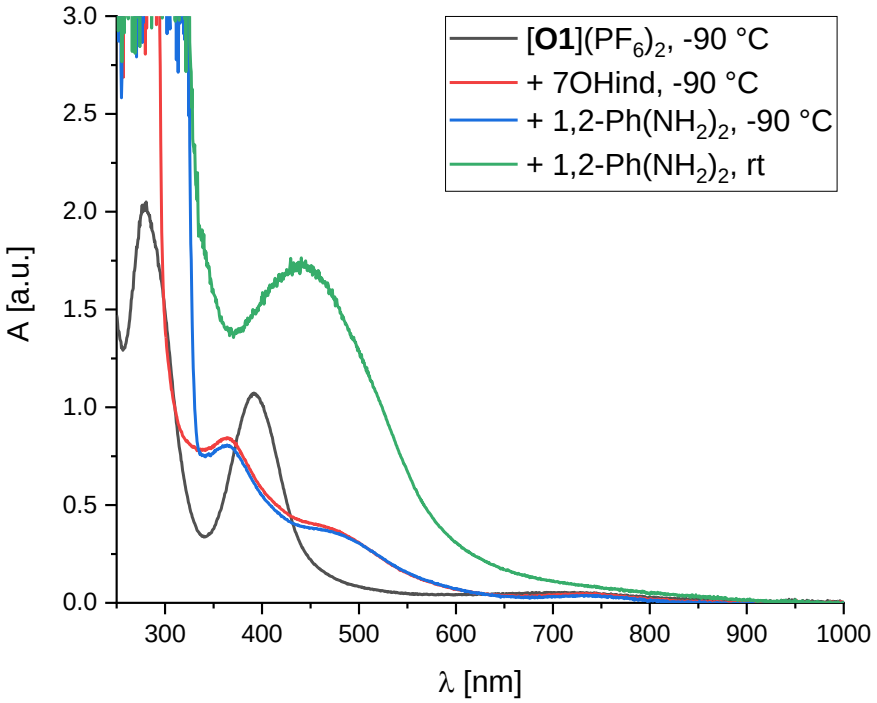

Figure S55: UV/Vis spectra of the reaction of 7-indolol with [**O1**]$(PF_6)_2$ (0.5 mM) in tetrahydrofuran at -90 °C and subsequent reaction with 1,2-phenylenediamine.

2.9. Crystallographic Data of Phenazines

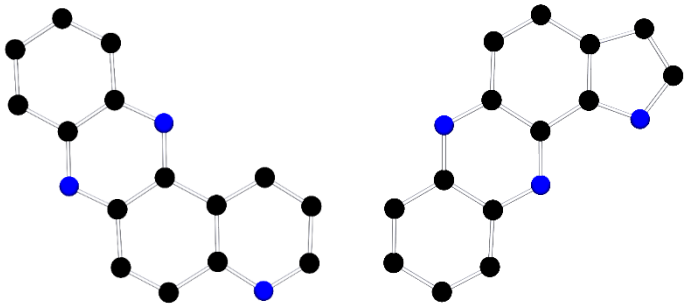

Figure S56: Molecular structures of **P3** and **P5** in the solid state. Hydrogen atoms were omitted for clarity.

Table S9: Crystallographic data and parameters of catalysis products **P3** and **P5**.

	P3	**P5**
Empirical formula	$C_{15}H_9N_3$	$C_{14}H_9N_3$
Formula weight [g mol^{-1}]	231.25	219.24
T [K]	100	100
λ [Å]	1.54186	1.54186
Crystal system	Monoclinic	Orthorhombic
Space group	P2(1)/c	Pbca
a [Å]	15.982(3)	6.9990(14)
b [Å]	4.9914(10)	13.519(3)
c [Å]	13.623(3)	21.134(4)
α [°]	90	90
β [°]	93.90(3)	90
γ [°]	90	90
V [Å^3]	1084.2(4)	1999.6(7)
Z	4	8
ρ_{calc} [g cm^{-3}]	1.417	1.457
μ [mm^{-1}]	0.691	0.714
F(000)	480	912
Crystal size [mm]	0.230 x 0.110 x 0.040	0.170 x 0.140 x 0.080
hkl range	±17, ±5, -14 ≤ l ≤ 12	-8 ≤ h ≤ 6, -15 ≤ k ≤ 12, ±24
Reflections collected	6345	11866
Independent reflections	1546	1689
R_{int}	0.0572	0.0562

Number of parameters	163	154
R_1 [I≥2σ(I)]	0.0868	0.0730
wR_2 (all data)	0.2424	0.1713
Goodness-of-fit	1.140	1.207
Largest diff. peak hole [eÅ^{-3}]	0.273, -0.245	0.282, -0.258
CCDC	1950656	1950657

2.10. Reactivity of Tyrosinase

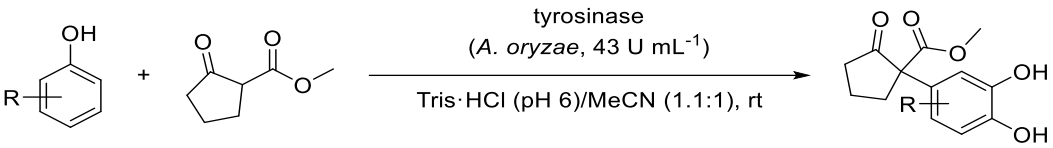

Scheme S10: Oxygenation of phenolic substrates mediated by tyrosinase and subsequent Michael addition to a cyclopentanone ester.

Reactivity studies of tyrosinase (from *A. oryzae*) were performed according to a published procedure.[33] The tyrosinase (with a volumetric activity of 43 U mL^{-1}) was dissolved in Tris·HCl buffer (pH 6) and treated with an acetonitrile solution of a phenolic substrate in the presence of CH-acidic cyclopentanone-2-carboxylic acid methyl ester at room temperature. The reaction was followed by thin-layer chromatography and NMR spectroscopy. Conversion of phenol mediated by tyrosinase led to the arylation product in 65% isolated yield (Table S10, entry 1).[33] However, using the same batch of tyrosinase, even after three days 1-naphthol, 2-naphthol as well as 6-quinolinol were not converted into the corresponding arylation products (Table S10, entries 2-4).

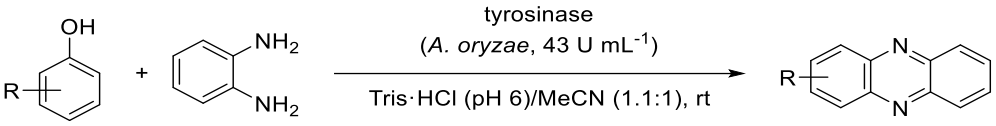

Scheme S11: Oxygenation of phenolic substrates mediated by tyrosinase and subsequent reaction with 1,2-phenylenediamine.

Reactivity studies of tyrosinase towards phenolic substrates were also performed in the presence of 1,2-phenylendiamine to give a phenazine product. However, conversion of phenol yielded no formation of phenazine after several days (Table S10, entry 5). Only polymer traces were detected. By using different indolols, the formation of various side products to a lesser extent was observed *via* NMR spectroscopy (Table S10, entries 6-9).

Table S10: Reactivity studies of tyrosinase.

entry	substrate	additive	time [d]	yield [%]
1	phenol	cyclopentanone ester (1.2 eq)	1	65
2	1-naphthol	cyclopentanone ester (1.2 eq)	3	0
3	2-naphthol	cyclopentanone ester (1.2 eq)	3	0
4	6-quinolinol	cyclopentanone ester (1.2 eq)	3	0
5	phenol	1,2-phenylenediamine (1.2 eq)	several	0
6	4-indolol	1,2-phenylenediamine (1.2 eq)	3	traces[a]
7	5-indolol	1,2-phenylenediamine (1.2 eq)	3	traces[a]

8	6-indolol	1,2-phenylenediamine (1.2 eq)	3	traces[a]
9	7-indolol	1,2-phenylenediamine (1.2 eq)	3	traces[a]

[a] Detection of undefined products in traces.

3. DFT Calculations

3.1. Energies, Geometric and Spectroscopic Parameters of the Active Species

Table S11: Energies of the theoretical Cu_2O_2 species (TPSSh/def2-TZVP, GD3BJ, THF-PCM):

	S^2	E [H]	Delta E [kcal mol^{-1}]
Bis(μ-oxo)		-4965.99338370	0.00
Peroxo		-4965.97488710	11.61
Peroxo BS	0.41	-4965.97724910	10.12

Table S12: Geometric parameters of the theoretical Cu_2O_2 species (TPSSh/def2-TZVP, GD3BJ, THF-PCM):

	Cu···Cu [Å]	Cu-N(gua) [Å]	Cu-N(amine) [Å]	Cu-O [Å]	O-O [Å]
Bis(μ-oxo)	2.750	1.914//1.915	1.963//1.965	1.800/1.806//1.801/1.804	2.331
Peroxo	3.527	1.932//1.931	1.998//2.000	1.900/1.921//1.900/1.928	1.473
Peroxo BS	3.542	1.932//1.932	2.000//1.997	1.938/1.905//1.909/1.931	1.487

Table S13: Spectroscopic parameters of the theoretical bis(μ-oxo) species (TPSSh/def2-TZVP, GD3BJ, THF-PCM):

	$\tilde{\nu}$ ($^{16}O_2$) [cm^{-1}]	$\tilde{\nu}$ ($^{18}O_2$) [cm^{-1}]	$\tilde{\nu}$ (N(amin)-Cu in $Cu_2{}^{16}O_2$) [cm^{-1}]	$\tilde{\nu}$ (N(amin)-Cu in $Cu_2{}^{18}O_2$) [cm^{-1}]
Raman	636	607	517	516
IR	681	652	512	511

3.2. Fukui Function of Phenolic Substrates

Table S14: Fukui function of phenolic substrates (TPSSh/def2-TZVP, GD3BJ).

phenolic substrate	Fukui function (f_k^-)
2-naphthol (entry 4 of Table 1)	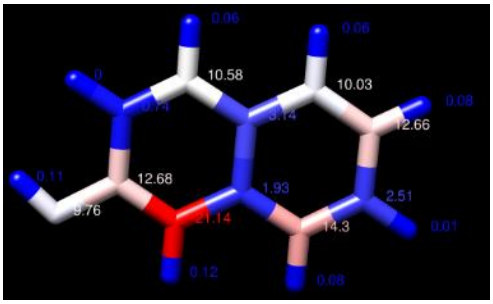
3-quinolinol (entry 5 of Table 1)	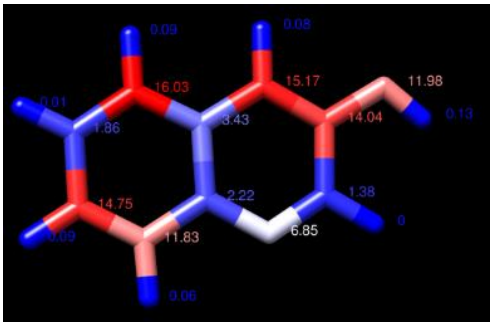
6-quinolinol (entry 7 of Table 1)	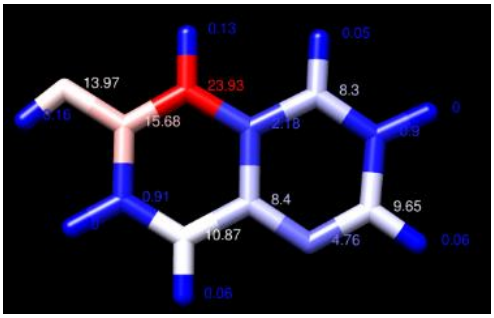
5-indolol (entry 11 of Table 1)	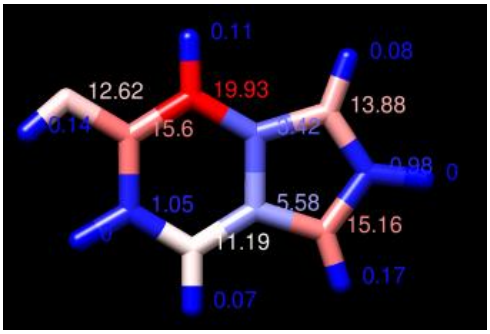

6-indolol (entry 12 of Table 1)	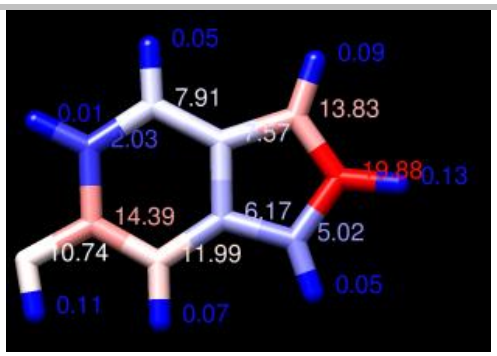

Calculation of the electrophilic Fukui function of 2-naphthol predicts a value of 21 for the carbon atom on 1-position and a value of 0.7 for the carbon in 3-position, hence, indicating that an electrophilic attack would be favored in 1-position.
Calculation of the electrophilic Fukui function of 3-quinolinol predicts a value of 1.3 for the carbon atom on 2-position and a value of 15 for the carbon in 4-position, hence, indicating that an electrophilic attack would be favored in 4-position.
Calculation of the electrophilic Fukui function of 6-quinolinol predicts a value of 23 for the carbon atom on 5-position and a value of 0.9 for the carbon in 7-position, hence, indicating that an electrophilic attack would be favored in 5-position.
Calculation of the electrophilic Fukui function of 5-indolol predicts a value of 19 for the carbon atom on 4-position and a value of 1.05 for the carbon in 6-position, hence, indicating that an electrophilic attack would be favored in 4-position.
Calculation of the electrophilic Fukui function of 6-indolol predicts a value of 2 for the carbon atom on 5-position and a value of 11 for the carbon in 7-position, hence, indicating that an electrophilic attack would be favored in 7-position.

3.3. Fukui Function of Quinones of the Phenolic Substrates

Table S15: Fukui function of quinones of the phenolic substrates (TPSSh/def2-TZVP, GD3BJ.

quinone	Fukui function (f_k^+)
quinoline-3,4-dione	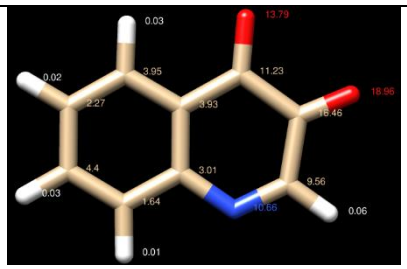
quinoline-5,6-dione	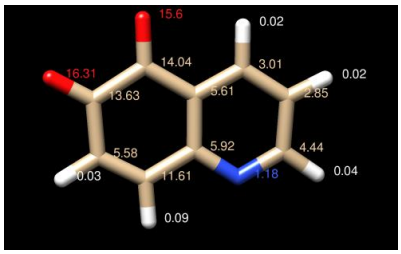
quinoline-7,8-dione	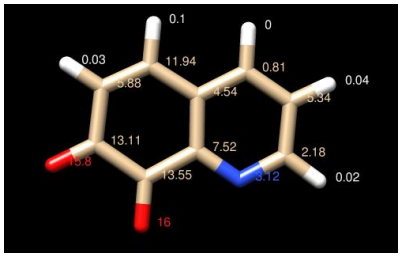

2-methyl quinoline-7,8-dione	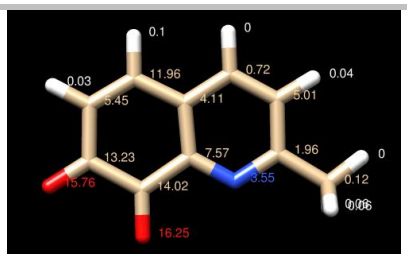
indole-4,5-dione	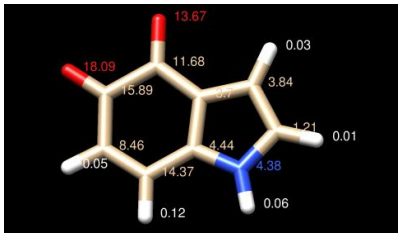
indole-6,7-dione	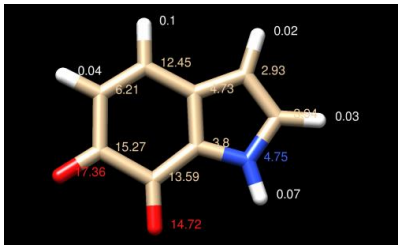

References

[1] G. J. Kubas, B. Monzyk, A. L. Crumbliss, *Inorg. Synth.*, **1979**, 90–92.

[2] V. Raab, J. Kipke, R. M. Gschwind, J. Sundermeyer, *Chem. Eur. J.* **2002**, *8*, 1682–1693.

[3] W. Kantlehner, E. Haug, W. W. Mergen, P. Speh, T. Maier, J. J. Kapassakalidis, H.-J. Bräuner, H. Hagen, *Liebigs Ann. Chem.* **1984**, *1984*, 108–126.

[4] S. Herres-Pawlis, A. Neuba, O. Seewald, T. Seshadri, H. Egold, U. Flörke, G. Henkel, *Eur. J. Org. Chem.* **2005**, *2005*, 4879–4890.

[5] a) P. Tremouilhac,A. Nguyen, Y.-C. Huang, S. Kotov, D. S. Lütjohann, F. Hübsch, N. Jung, S. Bräse, *J. Chemoinform.* **2017**, *9*, 54; b) https://chemotion.net/

[6] B. Schulz, J. Bäckström, D. Budelmann, R. Maeser, M. Rübhausen, M. V. Klein, E. Schoeffel, A. Mihill, S. Yoon, *Rev. Sci. Instrum.* **2005**, *76*, 073107-1-073107–12.

[7] B. Grimm-Lebsanft, C. Brett, F. Strassl, D. Rukser, M. Biednov, F. Biebl, M. Naumova, A. Hoffmann, L. Akinsinde, D. Brückner, S. Herres-Pawlis, M. Rübhausen, *Inorg. Chim. Acta* **2018**, *481*, 176–180.

[8] W. A. Caliebe, V. Murzin, A. Kalinko, M. Görlitz, *AIP Conf. Proc.* **2019**, 060031-1–060031-6.

[9] B. Ravel, M. Newville, *J. Synchrotron Radiat.* **2005**, *12*, 537–541.

[10] Demeter 0.9.26 with perl 5.024000 and using Ifeffit 1.2.12 on Windows 10.

[11] J. L. DuBois, P. Mukherjee, T. D. P. Stack, B. Hedman, E. I. Solomon, K. O. Hodgson, *J. Am. Chem. Soc.* **2000**, *122*, 5775–5787.

[12] Gaussian 16, Revision B.01, M. J. Frisch, G. W. Trucks, H. B. Schlegel, G. E. Scuseria, M. A. Robb, J. R. Cheeseman, G. Scalmani, V. Barone, G. A. Petersson, H. Nakatsuji, X. Li, M. Caricato, A. V. Marenich, J. Bloino, B. G. Janesko, R. Gomperts, B. Mennucci, H. P. Hratchian, J. V. Ortiz, A. F. Izmaylov, J. L. Sonnenberg, D. Williams-Young, F. Ding, F. Lipparini, F. Egidi, J. Goings, B. Peng, A. Petrone, T. Henderson, D. Ranasinghe, V. G. Zakrzewski, J. Gao, N. Rega, G. Zheng, W. Liang, M. Hada, M. Ehara, K. Toyota, R. Fukuda, J. Hasegawa, M. Ishida, T. Nakajima, Y. Honda, O. Kitao, H. Nakai, T. Vreven, K. Throssell, J. A. Montgomery, Jr., J. E. Peralta, F. Ogliaro, M. J. Bearpark, J. J. Heyd, E. N. Brothers, K. N. Kudin, V. N. Staroverov, T. A. Keith, R. Kobayashi, J. Normand, K. Raghavachari, A. P. Rendell, J. C. Burant, S. S. Iyengar, J. Tomasi, M. Cossi, J. M. Millam, M. Klene, C. Adamo, R. Cammi, J. W. Ochterski, R. L. Martin, K. Morokuma, O. Farkas, J. B. Foresman, D. J. Fox, Gaussian, Inc., Wallingford CT, **2016**.

[13] J. Tao, J. P. Perdew, V. N. Staroverov, G. E. Scuseria, *Phys. Rev. Lett.* **2003**, *91*, 146401.

[14] a) F. Weigend, R. Ahlrichs, *Phys. Chem. Chem. Phys.* **2005**, *7*, 3297-305; b) A. Schäfer, C. Huber, R. Ahlrichs, *J. Chem. Phys*.

1994, *100*, 5829; c) K. Eichkorn, F. Weigend, O. Treutler, R. Ahlrichs, *Theor. Chem. Acc*. **1997**, *97*, 119.

[15] L. Goerigk, S. Grimme, *Phys. Chem. Chem. Phys.* **2011**, *13*, 6670.

[16] S. Grimme, S. Ehrlich, L. Goerigk, *J. Comput. Chem.* **2011**, *32*, 1456–1465.

[17] M. Rohrmüller, S. Herres-Pawlis, M. Witte, W. G. Schmidt, *J. Comput. Chem.* **2013**, *34*, 1035–1045.

[18] M. Rohrmüller, A. Hoffmann, C. Thierfelder, S. Herres-Pawlis, W. G. Schmidt, *J. Comput. Chem.* **2015**, *36*, 1672–1685.

[19] A. Hoffmann, S. Herres-Pawlis, *Phys. Chem. Chem. Phys.* **2016**, *18*, 6430–6440.

[20] A. Hoffmann, M. Wern, T. Hoppe, M. Witte, R. Haase, P. Liebhäuser, J. Glatthaar, S. Herres-Pawlis, S. Schindler, *Eur. J. Inorg. Chem.* **2016**, *2016*, 4744–4751.

[21] F. Strassl, A. Hoffmann, B. Grimm-Lebsanft, D. Rukser, F. Biebl, M. Tran, F. Metz, M. Rübhausen, S. Herres-Pawlis, *Inorganics* **2018**, *6*, 114.

[22] S. I. Gorelsky, A. B. P. Lever, *J. Organomet. Chem.* **2001**, *635*, 187–196.

[23] a) Stoe & Cie, *X-Area Pilatus3_SV 1.31.131.0*, Stoe & Cie GmbH, Darmstadt, Germany, **2017**; b) Stoe & Cie, *X-Area Recipe 1.33.0.0*, Stoe & Cie GmbH, Darmstadt, Germany, **2015**; c) Stoe & Cie, *X-Area Integrate 1.71.0.0*, Stoe & Cie GmbH, Darmstadt, Germany, **2016**; d) Stoe & Cie, *X-Area LANA 1.71.4.0*, Stoe & Cie GmbH, Darmstadt, Germany, **2017**.

[24] Bruker, *XPREP 5.1*, Bruker AXS Inc., Madison, Wisconsin, USA, **1997**.

[25] G. M. Sheldrick, *Acta Crystallogr. Sect. A* **2015**, *71*, 3–8.

[26] G. M. Sheldrick, *Acta Crystallogr. Sect. C* **2015**, *71*, 3–8.

[27] C. B. Hübschle, G. M. Sheldrick, B. Dittrich, *J. Appl. Crystallogr.* **2011**, *44*, 1281–1284.

[28] M. V. Barybin, P. L. Diaconescu, C. C. Cummins, *Inorg. Chem.* **2001**, *40*, 2892–2897.

[29] R. L. Danheiser, R. F. Miller, R. G. Brisbois, S. Z. Park, *J. Org. Chem.* **1990**, *55*, 1959–1964.

[30] S. Herres-Pawlis, P. Verma, R. Haase, P. Kang, C. T. Lyons, E. C. Wasinger, U. Flörke, G. Henkel, T. D. P. Stack, *J. Am. Chem. Soc.* **2009**, *131*, 1154–1169.

[31] A. Hoffmann, C. Citek, S. Binder, A. Goos, M. Rübhausen, O. Troeppner, I. Ivanović-Burmazović, E. C. Wasinger, T. D. P. Stack, S. Herres-Pawlis, *Angew. Chem. Int. Ed.* **2013**, *52*, 5398–5401.

[32] H. Hussain, S. Specht, S. R. Sarite, M. Saeftel, A. Hoerauf, B. Schulz, K. Krohn, *J. Med. Chem.* **2011**, *54*, 4913–4917.

[33] a) R. Krug, D. Schröder, J. Gebauer, S. Suljić, Y. Morimoto, N. Fujieda, S. Itoh, J. Pietruszka, *Eur. J. Org. Chem.* **2018**, 1789–1796; b) L. Penttinen, C. Rutanen, J. Jänis, J. Rouvinen, N. Hakulinen, *ChemBioChem* **2018**, *19*, 2348–2352.